Scanning Tunneling Microscopy Study of DNA related Molecules on Solid Surfaces

by Hiroyuki TANAKA

Division of Atom Scale Science,
Institute of Scientific and Industrial Research,
Faculty of Science, Osaka University

A DISSERTATION IN CHEMISTRY
PRESENTED TO THE GRADUATE SCHOOL OF SCIENCE
OF OSAKA UNIVERSITY IN THE REQUIREMENT FOR
THE DEGREE OF DOCTOR OF SCIENCE

JANUARY 1997

Contents

Chapter 1

General Introduction

1.1 Introduction

The scanning tunneling microscope (STM) was invented by Binnig and Rohrer in 1981[1]. This new instrument has proved to be an extremely powerful tool for many disciplines in condensed-matter physics, chemistry and biology[2,4]. The STM can resolve local electronic structure and manipulate atom/molecule(s) at an atomic scale on conducting solid surfaces in real space.

One of the most interesting and important samples for STM study is DNA, because it is the medium encoding the information which determines the structural and functional properties of all living organisms. Many studies have been done to resolve the nucleotide sequence of the DNA[5-8]. However, it appears that none of these studies have been successful[4]. This is partly due to the lack of the reliable sample preparation method of the DNA for STM study. Unreliable sample surface often results in the observation of "artifacts" instead of the "real" DNA images.

The sample preparation is strongly related to both kind of substrates and observation conditions(in vacuum, in air, temperature of the system,.. for example). Moreover, if one wants to observe "molecule-molecule interactions" (which is an essential driving force of the "self-assembled structure" such as the DNA) by STM, "substrate-molecule interactions" should be deliberately considered, because too strong interactions between substrate and molecule surely alter the nature of the molecules.

In addition to the difficulties of sample preparation method and selection of appropriate substrate, "STM images" are not self-evident, that is, it is often difficult to understand what STM images means.

The STM is a scanning microscope which maps a constant charge density contour of the sample surface by detecting tunneling current flowing between the sample and probing "tip". This "constant current" imaging mode is sketched in Fig.1.1.

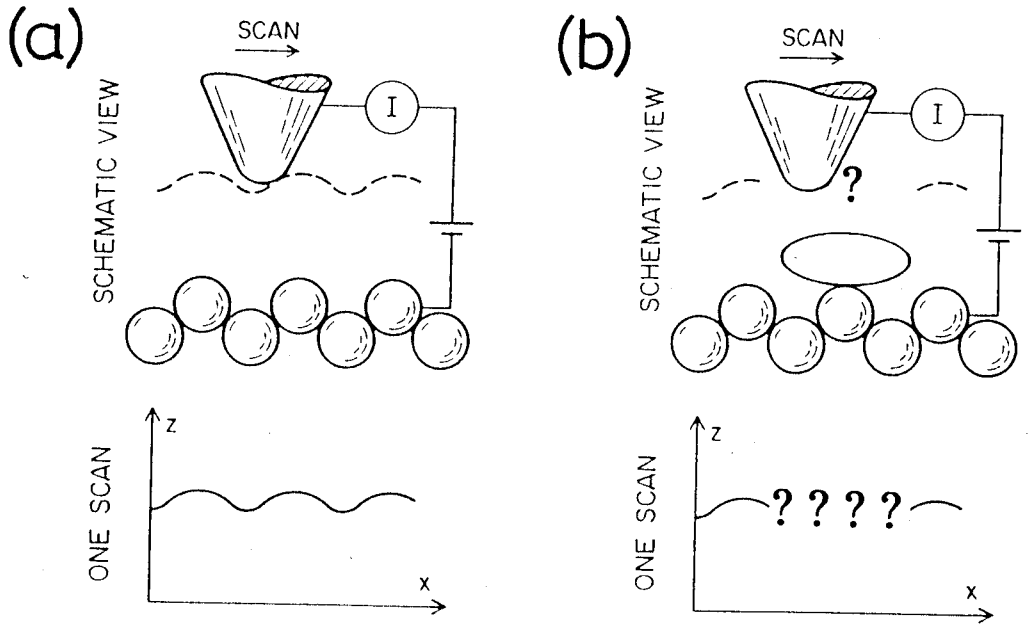

Fig.1.1 Schematic illustration of the constant current mode of STM operation(From Ref. [9]). (a) A clean surface. (b) A molecule-substrate system.

A molecule-substrate system is probed by scanning tip while adjusting vertical relative height of the tip to maintain tunneling current constant. The resultant contour (dotted envelope) may not correspond directly to the atomic position.

The tunneling current, I, is

$$I \propto \rho_s \rho_t \exp(-s \phi^{1/2}) \qquad (1.1)$$

where s is the sample-tip separation, ϕ is a parameter related to the barrier height for tunneling electrons between the sample and tip, ρ_s is the electron density of the tip, and ρ_s is the electron density of the sample. Although this expression is oversimplified, it is clear that the contrast in the STM image is convolution of the electronic structure of the sample, the electronic structure of the tip, and the tunneling barrier function(related to the surface work function).

The problem is that STM image of insulative molecules is actually observed for

many adsorbed-substrate systems[2-4]. To solve this problem, electronic states of the adsorbed system must be known as a first step. Because there are interactions between molecule-substrate and even from presence of probing tip which probably alter the electronic states of the system. However, a large ab initio theoretical calculation necessary for adsorbed system is still too time consuming to perform, that is, the theoretical description is very complex and far from complete to interpret the whole electronic structure of tip-molecule-surface system[10].

This thesis is an attempt from experimental stand point to elucidate the possibility of the imaging, sequencing and manipulation of the DNA-related molecules using STM based on the understanding of the interactions of molecule-substrate and between molecules.

In the next chapter (1.3 Scanning Tunneling Microscopy in Biological Molecules), essential facts and concepts which should be stated before the main text, are briefly reviewed in following order.

1.3.1 Substrate surfaces, 1.3.2 Imaging, 1.3.3 Self-assembly,

1.3.4 Manipulation

These sections are necessary to understand the discussion in the main text and to clarify the state of current progress of this field and the importance of this present study.

1.2 Motivation of the Present study

The advent of newly developed surface science tool, STM, has opened up a new era for the world of science as well as engineering. In fact, STM has resolved some "mysteries" of the nature and enabled so called "nano-technology". Both would have never been realized without STM. However, it has raised more questions than it has resolved. The few of the questions are:

(1) Is it possible to prepare samples of DNA-related molecules for UHV-STM study in reproducible and reliable manners? (Chapter 3-5,7.)

(2) Is there any possibility for sequencing of DNA using STM?

Is it possible to discriminate DNA base molecules? (Chapter 3-5,7.)

(3) How can we interpret STM images of DNA-related (insulative organic) molecules

adsorbed on solid surfaces? (Chapter 6.)

(4) Is it possible to observe self-assembly of DNA base molecules on solid surfaces? Is it possible to prepare such molecule-substrate system? (Chapter 5.)

(5) What factors contribute to the formation of self-assembly of DNA base molecules on solid surfaces. (Chapter 5, 6.)

(6) How can we manipulate DNA-related molecules? What the mechanism is? (Chapter 3, 8)

The ultimate goal of the present study involves one that has been tried and resigned to pursue. In chapter 2, basic instrumentation of STM is shown with developing and modifying process (usually required for unconventional study) of used apparatus. STM imaging and manipulation of isolated and self-assembled DNA base molecules (in chapter 3-5) and intact DNA oligomer (in chapter 7 and 8) adsorbed on various solid surfaces are shown in answer to the above questions.

In chapter 6, mechanisms of imaging, self-assembly, and in chapter 7,8 manipulation of DNA-related molecules are discussed on the basis of interactions of molecule-substrate, molecule-molecule and molecule-tip, followed by concluding remarks of chapter 9.

These works have been published in the following journals.

(1) STM-imaging of a $SrTiO_3(100)$ surface with atomic-scale resolution
Surface Science, 1992 278 L153-L158.
T. Matsumoto, H.Tanaka, T. Kawai and S. Kawai

(2) Surface Structure and Electronic Property of Reduced $SrTiO_3(100)$ Surface Observed by Scanning Tunneling Microscopy/Spectroscopy
Japanese Journal of Applied Physics, 1993 32 pp1405-1409.
H.Tanaka, T. Matsumoto, T. Kawai and S. Kawai

(3) Scanning Tunneling Microscopy Study of Laser Molecular Beam Epitaxy on $SrTiO_3(100)$ Surface Surface Science, 1994 312 pp21-30.
T. Matsumoto, H.Tanaka, T. Kawai and S. Kawai

(4) Bias Dependence of Scanning Tunneling Microscopy Study Images of Sr Atoms Adsorbed on $SrTiO_3(100)\sqrt{5}\times\sqrt{5}$ Surfaces
Japanese Journal of Applied Physics, 1996 35 L1692-1694.
A. Kubo, H.Tanaka, Hi Tabata, T. Matsumoto and T. Kawai

(5) Interaction of Oxygen Vacancies with O_2 on Reduced $SrTiO_3(100)\sqrt{5}\times\sqrt{5}$ R26.6° Surface Observed by STM
Surface Science, 1994 318 pp29-38.
H.Tanaka, T. Matsumoto, T. Kawai and S. Kawai

(6) Surface Structure of Reduced $SrTiO_3(111)$ Observed by Scanning Tunneling Microscopy
Surface Science, 1996 365 437-442.
H.Tanaka and T. Kawai

(7) Distinct imaging of the nucleic acid bases on $SrTiO_3(100)$ by scanning tunneling microscopy
Journal of Vacuum Science Technology B 13(4) 1995 pp1411-1414.
H.Tanaka and T. Kawai

(8) Scanning tunneling microscopy imaging of the DNA base molecules on reduced $SrTiO_3(100)$ surfaces
Material Science and Engineering C3 1995 pp143-148.
H.Tanaka and T. Kawai

(9) Elucidation of hydrogen-induced (1×2) reconstructed structures on Pd(110) from 100 to 300 K by scanning tunneling microscopy
Physical Review B 1995 51 pp4529-4532.
J. Yoshinobu, H.Tanaka and M. Kawai

(10)Oxygen-induced reconstruction of the Pd(110) surface: an STM study
Surface Science Letters, 1995 327 L505-L509.
H.Tanaka, J. Yoshinobu and M. Kawai

(11)Adsorption, migration, and superlattice formation of benzene on Pd(110)
Physical Review B 1996 53 pp7492-7495.
J. Yoshinobu, H.Tanaka and M. Kawai

(12)Imaging of Nucleic Acid Base Molecules on Pd(110) Surfaces by Scanning Tunneling Microscopy
Japanese Journal of Applied Physics, 1996 35 ppL244-L246.
H.Tanaka, J. Yoshinobu, M. Kawai and T. Kawai

(13)Two Dimensional Self-Assembly of DNA Base Molecules on Cu(111) Surfaces
Surface Science, 1996 364 L575-L579.
H.Tanaka, T. Nakagawa and T. Kawai

(14)Two-dimensional self-assembly of uracil molecules on Cu(111) surfaces: a low temperature STM study
Surface Science Lett., 1997 in press..
T. Nakagawa, H.Tanaka and T. Kawai

(15)STM imaging and manipulation of DNA oligomer adsorbed on Cu(111) surfaces by a pulse injection method
Journal of Vacuum Science Technology B 1997 in press.

H. Tanaka and T. Kawai

(16)STM Observation of Copper-Phthalocyanine and Nucleic Acid Base Molecules on reduced $SrTiO_3(100)$ and Cu(111) Surfaces
Japanese Journal of Applied Physics, 1996 35 Part 1,No.6B.
H.Tanaka and T. Kawai

The papers (1)-(8) deal with the preparation and characterization of the clean $SrTiO_3(100)\sqrt{5}\times\sqrt{5}$ surface that has been obtained for the first time. It has been revealed that the interaction on the $SrTiO_3(100)\sqrt{5}\times\sqrt{5}$-molecule system is relatively weak and the discrimination of the DNA base molecules was achieved. The results for DNA base molecules adsorbed on the $SrTiO_3(100)\sqrt{5}\times\sqrt{5}$ will be mainly shown and discussed in the chapter 3 in this paper.

The next papers (9)-(12) are the works to elucidate the interaction and dynamic reaction process on the Pd(110)-molecule system. The nature of the chemically reactive Pd(110) substrate has been revealed, i.e., the DNA base molecules were strongly adsorbed on the surface (they do not diffuse), and their molecular orbitals were observed by STM. This will be presented in the chapter 4.

The next paper (13)-(14) have revealed that the self-assembly of DNA (and RNA) base molecules, adsorbed on Cu(111), occurs through the intermolecular hydrogen-bonding by STM for the first time. This will be appeared and discussed in the chapter 5.

The paper (15) contains a new deposition technique for biological molecules and imaging/manipulation of the DNA oligomer on Cu(111). This will be appeared and discussed in the chapter 7, 8.

The paper (16) include systematic discussion on the role of substrates ($SrTiO_3(100)$ and Cu(111)) on the imaging and self-assembly mechanism of the adsorbed DNA base molecules. The related discussion will be appeared in the chapter 6.

1.3 Scanning Tunneling Microscopy in Biological Molecules.

In biological systems, a potential of STM to operate in fluids is a great advantage, because it enables the observation of dynamic processes in a direct way. However, it is often true that the ultrahigh vacuum (UHV) condition is the most well-defined condition for the surface science study, including STM study. In order to focus on the basic

imaging and manipulation mechanism of the STM and interactions in adsorbed systems (molecule-molecule, molecule-substrate and molecule-tip) for the DNA related molecules, all the experiments have been conducted under the most "well-defined" UHV condition by developing sophisticated sample preparation technique in this present study as a new approach for the study of biological molecules.

In the following section, the role of and requirements for the substrates are pointed out first, because STM experiment needs a substrate for molecules to be imaged or manipulated. The processes of adsorbed system are also stated. That is one of the factors that governs the mechanisms of image, self-assembly and manipulation.

1.3.1 Substrate Surfaces

In order to observe or manipulate organic molecules, the following issues should be considered:

(1) The roughness of the substrate should be considerably less than the apparent size of the molecular species, because this allows clear distinction between substrate and molecular feature in STM images. Atomically flat clean surfaces of single/poly crystals can be routinely prepared by conventional methods such as annealing, ion sputtering, cleaving or molecular beam epitaxy method.

(2) The substrates must have enough electrical conductivities. (The atomic force microscopy studies do not require this.) This means that insulators such as mica or sapphire can not be used though they expose atomically flat surfaces.

(3) The binding strength of molecules to the surface at finite temperatures must be large enough to immobilize them. If the strength is too weak, the molecules will be dragged by the tip during scanning through the tip-molecule interactions. Moreover, the molecules may intrinsically diffuse over the surface or even desorb from the surface. On the other hand, too strong binding between the molecule and substrate may break the bonds keeping atoms as a molecule.

This is related to the kind of chemical bonding between molecule and surface and also crystallographic geometry such as (111) surface of face-centered cubic crystal or (110) surface of body-center cubic.

(4) An adequate temperature of the sample must be chosen, because this factor affects the surface diffusion/desorption and dissociation process of the molecules.
(5) The electronic and geometric structures of adsorbed system and transport properties(imaging mechanism) must be understood to interpret STM images of molecular species.

As described above, interactions between the molecule and substrate play important roles which provide immobilization of the adsorbed molecules or surface diffusion for formation of self-assembly and have much to do with interpretation of molecular images. Subsequently, the concepts on process of molecule-substrate interaction, such as "physisorption", "chemisorption", "theory of chemisorption" and "surface diffusion" are shown to precede "employed substrates".

Physisorption

There are two major adsorption processes that govern interaction between molecule and substrate; physical adsorption(or physisorption) and chemical adsorption(or chemisorption).

In the case of physisorption, an adsorbed molecule is bound to the surface via a rather weak van der Waals type of bonding. This bond involves no charge transfer between the substrate and adsorbed molecule. The attractive force is provided by the instantaneous dipole moments of the adsorbed molecule and its nearest neighbor surface atoms. The binding energies for physisorbed molecules are typically 0.2 eV or less. Such bonds are found in the adsorption of inert gases on metals. This weak interaction is insufficient to lead to bond breaking. This means a physisorbed molecule retains its identity.

If t_0 is the period of a single surface atom vibration in the well of the depth E_{des}, then the stay time t of this atom on the surface is given by

$$t = t_0 \exp (E_{des}/kT) \qquad (1.2)$$

The time t_0 is usually of the order of 10^{-12}s, and equation(1.2) can be used to show that stay time greater than about 1 s will not occur until $E_{des} > 28\ kT$. Thus an adsorption energy of 0.2 eV will give t>1s only below temperatures of about 100K.

Since the STM imaging typically requires a few seconds to minutes to obtain single image, physisorbed atoms (molecules) can be imaged by STM at only below 100K and can not be imaged at room temperature.

Chemisorption

In the case of chemisorption, an adsorbed molecule is bound to the surface via a rather strong bond. This bond involves charge transfer between the substrate and adsorbed atom. Usually there is an admixture of the wave functions of the valence electrons of the molecule with the valence electrons of the substrate into a new wave function. The electrons responsible for the bonding can then be thought of as moving in orbitals between substrate and adsorbed molecules. The simple potential diagram for a chemisorption is shown in Figure1.2. Some of the impinging molecules are accommodated by the surface and become weakly bound in a physisorbed state (also called a precursor state) with binding energy Ep. During their stay time in this state, electronic or vibrational processes can occur which allow them to surmount the small energy barrier Ec (activation energy: Ec+Ep) and electron exchange occurs between adsorbate and substrate. The adsorbed molecule now stays in a much deeper well, Ea.

The binding energies (heats of adsorption) in chemisorption are typically in the region of 2 eV and larger than those of physisorption(0.2 eV). In the case of chemisorption, adsorbed molecules stays at the surface longer than an hour even at room temperature. This means chemisorbed molecules can be imaged by STM at room temperature.

As stated earlier, the electronic structure of the sample contribute to STM image, understanding of the electronic structure of chemisorbed molecule-substrate system is necessary for interpretation of STM image. One of most the important theory of chemisorption is presented bellow.

Theory of chemisorption

The theoretical description of chemisorption is very complex and far from complete[10]. In fact the theoretical calculation of adsorbed system seems not be realized without approximations about the description of the electron-electron

interactions or the construction of an extremely simple model. However, there is an important theory known as the *News- Anderson* model[10]. In this model, there are two limiting cases which emerge from the application of this model to a system consisting of an adsorbate with a single valence state on a metal surface. These two extremes are sketched in Fig.1.3. In Fig.1.3(a) is the density of states in the metal is flat and the adsorbate state is broadened from a single level in the isolated atom to a Lorenzian distribution centered about the original energy level. This is *week chemisorption*. The other extreme occurs when the electron in the metal are confined to a band which is narrow compared to the coupling between the atom and the metal. This is indicated in

Surface Diffusion

Adsorption processes are an important factor, as presented above. In STM experiment, another relevant factor must be considered also. That is surface diffusion process of adsorbate. In this section surface diffusion is briefly explained.

At finite temperature, the thermal energy fluctuations sometimes give the adsorbed molecule(atom) sufficient energy for it to leave its initial site in the surface and become an adsorbed molecule(atom) in neighboring position of potential energy minimum. This is the simplest picture of self-diffusion.

The activation energy for diffusion(E_{dif}) over the surface need not be the same for desorption(E_{des}) because the molecules may be able to move through valley between potential peaks without leaving the surface completely. The activation energy for migration is generally about 10-20 per cent of that for desorption. The stay time t of adsorbed molecule(atom) upon the surface is given by same as Eq.(1.2), replacing E_{des} by E_{dif}.

Since E_{dif} is smaller than E_{des}, it is E_{dif} that decides whether the adsorbed molecules freeze their transitional motion over the surface at finite temperature such as room temperature. However, large $E_{des}(E_{dif})$ means that the nature of the adsorbed molecules(atoms) is strongly distorted by the bond between the molecules and the substrate. It would result in a dissociation of the adsorbed molecules. In order to observe intact molecules by STM, this must be avoided by any means.

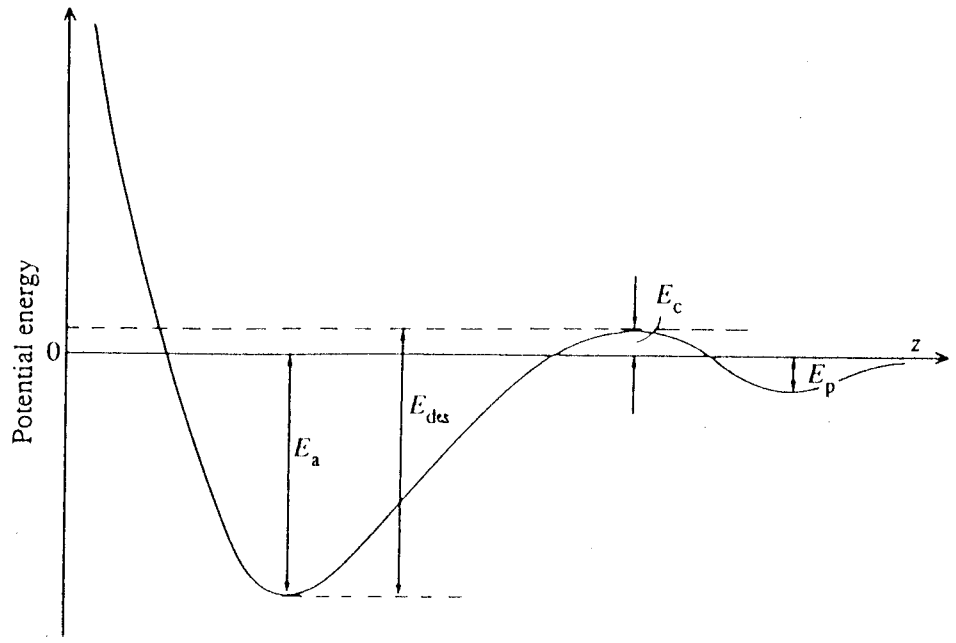

Fig. 1.2 A potential diagram for chemisorption.

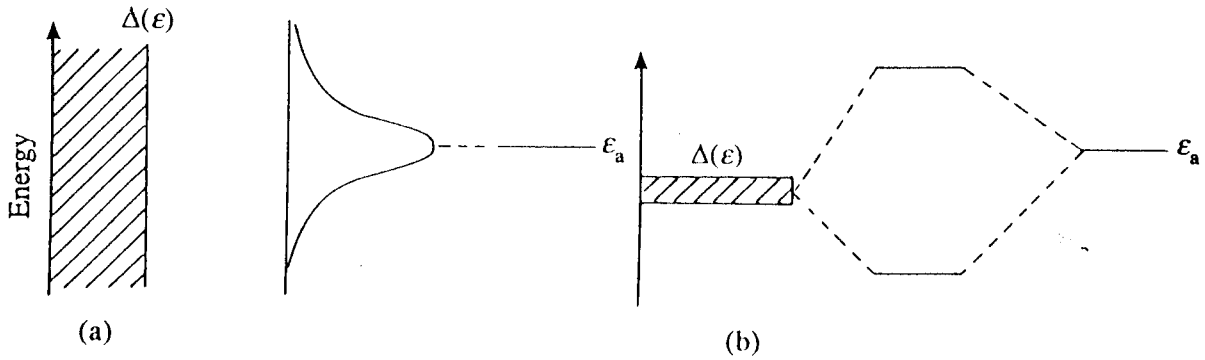

Fig. 1.3 The local density of states of an adsorbate in the Newns-Anderson model. (a) The single level in the adsorbate is broadened into a Lorentzian distribution when the chemisorption is weak. (b) The same level is split into two states when the chemisorption
is strong. (From Ref. [10])

Fig.1.3(b) where it can be seen that the single level in the isolated atom has split into two states-known as *bonding* and *anti-bonding*.

In the case, E_{des} is large enough to keep molecules at the surface and E_{dif} is small enough for the adsorbed molecules to diffuse over the surface, the molecule-molecule interaction is expected. The molecule-molecule interaction is important for the self-assembly that is presented in the section 1.3.3.

Employed Crystal substrates

The above sections have pointed out the importance of the substrate in many aspects. Therefore, the selection of substrate for the study must be deliberately done. In the STM study on organic molecules such as DNA, the following facts must be also considered. Crystal substrates have been usually used for the adsorption of organic(biological) molecules. This is because a crystal exposes an atomically flat surface which is necessary for STM observation. A typical corrugation of less than 0.1 nm is usually observed. As a matter of course, graphite substrates have been used as a most common and convenient substrate due to its easy preparation, i.e., it is usually enough only to cleave by a mending tape. The STM image of DNA with the highest resolution(the double-helical structure, and the base pairs) were obtained under UHV conditions using graphite substrate[6]. However Clemmer and Beebe [11] have demonstrated and claimed that as-cleaved graphite surfaces sometimes exhibit structural features which can mimic the presence of 'DNA', which are called "artifacts". Moreover, interpretation of STM image of macro molecules such as DNA is not understood completely. It should be mentioned that the STM study aiming at DNA sequencing on graphite surface seems to have almost disappeared lately. It may be better not to use graphite as substrates for DNA at least.

The crystal substrates used in the present study are listed below, and the characteristic natures of these substrates are shown in Fig.1.4.

(a) $SrTiO_3(100)\sqrt{5}x\sqrt{5}$-R26° surface

This is a reduced (100) surface of perovskite structure. The top most(exposed surface) layer is TiO_2 with an ordered oxygen vacancy of $\sqrt{5}x\sqrt{5}$ periodicity. The $SrTiO_3$ is an insulator with the band gap of 3.2 eV when stoichiometric. Upon annealing at 1200C in vacuum, oxygen vacancies are introduced which induce electronic states

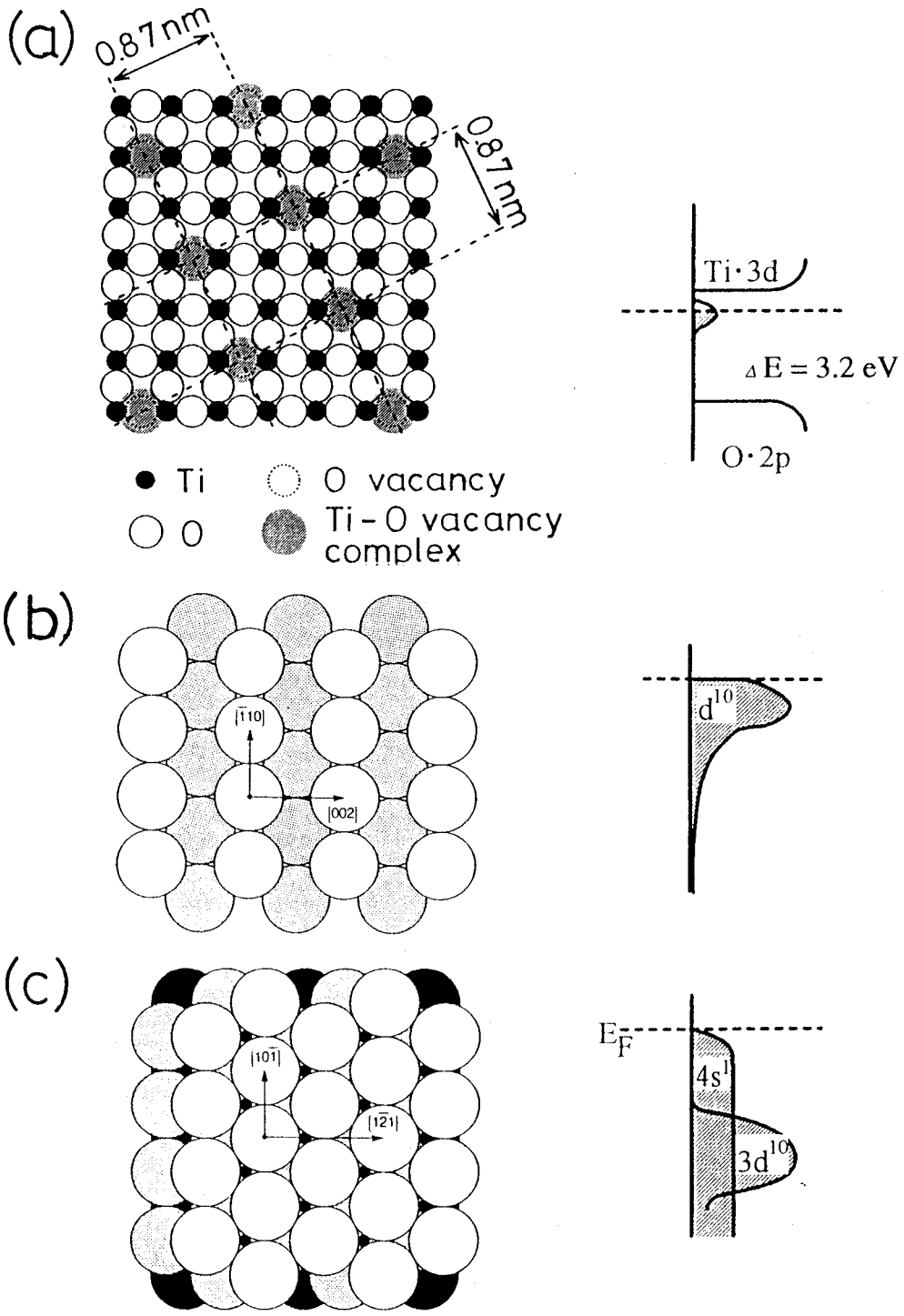

Fig. 1.4 The simple models of the surface structure and electronic structure (density of states near the Fermi level (E_f)) of the three different substrate surfaces. (a) $SrTiO_3(100)$ $\sqrt{5}x\sqrt{5}$-R26° , (b) Pd(110), (c) Cu(111).

near the Fermi level to become a n-type semi-conductor. Atomic feature of $\sqrt{5}x\sqrt{5}$ corresponds to a map of the each oxygen vacancy site as shown in Fig.1.4(a) [12].

(b) Pd(110) surface

Pd is known as a chemically reactive material[13][14]. This active nature is supposed to arise from its 4d electronic states that rest at the Fermi level (Fig.1.4(b)). Pd has a face-centered cubic (fcc) structure. The (110) surface has a C_{2v} symmetry which may induce anisotropy in surface diffusion process.

(c) Cu(111) surface

Copper is a less chemically reactive metal. This is due to the electronic states of the broad 4s band at the Fermi level (Fig.1.4(c)). The (111) surface of Cu which is also a fcc metal has a close-pack (the smallest corrugated) surface [15].

The specific preparation processes of such surfaces used in the study are described in each experimental sections. It should be mentioned that preparation of a well-defined clean surface is a serious problem, because a recipe for certain clean surface may not be found in the literatures. In that case, the time and effort must be spent on it as a starting point.

1.3.2 Imaging

Before the invention of the STM, the tunneling process was discovered and has been studied experimentally and theoretically. In classical physics, an electron with an energy smaller than a potential barrier height of an energy barrier, will never be able to traverse this barrier. However, in quantum theory, this electron can traverse the barrier. The wave nature of microscopic particles impinging upon a potential energy barrier is expressed in the experimental observation of a finite probability of finding the particles beyond the barrier and they are then said to have tunneled through it.

In this section, a basic theory which is essential for interpretation of STM images, i.e., tunneling theory, is shown.

One-Dimensional Tunneling Theory

The tunneling current flowing between two electrodes separated a thin insulating barrier, when high or very low voltages were applied, was theoretically studied by Sommerfeld and Bethe [16] using the WKB approximation(developed by Wentzel, Kramers and Brillouin in elementary textbooks of quantum theory). The following expression for the probability $D(E)$ that an electron can penetrate into a one-dimensional potential barrier $V(z)$ of arbitrary shape is found within the WKB approximation, as follow:

$$D(E) = \exp\{-(2/h)\int_{s1}^{s2}[2m(V(z)-E)]^{1/2}\,dz\} \tag{1.3}$$

$$= \exp\{-2\int_{s1}^{s2}\kappa(z,E)\,dz\}$$

where s_1 and s_2 are the classical tunneling points and $(s_1 - s_2)$ is the width of the barrier, as shown in Fig.1.5. The WKB approximation is adequate only if the energy E is not near or above the top of the barrier ($E << V$) and if the sides of the barrier at s_1 and s_2 are gently sloping.

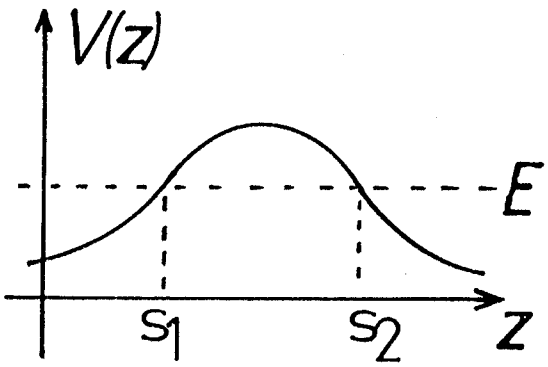

Fig.1.5 Potential diagram for tunneling by WKB approximation.

Interpretation of STM images

As will be described in chapter 2, the constant current imaging mode is used in the present study as well as in the most of the literatures. In this mode a voltage V is applied to the sample (with the tip at ground), only those states lying between E_f and $E_f + eV$

contribute to the tunneling process (Fig.1.6). The polarity and magnitude of the applied voltage, then determine which state can contribute to the resulting topographic image.

Figure 1.6 shows an energy level diagram for the system consisting of the sample and tip that are separated by vacuum. Based on the simple one-dimensional planar tunneling models, using the WKB approximation, the WKB theory predicts that the tunneling current is given by

$$I = \int_0^{eV} \rho_s(r, E)\ \rho_t(r, -eV + E)\ T(E, eV, r)\, dE \qquad (1.4)$$

where $\rho_s(r, E)$ and $\rho_t(r, E)$ are the density of states (DOS) of the sample and tip, respectively, at location r and the energy E, measured with respect to their individual Fermi levels. For negative sample bias, $eV<0$ and for positive sample bias, $eV>0$. The transmission coefficient $T(E, eV)$ for electrons with energy E and applied bias voltage V is given by

$$T(E, eV) = \exp\left[-\{(2Z(2m)^{1/2})/h\}\{(\phi_s + \phi_t)/2 + eV/2 - E\}^{1/2}\right] \qquad (1.5)$$

where ϕ_s and ϕ_t are the work functions of the sample and tip (see Fig.1.6). This formula indicates that the transmission coefficient increases monotonically with the applied bias voltage. However, following factor may contribute to "apparent shape" and lateral resolution of STM images.

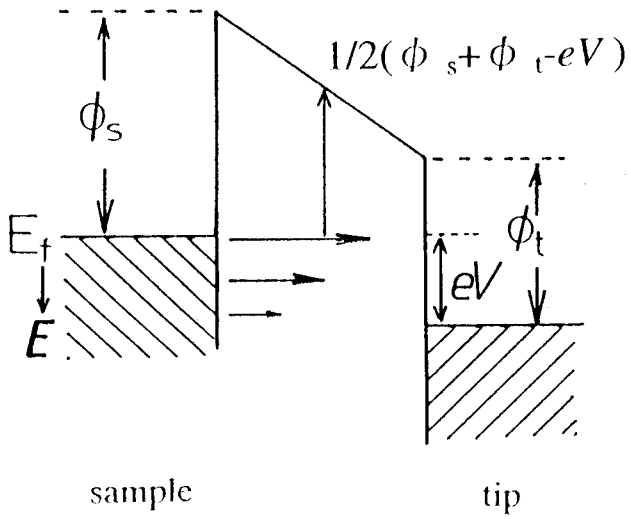

Fig. 1.6 Energy diagram of sample and tip (applied negative sample bias).

The band structure has an effect on tunneling process because the rate of decay of the wavefunctions of the sample and tip in the vacuum region is determined by momentum *perpendicular* to the surface. The energy E of the state enters the tunneling probability because the effective height of the tunneling barrier depend on the electron energy

$$E = k^2/(2m) = [(k_x^2+k_y^2+k_z^2)/(2m)]. \quad (1.6)$$

In order to incorporate such effect, the E in Eq.(1.5) must be replaced by

$$E - h^2 [k_{\|}^2/(2m)]. \quad (1.7)$$

where $k_{\|}^2 = (k_x^2+k_y^2)^{1/2}$ is the parallel momentum. It is apparent that $T(E, eV)$ becomes largest when the parallel momentum is zero.

Thus, STM image (at constant tunneling current I, the contour followed by the tip) is a relatively complicated function of the DOSs of both sample and tip, together with the tunneling transmission probability.

1.3.3 Self-assembly

Under certain conditions, such as liquid phase, gas phase, gas-solid interface, etc., molecules undergo spontaneous formation of aggregates or complex supramolecular assemblies through the interaction between molecules. That is the phenomenon called self-assembly or self-organization. Lipids and biological cells are typical examples of naturally occurring self-assembled(organized) structures [17].

It is well known that molecule-molecule interaction through hydrogen bonding play a central role in DNA, RNA (such as the double-helical structure and the base pairs) and many biological molecules[18][19]. Considering the difficulty to obtain reliable high resolution image of whole DNA, as mentioned in section 1.3.1, it may be reasonable to go back to the individual molecules i.e., the DNA base molecules as a first confident step. In addition, they are rather simple molecule and well studied in both experimentally and theoretically [18][19]. Since STM has atomic/molecular resolutions on substrate surface in real space, the STM may indeed be one of the powerful tools for probing two-dimensional self-assembled DNA base molecules to elucidate the mechanism of self-assembly.

There are two important points on self-assembly (self-organization), especially in this study. One is the fact that the molecules self-assembled into a two-dimensional molecular crystal (usually monolayer film) can be often imaged by STM without dragging them by the tip, because the molecule-molecule interactions force them to immobilize on the substrate. Second, information of self-assembled structure can give insight into the mechanism of self-assembly that involves molecule-molecule and molecule-substrate interactions, the temperature of the system etc..

In order to clarify the state of the STM study of self-assembly, a brief history and basic mechanism of self-assembly of organic molecules is presented in this section, as follows.

A brief history of self-assembly of organic molecules in STM study

As mentioned above, self-assembling process depends on molecule-molecule and molecule-substrate interactions and temperature of the system. The molecule-molecule interactions originate mainly from van der Waals and electrostatic (hydrophilic, hydrophobic and hydrogen bonding) interactions.

The most clear example for the self-assembly due to van der Waals interaction of organic molecules is reported by Ohtani et al.,[20]. They studied benzene co-adsorbed with CO on clean Rh(111) substrates and found that a (3×3) superlattice structure is formed with two CO molecules per unit cell, as shown in Fig. 1.5(a). The model can be easily understood from the view point of the known van der Waals sizes of adsorbed species. In the case of non-polar molecules, the van der Waals interaction dominates to form close-packed structures.

The molecule-substrate interaction, especially the activation energy for diffusion is comparable to the thermal energy at room temperature (kT =0.025 V) in this CO, benzene/Rh(111) system. This allows the molecules to diffuse over the surface as long as the coverage is low. At saturated coverage, they cannot diffuse over the surface any longer because they are packed. It should be noted that above superlattice structure (resulting from van der Waals interaction) may not be called self-assembled structure.

Other famous self-assembled molecules which have been extensively studied by STM are liquid crystal and alkanes(-derived) molecules[21][22]. They are structurally

similar in that they have alkyl-chains as a main frame. (These molecule with a hydrophilic head and a hydrophobic tail groups are known to form two-dimensional layers using Langmuir-Blodget method[23].) As shown in Fig.1.7(b), the observed two-dimensional structures adopt a similar structure, that is, the hydrophilic head (hydrophobic tail) groups are positioned next to the hydrophilic head (hydrophobic tail) groups of other molecules due to molecule-molecule interactions of hydrophilic and hydrophobic bonding. And the molecule-substrate interactions make the self-assembly form a domain structure with epitaxial orientation (Fig.1.7(c)).

From above examples, the shape and functional head/tail (group) of the molecule plays an important role in the intermolecular interaction. Moreover, the hydrogen bonding acts as dominant electrostatic interaction force when molecules have -OH or -NH_2 groups addition to hydrogen. The hydrogen bonding are typically formed as -OH***O-, -OH***N- with bonding energy of 0.1-0.5eV[24][25][26]. The value of 0.1-0.5 eV is much larger than that of thermal energy of kT =25 meV and may be even larger than that of activation barrier for diffusion.

STM observation of self-assembled DNA base molecules on Au(111) electrode under electrochemical condition has been reported by Lindsay and coworkers[27]. They have observed that some of the DNA bases are packed into two-dimensional superstructures through hydrogen bonding. However, the observed structures seem to depend on the electrochemical conditions (applied potential, charge transfer, water molecules, electrolyte, dissolved contaminants, etc.) and may be different from those adopted under vacuum or biological conditions. The poor (not reliable enough) quality of the images may indicate that the difficulties of STM observation of intact molecule under electrochemical condition.

As shown in above, in self-assembly process of organic molecule (and also for DNA base molecules), following factors are important:

The intermolecular interaction:

(1) The shape of the molecule: van der Waals packing.

(2) The group in the molecule: electrostatic hydrogen bonding; typically 0.1-0.5 eV

(3) The group in the molecule: hydrophilic, hydrophobic bonding; <0.1 eV

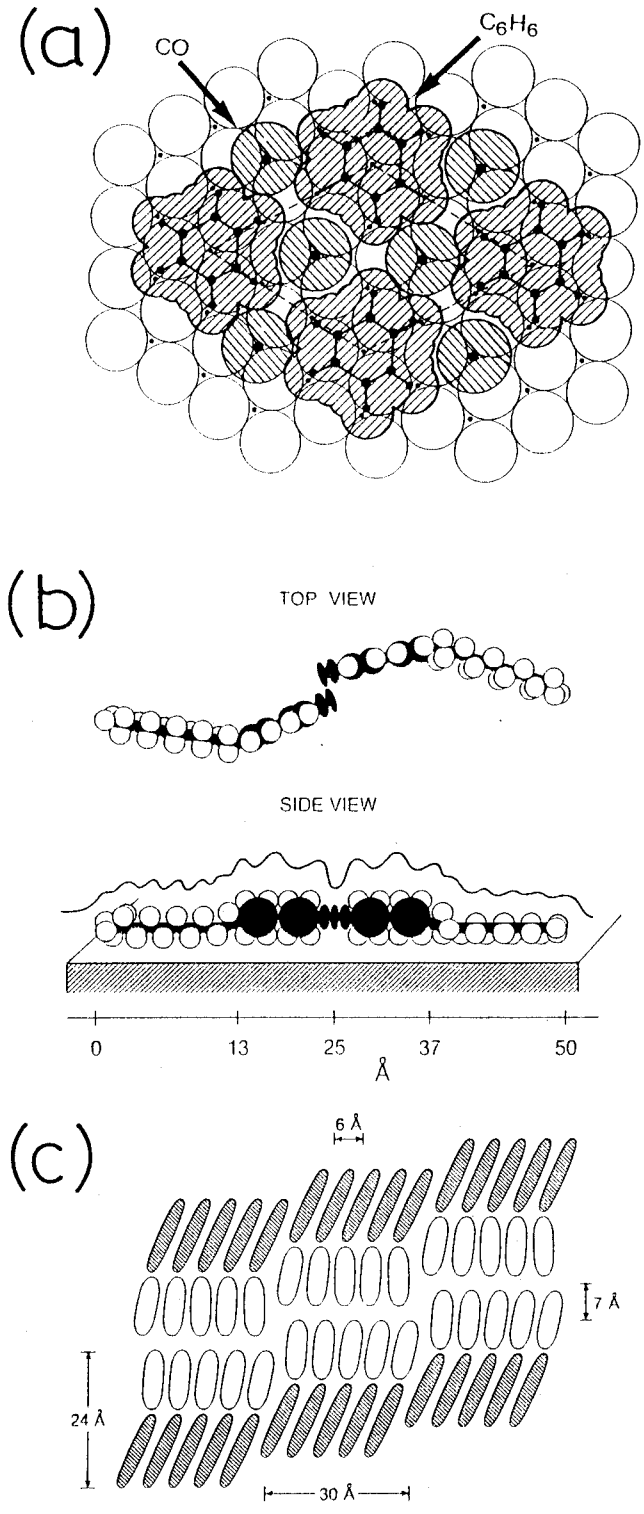

Fig. 1.7 (a) The structure model for Rh(111)-(3x3)(C_6H_6 + 2CO). (From Ref. [21]) (a)(b) The structure model for 10-alkylcyanobiphenil on graphite surface, showing the orientation of two molecules(a). The shaded and unshaded segments represent the alkyl tails and the cyanobiphenyl head groups, respectively. (From Ref.[22])

The molecule-substrate interaction:

(4) Adsorption energy(E_{des}): too strong (weak) interaction will result in dissociation (desorption) of adsorbed molecule; ~ 0.5 (weak) - 10 eV (strong).

(5) Diffusion energy(E_{dif}): too large E_{dif} prevents adsorbed molecules from diffusing and interacting each other to self-assemble; 10-20 % of that for E_{des} i.e., ~0.05-2eV.

(This value also depends on the symmetry of the surface structure.)

(6) The temperature of the system: thermal energy (kT) can activate the diffusion of adsorbed molecule; ~0.025 V at 300 K.

(7) Epitaxy and diffusion bias; the corrugation of E_{dif} is not isotropic along the surface due to the symmetry of, steps and defects on the surface. The ratio of E_{dif} (max)/E_{dif} (min) ~ 2.

As is classified above, these factors will decide whether self-assembly occurs or not, and resulting structure if it takes place. Consequently, the choice of a system of substrate, chemical species and crystal plane as well as conditions of temperature or ambient, is critical for the study of self-assembly.

1.3.4 Manipulation

The ability of STM to probe individual atom/molecules in real space implies an ability to perturb individual atom/molecules in real space. The "probe" in STM is tunneling current which flows between sample and probing tip according to the applied potential field. In view of this fundamental principle of STM, possible perturbation which can be cast upon a system includes following STM parameters:

(1)electrostatic field E (V/m) due to applied bias voltage V (V) between the gap s (m).

(2) (tunneling) current I (A), especially inelastic one.

(3) tip-sample proximity (interaction), such as van der Waals, chemical bonding

(The field and current have "polarity")

They may effect as either attractive or repulsive interaction.

Since the well-known memorial report by Eigler and Scweizer in 1990 [28], research aiming at atom/molecule manipulation has been done, though it may be still in its infancy. From the literatures, one can recognize the importance of the controllability

of STM parameters, *V*, *I* and *s*. In this section, typical mechanisms of manipulation are summarized in the order of STM parameters.

(I) Field related manipulation

1. Field evaporation.

The mechanism is essentially same as that of FIM. A strong electric field (on the order of volts/0.1 nm) is applied between the gap. An adsorbed atom/molecule or substrate atoms are polarized and are ionized by charge transfer. Finally, these ions are accelerated by Coulomb repulsion to evaporate from the surface(Fig.1.8(a))[29][30].

2. Field assisted diffusion.

A electric field applied between the gap induces electrostatic polarization of both tip and adsorbed atom/molecule(s)(Fig.1.8(b)). Then, an attractive interaction between tip and molecule occurs. This attractive force is not strong enough to move molecule from the substrate to tip. However, this may be strong enough for dragging it by the tip in the surface plane [28][31].

3. Field-induced diffusion.

An electric field applied between the gap impose its potential upon the diffusion potential for adsorbed atom/molecule(s). If gradient of the added potential is steep than that of corrugation of surface diffusion, the atom/molecule(s) can diffuse (Fig.1.8(c)) [32].

(II) Current related manipulation

1. Localized heating.

The energy of product of tunneling current and bias voltage will excite phonon. When current is too large, atom/molecule(s) in the current path will gain thermal energy to diffuse(Fig.1.8(d)).[33].

2. Electron stimulated desorption.

Electrons with high energy can break chemical bonds in adsorbed atom/molecules, causing ionized or radical atom/molecules to be ejected from the surface(Fig.1.8(e))[34]. This occurs at positively biased electrode into where accelerated electrons impinge.

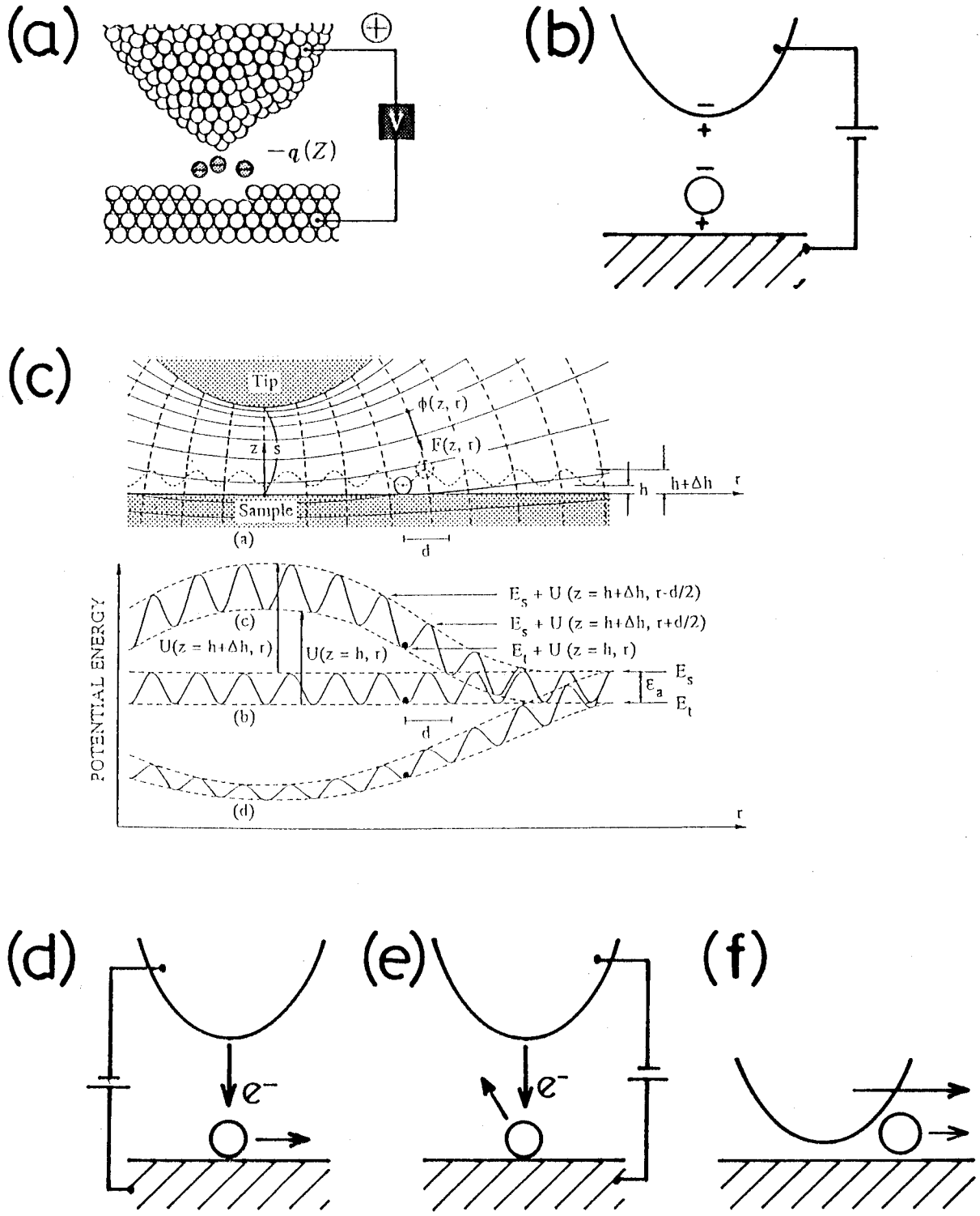

Fig1.8 The typical mechanisms for molecular manipulation by STM. (a) Field evaporation, (b)Field assisted diffusion, (c) Field-induced diffusion(from Ref[32]), (d)Localized heating, (e)Electron stimulated desorption and (f)Van der Waals repulsive force.

(III) Tip-sample proximity related manipulation

1. Van der Waals repulsive force.

Van der Waals repulsive force is responsible for the prevention of the complete collapse of matter to nuclear densities. This force emerges when the tip-sample distance is reduced(Fig1.8(f))[35].

Above literatures indicate that atom/molecule manipulation is not just imagination. The problem is that there have been no report on the manipulation of DNA related molecules at atomic/molecular level. This is, doubtlessly, partly due to the lack of reliable sample preparation, that is, substrate surface and deposition method, as already mentioned earlier.

Chapter 2

Scanning Tunneling Microscopy

2.1 Introduction

As already briefly explained in chapter 1.1, the principle of STM is surprisingly simple. In fact, before Binnig and Rohrer invented it, Young et.al., NBS in USA had invented an instrument, referred to the "topographiner" that had a design feature conceptually identical to the STM. They, however, managed to obtain a resolution of a few tens of nanometers. In other words, so called atomic resolution was not achieved. One of the reason for their low resolution was the ***noise*** they encountered both from *mechanical vibrations* and *the electronics*.

In order to achieve atomic resolution, both vibrational isolation and electronic noise reduction are essential.

This chapter consists of two sections.

(1) 2.2 STM design and instrumentation

In this section, basic physical principles of STM and required modification to improve accuracy and reproducibility of both STM and related ultra-high vacuum system are shown.

(1) 2.3 Modes of operation by STM

In this section, two modes of the STM operation are shown.

One is the constant current imaging mode. The other is the apparent tunneling barrier height mode.

2.2 STM design and instrumentation

Overview(physical principle)

As shown in Figure 2.1, the principles of STM are rather simple.
A conducting(metallic) tip mounted on a piezoelectric transducer is located very close(~1nm) to the source of the sample to be studied. A bias voltage, applied between the tip and the sample, causes a tunneling current. Such a current is a quantum-mechanical phenomenon which decides essential imaging mechanism. The imaging mechanism have already been discussed in chapter 1.3.2.

The tunneling current is amplified by the current amplifier to become a voltage, which is compared with a reference voltage. The difference is then amplified and passed through certain filter circuit again to drive the z piezo. The phase of the amplifier is chosen to provide negative feedback:
If the tunneling current is larger than the reference value, then the voltage applied to the z piezo tends to withdraw the tip from the sample surface, and vice versa. Therefore, an equilibrium a position is established through the feed back loop. As the scan over the xy plane, a two-dimensional array of equilibrium z positions, representing a contour plot of the equal tunneling-current surface, is obtained and stored.

The contour plot is displayed on a computer screen, typically as a gray-scale image. The image is similar to a black-and-white television picture. The bright spots represent high z values(protrusions), and the dark spots represent low z values(depressions). This mode of STM operation is called "The constant currant imaging mode."

STM systems

A system of STM consists of the mechanical part, "STM head", the controlling electronics and the computer for data acquisition automation. In the present experiment, a commercial STM system was installed in a vacuum system, as shown in Fig.2.2. It was, however, difficult to obtain reliable STM images with atomic resolution in reproducible and efficient manner without extensive modification of both commercial STM and UHV system, as shown in Fig.2.2.

For the present experiments, I have extensively modified and developed the apparatus as follows.

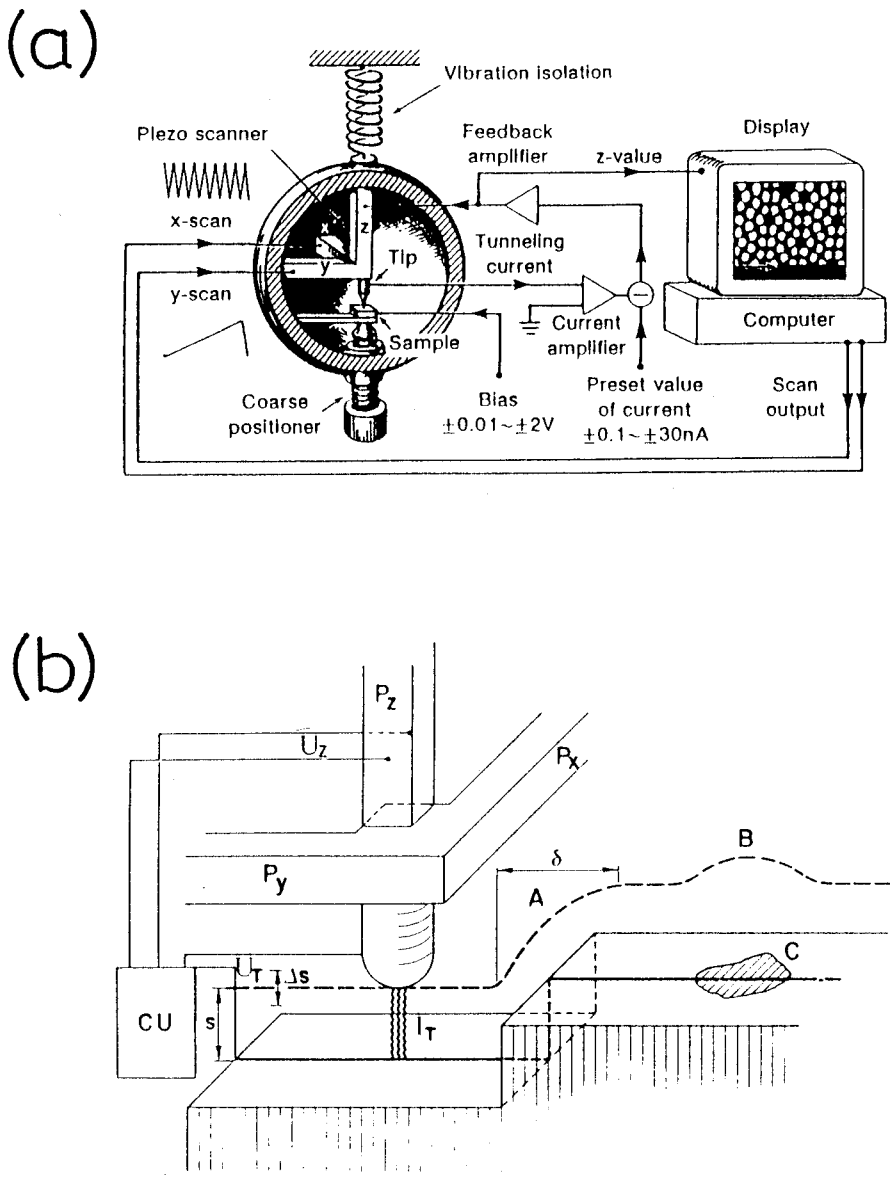

Fig. 2.1 Schematic diagrams of the scanning tunneling microscope. (a) from Ref. [2]. (b) from Ref.[1].

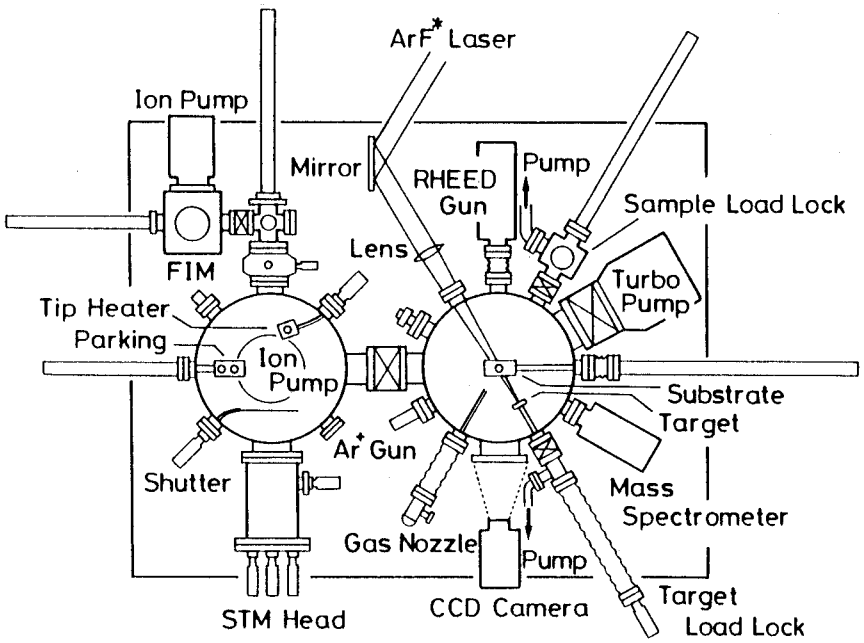

Fig.2.2 Schematic illustration of the UHV-STM system.

(1) Sample holder

With the sample holder that came with commercial STM, a sample(typically a piece of plate-shaped single crystal) is holed onto by tightening screws (see Fig.2.3(a)). This often results in a crack of the sample in annealing process due to thermal expansion and in loosening at transferring operation because its design allows direct mechanical impact through the screw and/or friction to the screw to either tighten or loosen.

As a sophisticated alternative design, instead of above awkward sample holder, following design was invented, as shown in Fig.2.3(b). The new one needs no screw but tiny pieces of springs which are made of a folded Ta sheet($1.5 \times 40 \times 0.15 mm^3$). The Mo "caisson" , the block support has a rectangular gutter in the side in which sample and

holding Ta spring are inserted. This spring design can give an appropriate holding tension with less effort. Moreover, the thermal expansion at annealing is absorbed by this elastic spring. Since the rigid Mo casinos protect sample from mechanical shockhazard, the possibility to damage sample at transferring operation is substantially reduced.

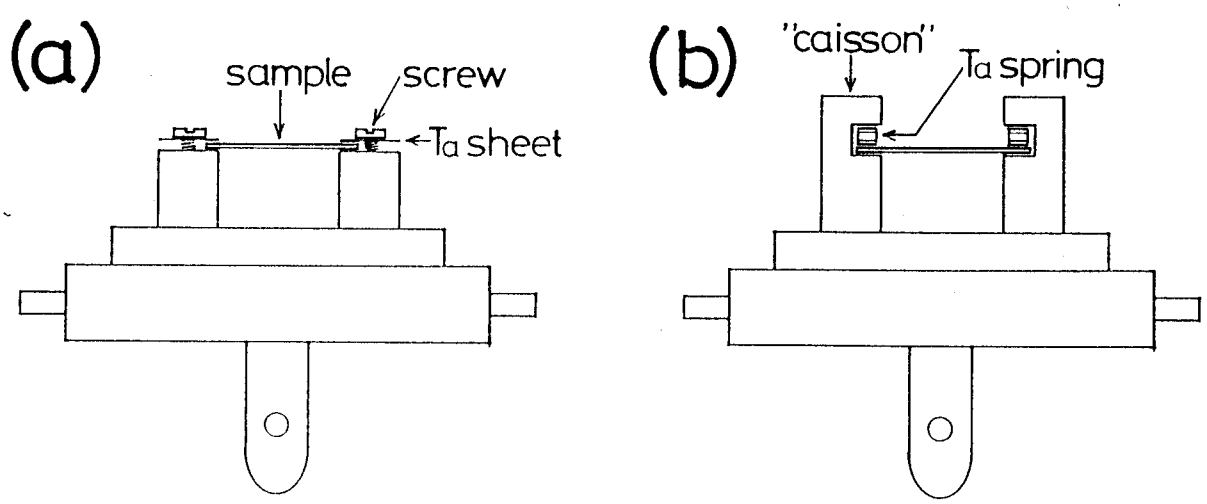

Fig.2.3 Side view of (a) delivered and (b) invented sample holders.

(2) Vibration isolation

Effective vibration isolation is one of the critical elements in achieving atomic resolution by STM. The typical corrugation amplitude for STM images is about 0.01 nm. Therefore, the disturbance from external vibration must be reduced to less than 0.001 nm.

To date, vibration system based on suspension spring with eddy-current damping is probably the most efficient one. Its basic concept is following:

The frame for the instrument always has vibrations transmitted from the ground an the air. The vibrations have frequency contents(from DC to ultrasonic region). The suspension consist of spring and massive frame on which STM is mounted. The suspension behaves as so called a low pass filter(high cut filter) with a resonant

frequency. The vibrations of the frequency much higher than resonant frequency of the suspension system, are reduced. The vibrations of the frequency much lower than the resonant frequency for the STM system of sample and tip, including piezoelectric scanner, will not disturb the STM. Therefore, to reduce vibrations, the resonant frequency of the suspension system must be lower and that of the STM must be higher.

When a conductor moves in a magnetic field, damping forces are generated by eddy currents induced in the conductor. The magnetic damper, with its reliability and thermal stability, has been utilized in various branches of engineering. Our STM originally has only suspension spring system without damping system when it was delivered. This often results in accumulation of vibrational energy of relatively low frequency(few Hz), which is the resonant frequency of the suspension system. It is hard to eliminate the vibration without damping system. The vibration always appeared as a modulation with an amplitude of 0.1nm in the STM images! In order to suppress the resonance of the suspension system, I have attached eddy-current damping and this has been proven to be effective. The modification was quite simple. The installation was that placing 4 pieces of Co_5Sm magnets($5x10x20mm^3$) on the bottom of the suspension system and Cu block($10x40x100mm^3$) just below them, as shown in Fig.2.4. The adjustment required was setting the magnets to Cu block at the distance of approximately 2mm, so that they will not contact each other.

After this modification, the noise from vibration transmitted from the ground has become completely negligible.

As described above, the noise from the vibrations are sufficiently reduced. It is true, however, that the noise from electronics is still not negligible. Accordingly, I have modified electronic circuits as follows.

(3) Current amplifier

The tunneling current in STM is very small, typically from 1 pA to 10 nA. The current amplifier is thus an essential element of an STM, which amplifies the tiny tunneling current and converts it into a voltage. (strictly speaking, it is a transimpedence amplifier, because the output is voltage instead of current.) The performance of the

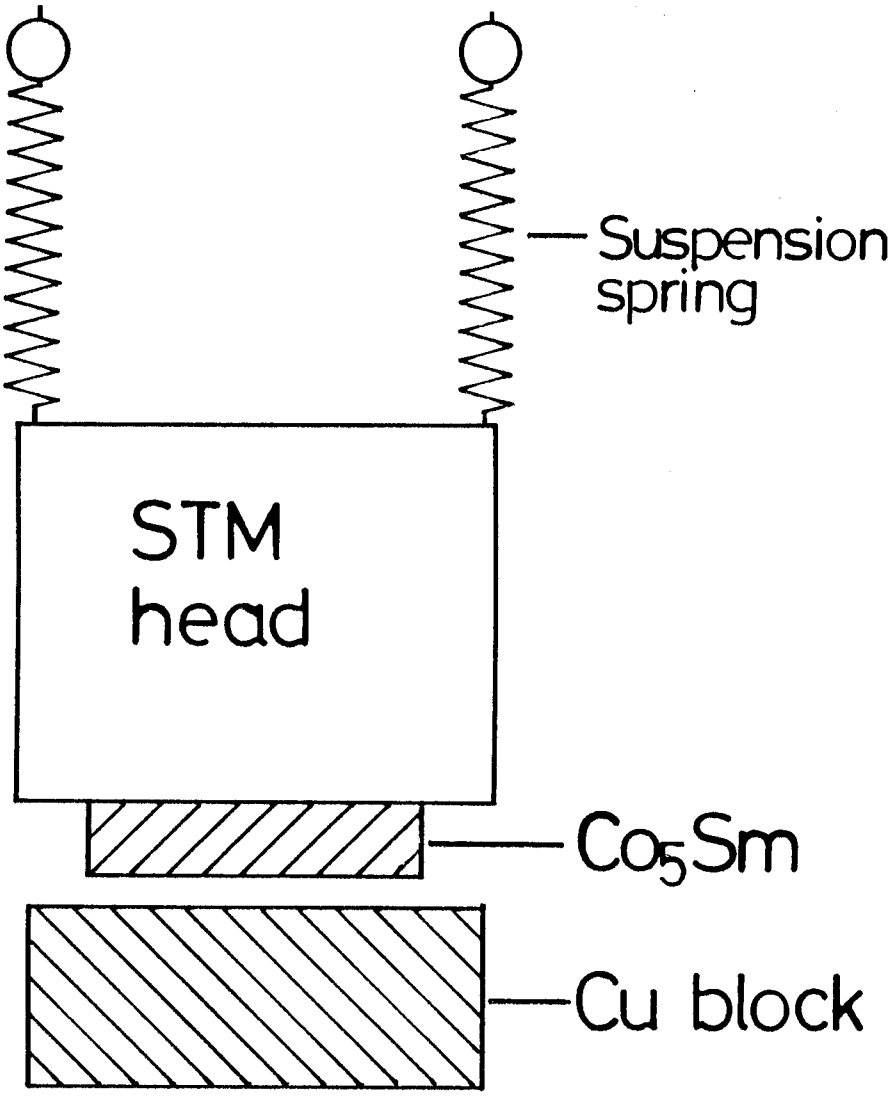

Fig.2.4. Schematic illustration of eddy-current damper system.

current amplifier, to a great extent, influences the performance of the STM. There are natural limits for the overall performance of current amplifiers, as determined by the thermal noise, stray capacitance, and the characteristics of the electronic components.

It is also important to minimize tunneling current when imaging insulative sample otherwise scanning process bring about an unwanted perturbation or modification upon the sample. Since the present study deals with insulative molecules, the improvement of the current amplifier is essential.

As a one of the solutions, I selected a commercial current amplifier(Keithley 428) for the use. This current amplifier can provide a current-to-voltage conversion ratio of 10^8V/A with frequency response of 7kHz(-6dB) that is much higher than the resonant frequency of the STM unit. Although the performance of this current amplifier(Keithley 428) is much better than that used in the purchased STM system, a drastic modification of the STM system has been done, including the removal of commercial current amplifier unit, spot-welding of coaxial cable between the piezoelectric unit and electric feedthrough, and reorganization of electronics circuit. After this modification, the tunneling current can be minimized by one order of magnitude with a better frequency response.

(4) Feedback circuit

The output of the logarithmic amplifier is compared with a reference voltage, which represents the set point of the tunneling current. The error signal is then sent to the feedback circuit, judicially designed amplifier, which sends a voltage to the z piezo. The phase of the collection of all the amplifiers is chosen to constitute a negative feedback: If the tunneling current is larger than the preset current, then the voltage applied to the z piezo tends to withdraw the tip from the sample surface, vice versa. Therefore, an equilibrium z position is established through the feedback loop. As the tip scans in the x direction, the contour height z also changes with time. The function of the feedback circuit is to make the tip accurately follow the constant tunneling current contour at the highest possible speed. The feedback circuit usually consists of a proportional(**P**) amplifier and analog integrator(**I**). These units (**P**,**I**) are well known in the familiar **PID** feedback loop system. To make the feedback circuit work at the best

performance (highest speed), the values of the P and I must be optimized.

The purchased STM in our laboratory, however was not designed to adjust these **P** and **I** values during experiments. This often caused instabilities of the feedback system or requirements of additional data acquisition time.

To improve controllability of the feedback system, I have modified the feedback electronic circuit, so that the **P** and **I** values can be optimized.

(5) Ground loops

When two or more electronic circuits and/or instruments are connected together, care must be taken to avoid unwanted signals caused by ground loops. Ground loops usually occur when a circuit(instrument) is connected to other circuit (instrument) with more than one signal return path such as power line ground. The resulting ground loop causes current to flow through the instrument ground signal leads and then back trough power line ground. This circulating current develops a small but undesirable voltage between the ground terminals of the two circuits. This voltage will be added to the signal voltage, appearing as a noise. If the current source is grounded, it may be necessary to isolate the device from power line ground.

As for the commercial STM used in the present study, the noise originated from ground loops was not negligible. The amplitude of the noise was typically 0.1 nm or larger in z scale in images. The reason of this noise(from ground loops) is clear, as described above. The only solution is to eliminating all the ground loops by isolating all the grounds of the circuit from the power line ground. Since the STM head unit(current source) is grounded, all the grounds except for the STM head were isolated from the power ground. This thorough modification has given successful improvement.

(6) Coarse positioner

An important elements of an STM is the coarse positioner, which moves the relative position of the tip versus the sample in steps exceeding the range of the piezodrive (typically a fraction of a micrometer). The step sizes for this movement have to be smaller than the total range of the z piezodrive for the tip in order to avoid accidental contact between tip and sample during the approach. One of the most

simplest coarse positioners is realized using the devices, conventional rotary feedthrough and a fine-pitch screw.

Although the commercial STM in our laboratory was equipped with a coarse positioner consisting of rotary feedthrough and a fine-pitch screw, there were two parts to be improved. One was the rotary feedthrough whose coupling mechanism was "bellow" type. It turned out that this type of rotary feedthrough loses smooth response or become choppy in movement in the course of operation, specially by small recursive motion. Because a small recursive motion makes the bellows accumulate the local distortion and stiff to require much more force to transmit the motion. This means that the steps of coarse positioner tend to change into much larger than the total range of the z piezo drive. In this case, the contact between tip and sample is inevitable.

The solution is, however, essentially quite simple. The below-type rotary feedthrough was replaced with a "magnetically coupled" one, that was done in the present studsy.

The other problem was that the coarse positioner system was not designed to perform so called "automatic approaching". Actually the approaching was performed by just approaching continuously the tip to the sample using a DC motor until tunneling current is detected. This approaching procedure does not always lead to the coarse positioning without contact, because it needs finite time(approximately a few milliseconds) for the tip(z piezo) to attain the equilibrium z point. In order to achieve reproducibly wholesome approaching, an automatic approaching system was developed. The process of is as follows:

1. Withdraw the z piezo to the limit.
2. Take one step forward with the coarse positioner(using Motor).
3. Move the tip forward.
4. If a tunneling current is detected, then stop. Otherwise repeat the loop.

After this development, an almost ideal approaching is routinely realized.

(7) Tip treatment and preparation

The importance of the tip treatment in STM was recognized by Binnig and Rohrer from the very beginning of their experiment. Because geometric and electronic

properties of the tip play a role equivalent to that of sample, as discussed in chapter 1.3.2. There are various experimental methods of tip preparation and treatment. It is, however, true that little characterization of the tip has been carried out. This is mainly due to the lack of a suitable technique except for field ion microscopy, which enables one to observe the apex of a metallic needle(tip) with atomic resolution. Few of other reasons may be as follow:

(1) Atomic resolution might happen spontaneously by repeated tunneling and scanning for an unpredictable time duration.

(2) A STM tip provided atomic resolution often looks blunt under scanning electron microscope(SEM).

(3) A STM tip looks perfectly sharp under SEM, would not provide atomic resolution.

(4) A tip mechanically cut(with a nipper) out from a Pt-Ir wire often works even if it looks like blunt under SEM or optical magnifier(lupe).

Therefore, there appears no reliable and reproducible method of tip treatment. Tip treatment and characterization is one of the central experimental problems in STM. A lot more development and understanding should be achieved.

In spite of the lack of reliable and reproducible tip treatment, STM experiment does demand a tip. A simple and easy method developed in the present study is described in the following:

The developed method is based on the dc "dropoff" method. This art of making tips using electrochemical etching is developed in the 1950s for preparing samples for FIM. The basic setup is shown in Fig.2.5. It consist of a beaker containing an electrolyte of 1M aqueous solution of KOH. A piece of W wire whose one of the end is covered with insulative material, typically a glue made of rubber, is placed near the center of the beaker. The height of the W wire relative to the surface of the electrolyte can then be adjusted, so that only the interface between the W and insulative coat is wet. The counter electrode is a piece of stainless steel, carbon rod or platinum placed in the beaker. An ac voltage stepped down through a variable transformer(slidac), 2 Vrms to 20 Vrms, is applied to the electrodes. (It works with a dc voltage also.) Etching occurs at the W-electrolyte interface. When the neck of the wire near the interface becomes thin enough,

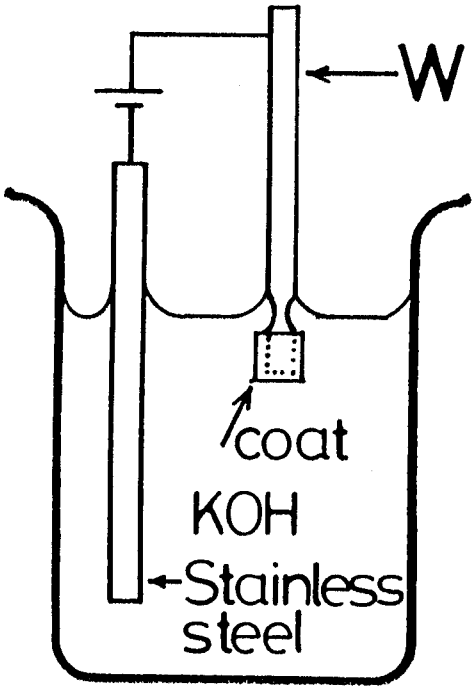

Fig.2.5 Electrochemical etching of tungsten tips.

the weight of the wire in electrolyte fractures the neck. The lower half of the wire drops off. The sudden rapture leaves a ragged edge of work hardened asperities at the very end of the tip. To remove the residual KOH from the tip surface, a thorough rinsing with distilled water and pure alcohol is necessary.

(8) Scanning tunneling spectroscopy (I-V measurement)

By interrupting the feedback loop and keeping the tunneling gap constant and applying a voltage ramp on the tunneling junction, the tunneling current as a function of bias provides information that is the convolution of the tip density of states(DOS) and sample DOS (see Eq.(1.4)).

Although the commercial STM in our laboratory was equipped with a sample-and-hold circuit in the feedback system and computer software to sweep the bias voltage, the STS design was of fatal imperfections. One of them was that the time profile of the STS bias voltage had precipitous changes($dV/dT \sim \infty$), which cause undesirable and destructive damages to the sample-tip system, as indicated by arrows in Fig.2.6(a). After making the STS bias to sweep gently, the STS can be measured in an indestructive and reproducible manner (Fig.2.6(b))[36].

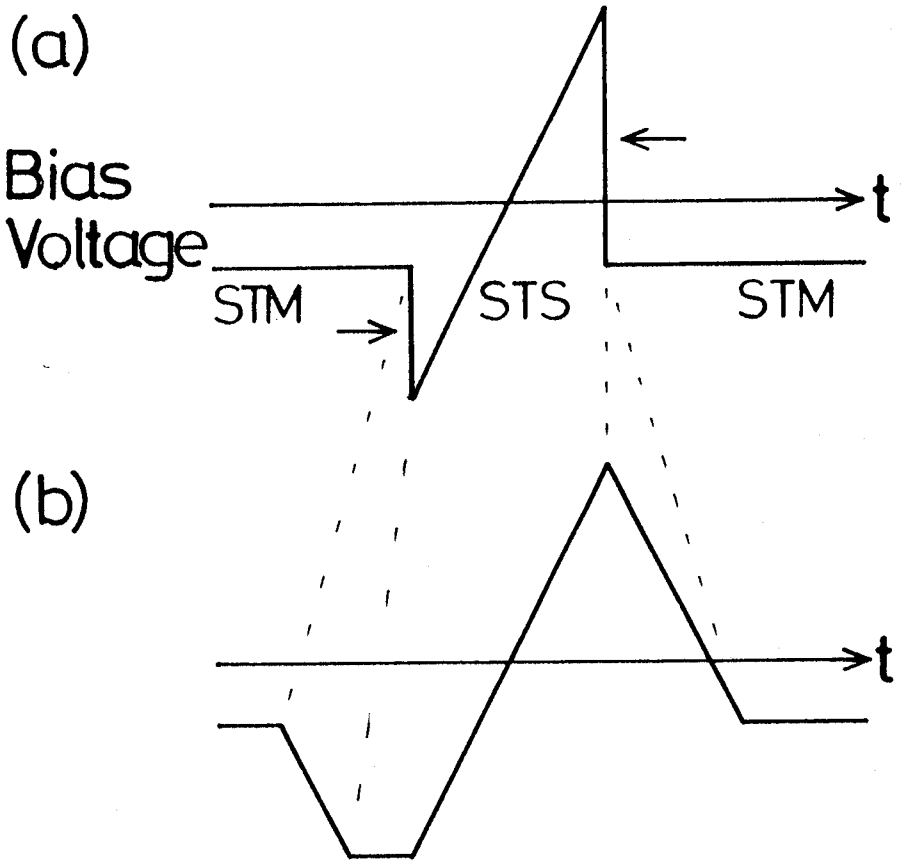

Fig.2.6 Timing chart of STS bias voltage. (a) before and (b) after modification.

(9) Apparent local tunneling barrier height(*I-s* measurement)

In this section experimental detail is mainly described. The theoretical detail is described in section 1.3.2 and 2.3. In short, this is based on the exponential decaying wavefunction in the barrier region.

The commercial STM in our laboratory is not designed to measure the tunneling current versus the tip-sample distance (*I-s*) curve. To make the STM measure *I-s* curve with a minimum modification, the bias sweep logic of the STS circuit is used. Actually, the electronic circuit was modified, so that in STS measurement, the tip distance is varied by the voltage generated from the STS circuit instead the bias voltage. Therefore, an *I-s* curves can be obtained with the STM.

2.3 Topographic imaging by STM

There are various modes of operation of an STM. To reduce the volume, only two modes of operation of an STM and the information which can be extracted are described in this section. One is constant current imaging mode, and the other is apparent local tunneling barrier height mode. Because, the only two are performed in the present study.

(1) Constant current imaging

As already described in section 2.2, a feedback loop adjusts the height of the tip and the sample is kept constant. The height (z) adjustment is performed by applying an appropriate voltage Uz to the z piezoelectric drive while the lateral tip position (x,y) is determined by the corresponding voltages Ux and Uy applied to the x and y piezoelectric drives. Therefore, the recorded signal Uz(Ux,Uy) can be translated into the 'topography' $z(x,y)$.

The principle of this mode sounds rather simple. However, the interpretation of the obtained contour map $z(x,y)$ is not at all trivial, as described in section 1.3.2.

(2) Apparent local tunneling barrier height

As already described in section 1.3.2, the tunneling current I in STM depends exponentially on the tip-surface separation s:

$$I \propto \exp(-2\ \kappa\ s)$$

with a decay rate k is given by

$$\kappa = (2m\ \phi)^{1/2}/h$$

where f is an effective local potential barrier height.

From above equation, an apparent local barrier height in STM is defined by

$$\phi_A\,[\mathrm{eV}] = (h^2/8\mathrm{m})(\mathrm{d}\ln I/\mathrm{d}s)^2 \sim 0.95(\mathrm{d}\ln I/\mathrm{d}s[0.1\mathrm{nm}])^2$$

Experimentally, this quantity can be conveniently measured by varying the tip-sample distance through the z piezo at constant bias voltage.

Chapter 3

The DNA Base Molecules on Reduced $SrTiO_3(100)$: STM Imaging and Discrimination of Bases

3.1 Introduction

To differentiate chemical species using STM, the first step requires preparation of an atomically flat solid surface covered with molecules to be investigated. The difficulties are obtaining such surface and deposition of molecules in reproducible and reliable manners. The author constructed a UHV-STM system which enables various sample treatment for the preparation of an well-defined clean surface and deposition of the DNA base molecules under UHV conditions. In the present work, distinct imaging of the DNA base molecules was accomplished which indicate possibility of the DNA sequencing by means of STM. For the DNA base molecules, this attempt is the first experimental challenge for UHV-STM imaging of isolated bases and demonstration of discrimination of co-adsorbed different bases.

3.2 Experimental

Sample preparation

The substrates for the deposition of the bases were prepared as follows. Polished, (100)-oriented, plate-shaped crystals of $SrTiO_3$ were purchased from Earth-Jewelry Co. (Japan). The $SrTiO_3$ crystal was clamped onto a Si heater mounted on a holder made of Ta. The substrate was degassed at 1000℃ for 30 minutes in the preparation chamber and further annealed at 1200℃ for 1 minute in the STM chamber. After the anneal, the sample was transferred to the STM head. It was routinely possible to obtain atomic

resolution STM images of the substrate within 3 hours after the anneal[12]. The XYZ-scale was calibrated by imaging a Si(111)-7×7 surface.

Deposition process

The DNA base molecules, adenine, thymine, guanine and cytosine are planar molecules with the dimensions(skeleton sizes) 0.45 nm for adenine and guanine and 0.25 nm for thymine and cytosine, as shown in Figure 3-1. They were crystalline Sigma Graded bases and purified by sublimation in vacuum in the UHV chamber. The purified nucleic acid base was loaded into an electrically heated Ta source cell holder to bring about the deposition. After introduction into the preparation chamber, the cell holder was degassed for 30 minutes prior to the deposition process in the STM chamber. Deposition of more than one molecular species was performed by repeated deposition of each base using the same procedure as described above. The evaporated species were examined by mass spectroscopy. This revealed that isolated molecules are evaporated from the cell and deposition of intact single molecules is possible.

3.3 Results and discussion

3.3.1 Images

Reduced $SrTiO_3$(100) clean surface

Fig.3-2 (a) and (b) show 44 nm by 40 nm by 1.0 nm(x,y,z) STM images of the reduced $SrTiO_3$(100) clean surface obtained (a) before and (b) after the deposition of adenine. The crystal structure of $SrTiO_3$ is a perovskite structure with a lattice constant of 0.391nm. In Fig.3-2(a), small bright features are observed on the surface domain boundaries and also on the flat domains. They are considered to be Sr and/or SrO which have not been evaporated from the surface during annealing process even at higher temperatures. The surface has ordered oxygen vacancy of $\sqrt{5}\times\sqrt{5}$-R$\pm$26.6° superstructures which appear as bright spots of square lattices in the image. A domain boundary intersects neighboring domains which have a different phase of super structure (translational mismatch of square lattices) and/or slanting angle(+53° or -53°) each other[12].

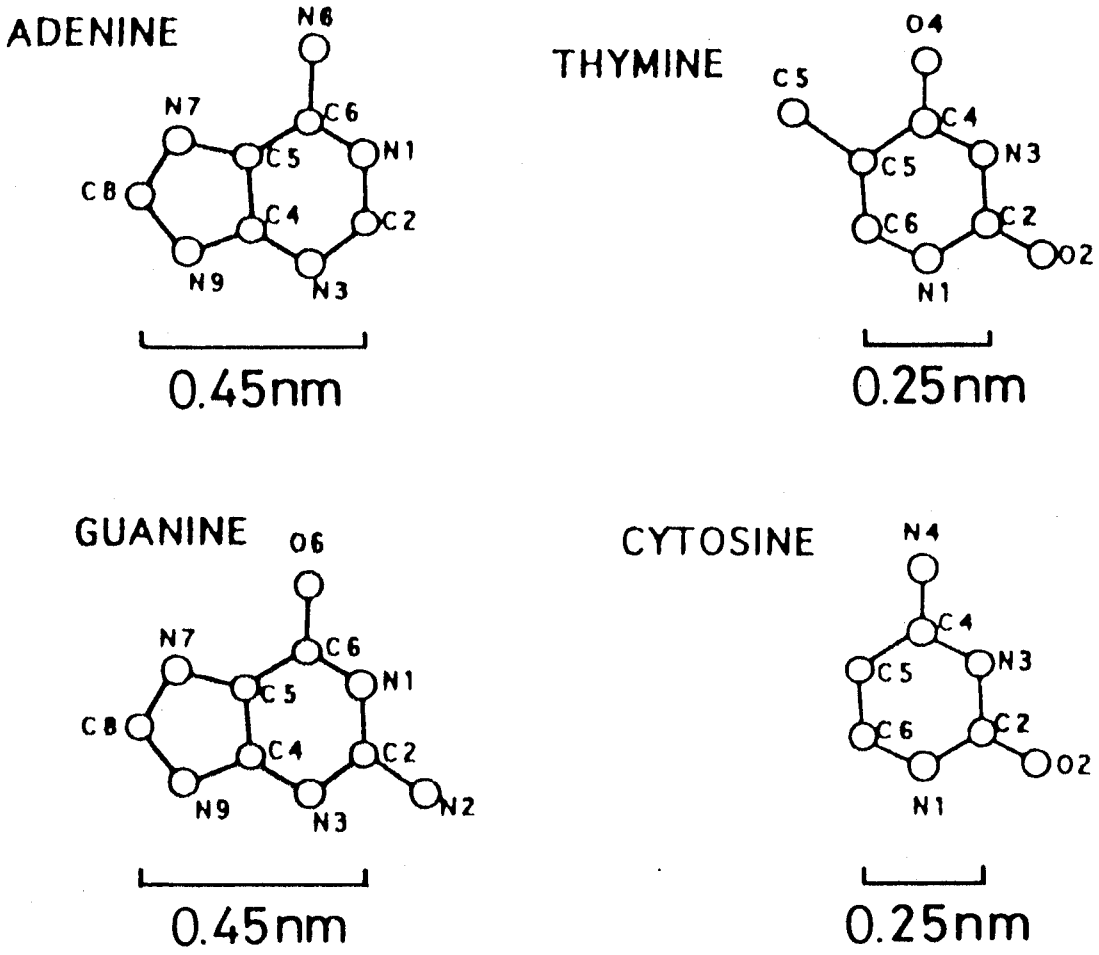

Fig. 3-1 Molecular structures of (a) adenine, (b) thymine, (c) guanine, and (d) cytosine with atomic labeling convention and with scales.

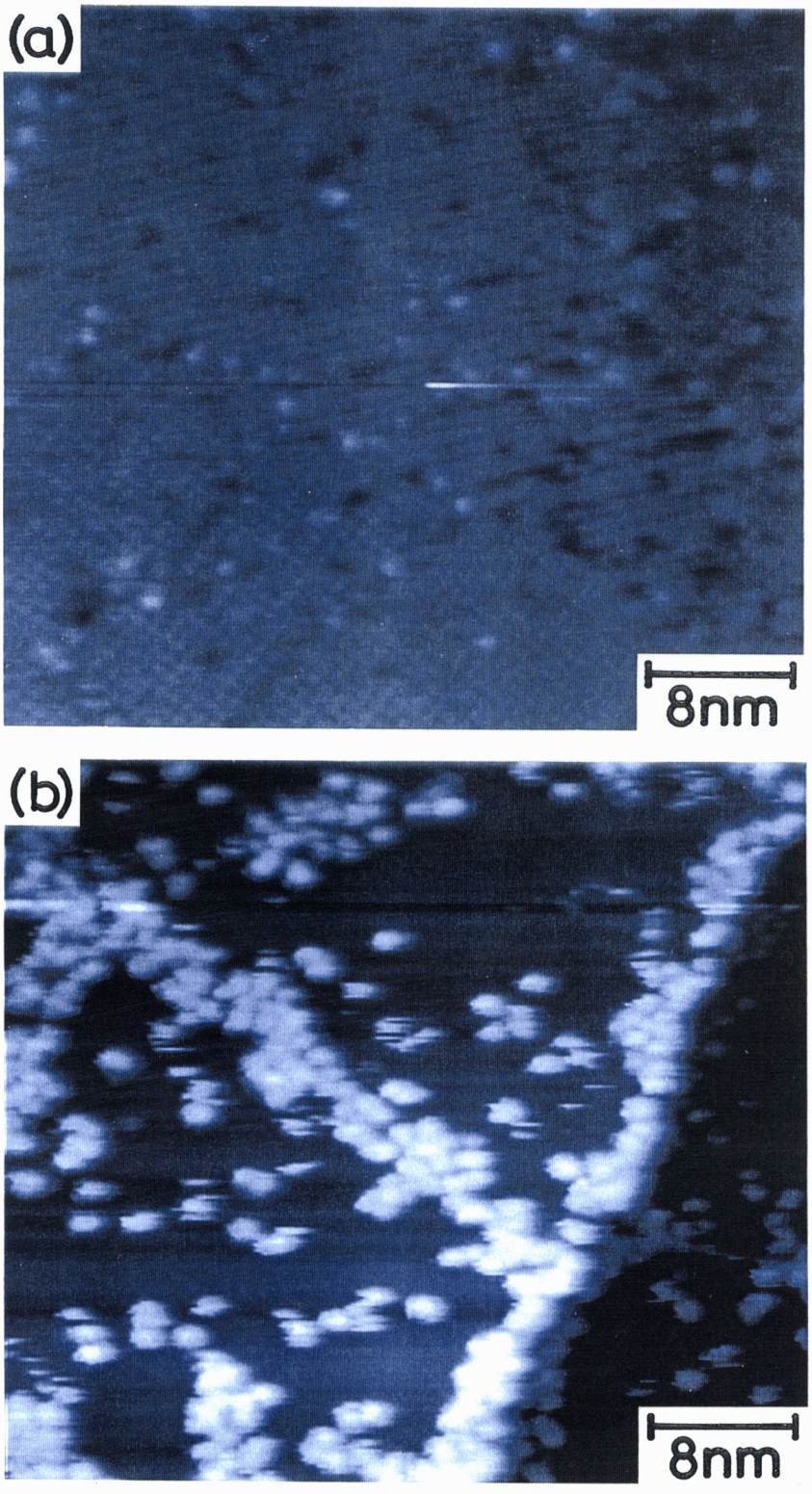

Fig. 3-2 Constant current STM image (44 nm by 40 nm by 1.0 nm(x,y,z)) of a reduced $SrTiO_3$ clean surface obtained (a) before and (b) after deposition of adenine(~0.2 monolayer). The crystal structure of $SrTiO_3$ is a perovskite structure with a lattice constant of 0.391 nm. (a) This image was obtained with a sample bias of -1.5 V and tunneling current of 0.2 nA. (b) This image was obtained with a sample bias of -3 V and tunneling current of 0.2 nA.

Adenine

Upon deposition (~0.2 monolayer) of adenine on the substrate, many round protrusions which are not observed before the deposition appear, as shown in Fig.3-2(b). This image shows that adenine molecules are deposited on the substrate and were observed by STM. There is a possibility that adsorption of adenine monomers on the domain boundaries change their structure. However, in the experiments, remarkable difference such as change of height or shape has not been recognized, though isolated adenine tend to have relatively large lateral dimensions. I consider that their structural changes would be trivial to be ignored. Note that adenine is evaporated in a molecular form to be deposited as individual adsorbed molecules on the surfaces as mentioned in the experimental section.

Fig. 3-3 (a) shows a higher magnification (22 nm by 21 nm by 0.8 nm(x,y,z)) STM image of adenine molecules with coverage of 0.2 monolayer deposited on the $SrTiO_3$ substrate. A cross section of Fig. 3-3 (a) is presented in Fig. 3-3 (b). The adsorbed adenine molecules appear to have a round shape. In addition, noisy lines of molecules are in the image. These lines imply some of the molecules are mobile on the surface. The literatures on adenine adsorbed on KBr(100) by infrared absorption studies[37], benzene on Pt(111) by STM[38], azulene on Pt(111) by STM[39], and so on, indicate that the molecules of π system lie flat on the surfaces. In our result, the image indicates that individual monomers are resolved as round shape with the fairly uniform height. Thus, I assume that the adenine adsorbates also lie flat on the $SrTiO_3$(100) surface. The typical heights and lateral dimensions of the adenine adsorbates in the image are 0.50 ± 0.05 nm and 1.4 ± 0.6 nm, respectively. These values are larger than expected based on the size of the molecules. For example, the lateral dimensions are about three times larger than the molecular dimension of 0.45 nm.

Manipulation

The observation of the mobile molecules is important in terms of adsorbate manipulation. In order to obtain further information about these molecules, a sequential STM image was recorded with various tunneling conditions. Fig. 3-4(a) and (b) show

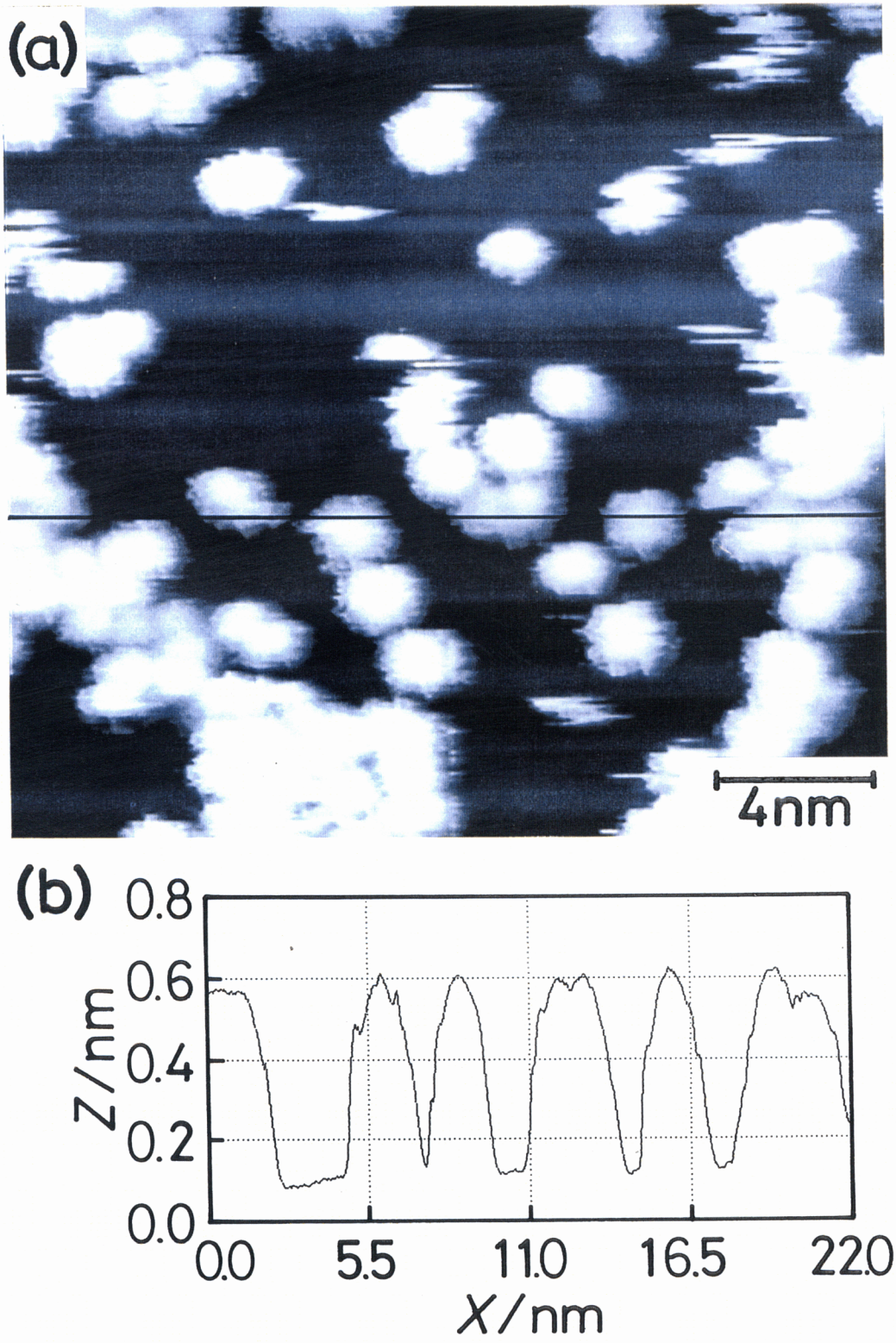

Fig. 3-3 (a) Constant current STM image (22 nm by 21 nm by 0.8 nm(x,y,z)) of adenine molecules, taken at sample bias of -3 V and tunneling current of 20 pA, adsorbed on a reduced $SrTiO_3$(100) clean surface by evaporation in UHV. (b) A cross section of (a). In this cross section, adenine adsorbates have the typical heights of 0.50 ± 0.05 nm and lateral dimensions of 1.4 ± 0.6 nm at sample bias voltage of -3V.

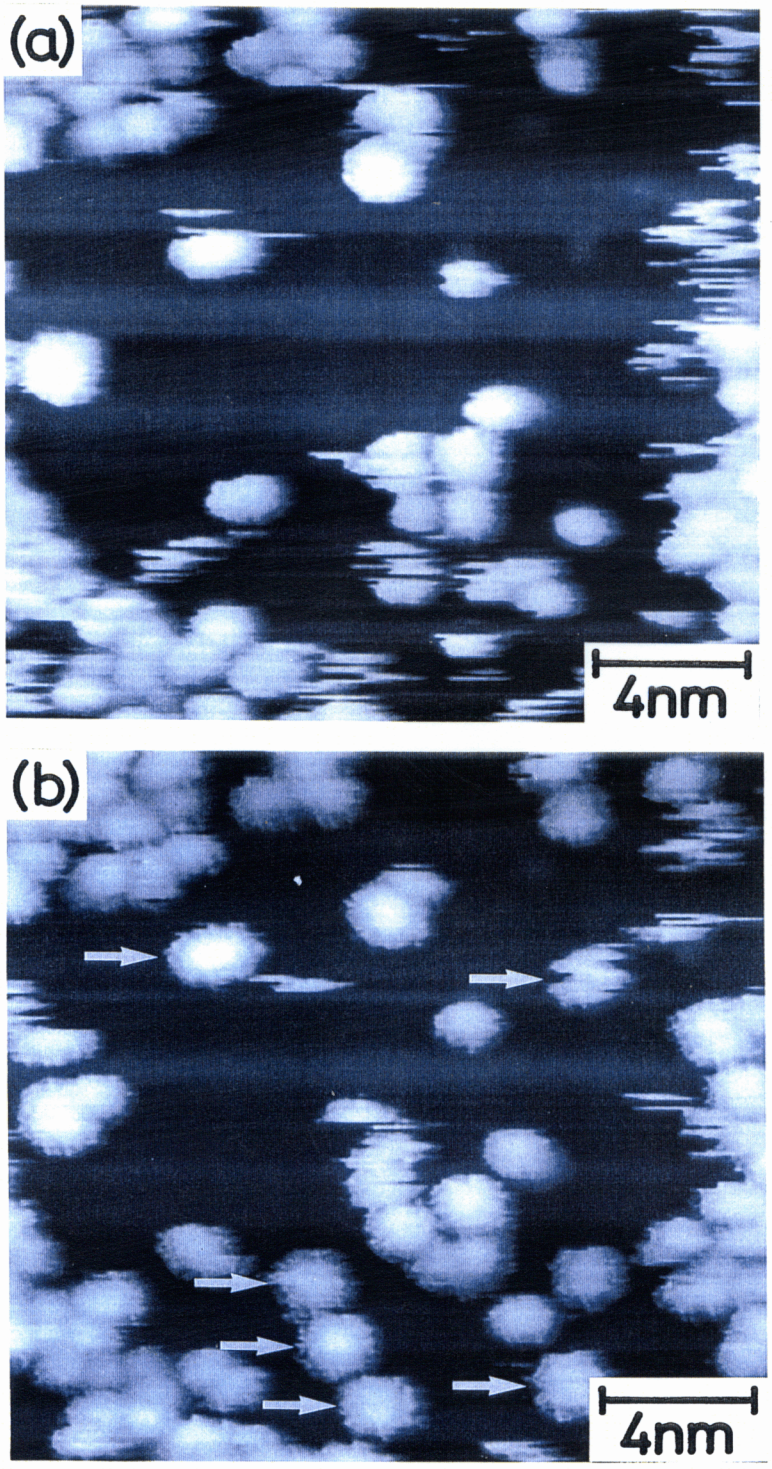

Fig. 3-4 Series of constant current images (20 nm by 19 nm by 1.0 nm(x,y,z)) of adenine adsorbed on a reduced $SrTiO_3$(100) clean surface. (a) The image was obtained with a sample bias of -3 V and tunneling current of 0.2 nA. (b) The image was obtained with a sample bias of -3 V and tunneling current of 20 pA. These two images show the identical area of the substrate. The arrows in (b) indicate some of the adenine molecules have changed their adsorption sites.

STM images of the identical area (20 nm by 19 nm by 1.0 nm(x,y,z)) of the adenine adsorbed on the substrate, taken with the same bias voltage of -3V and different tunneling current of (a) 0.2 nA and (b) 20 pA. In Fig.3-4(a)(0.2 nA), noisy lines were much observed in comparison to Fig.3-4(b)(20 pA). In addition, the distributions of the adenine adsorbates on the surface are different between Fig.3-4(a) and (b), as indicated by arrows in Fig.3-4(b). Although I can not determine the forces responsible for the sliding of the adenine molecules, it is revealed that adenine molecule can be slid by the STM tip scans under certain tunneling conditions.

Molecule-substrate interaction

As discussed above, some adenine molecules defuse over the surface within the period of taking a line of an image (0.2 s). The activation energy for surface diffusion is derived from an Arrhenius equation shown as (1.2). $t = t_0 \exp(E_{des}/kT)$

assuming $T = 300$ K, $t_0=10^{-13}$ s, $t = 0.2$ s, $k = 1.38\text{x}10^{-23}$ J/K ($= 8.62\text{x}10^{-5}$ eV/K), and

E_{dif} ~0.7 eV is estimated.

The adsorption energy is derived from the equation, assuming $T = 300$ K, $t_0=10^{-13}$ s,

t = 1 day (because molecules can be found within 1 day), $k = 1.38\text{x}10^{-23}$ J/K ($= 8.62\text{x}10^{-5}$ eV/K),

E_{des} ~1.0 eV is estimated.

This value is relatively weak for that expected for chemisorption (typically 2eV) and is however, much stronger than that for physisorption(typically 0.2 eV).

Thymine

The deposition of thymine was performed by the similar evaporation method as that of adenine. Fig. 3-5 (a) and (b) show the images with area of 20 nm by 20 nm by 0.8 nm(x,y,z) and a cross section of (a), respectively. The adsorbed thymine molecules also appear as round objects. Comparing thymine (Fig. 3-5) with adenine (Fig. 3-3), the heights and lateral dimensions of the thymine adsorbates are smaller than those of the adenine adsorbates. The typical heights and lateral dimensions for thymine are about 0.35 ± 0.05 nm and 0.8 ± 0.2 nm, respectively. I assume that these round shapes

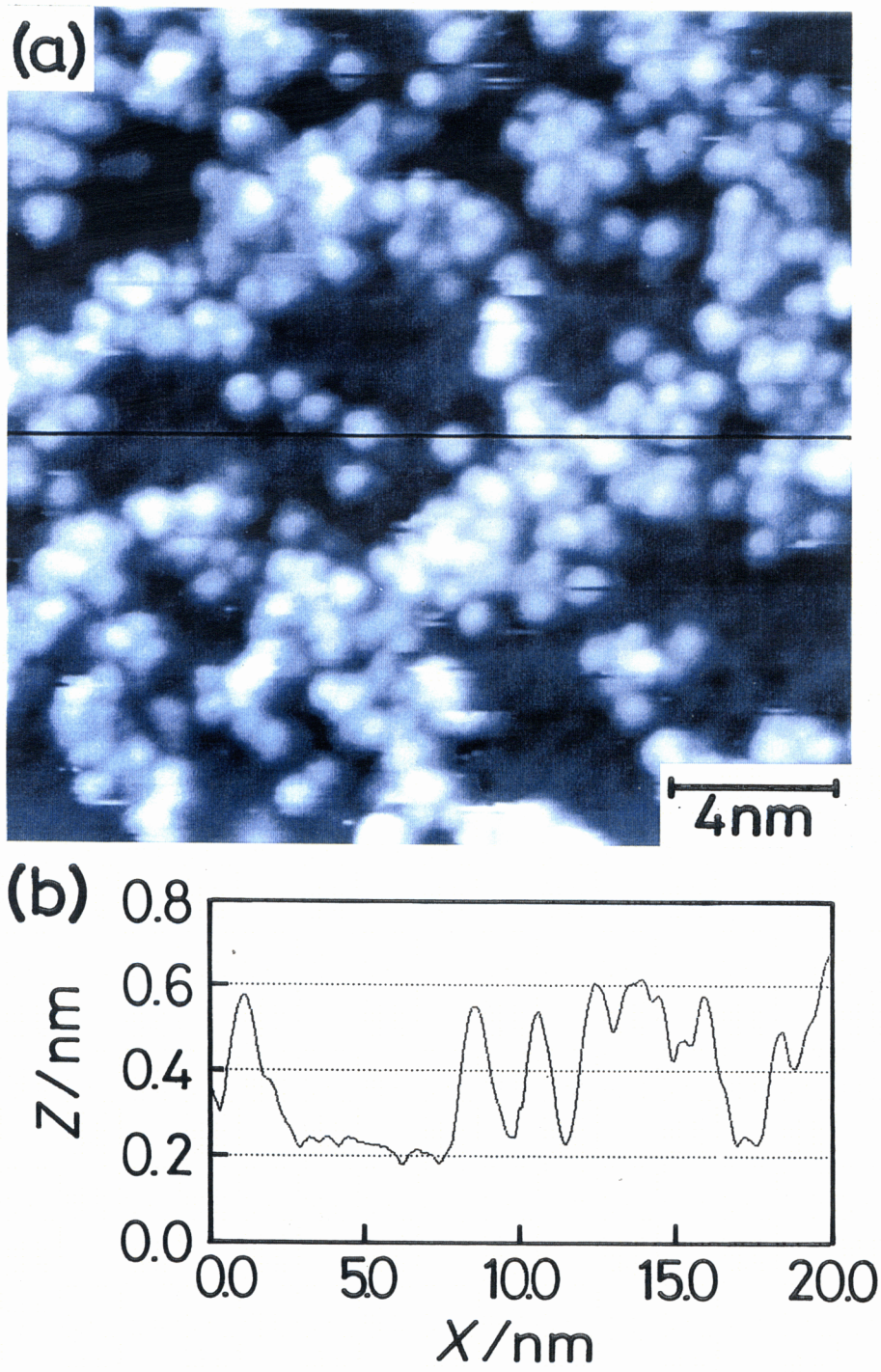

Fig. 3-5 (a) Constant current STM image (20 nm by 20 nm by 0.8 nm(x,y,z)) of thymine on a reduced $SrTiO_3$(100) clean surface, taken at sample bias of -3 V and tunneling current of 20 pA. (b) A cross section of (a). In this cross section, thymine adsorbates have the typical heights of 0.35 ± 0.05 nm and lateral dimensions of 0.8 ± 0.2 nm at sample bias voltage of -3 V.

represent individual thymine molecules, for the same reasons as discussed above for adenine. The most notable result is that the adenine and thymine can be differentiated by comparing the heights and the lateral dimensions in the STM.

Guanine and Cytosine

Guanine and cytosine were also deposited on the reduced $SrTiO_3(100)$ surfaces. By comparing the dimensions of both adsorbates, guanine and cytosine can be discriminated in the same way as adenine and thymine.

Tip dependence

I have measured and presented the typical heights and lateral dimensions for the bases. However these dimensions are the largest values measured and I have observed values down to half times smaller.

The large variation of these apparent dimensions may be explained as follows. The corrugation in STM images depends strongly on the convolution of the sample shape and the tip shape. Moreover, the tunneling conductance is a convoluted function of the relevant electronic states of both the sample and the tip. Considering these basic imaging mechanisms of STM, it is plausible that the tip condition, in particular with respect to atomic or molecular species at the apex of the tip and the corresponding differences in the electronic states form a major factor contributing to the variations in the observed dimensions.

Bias dependence

The bias dependence of the image of the bases is also of interest. Fig. 3-6 (a) and (b) show adenine images(18 nm by 18 nm by 0.8 nm(x,y,z)) taken at the sample bias of +2 V and +3 V, respectively. These images were obtained on the identical area of the substrate. In Fig. 3-6 (a)(+2) the adenine adsorbates appear as protrusions, while in Fig. 3-6 (b)(+3) the adenine adsorbates appear to be depressions rather than protrusions. This bias dependence suggests that the observed corrugations of the nucleic acid bases vary with the applied sample bias voltage and, that is, bias dependence may facilitate a reproducible distinction among

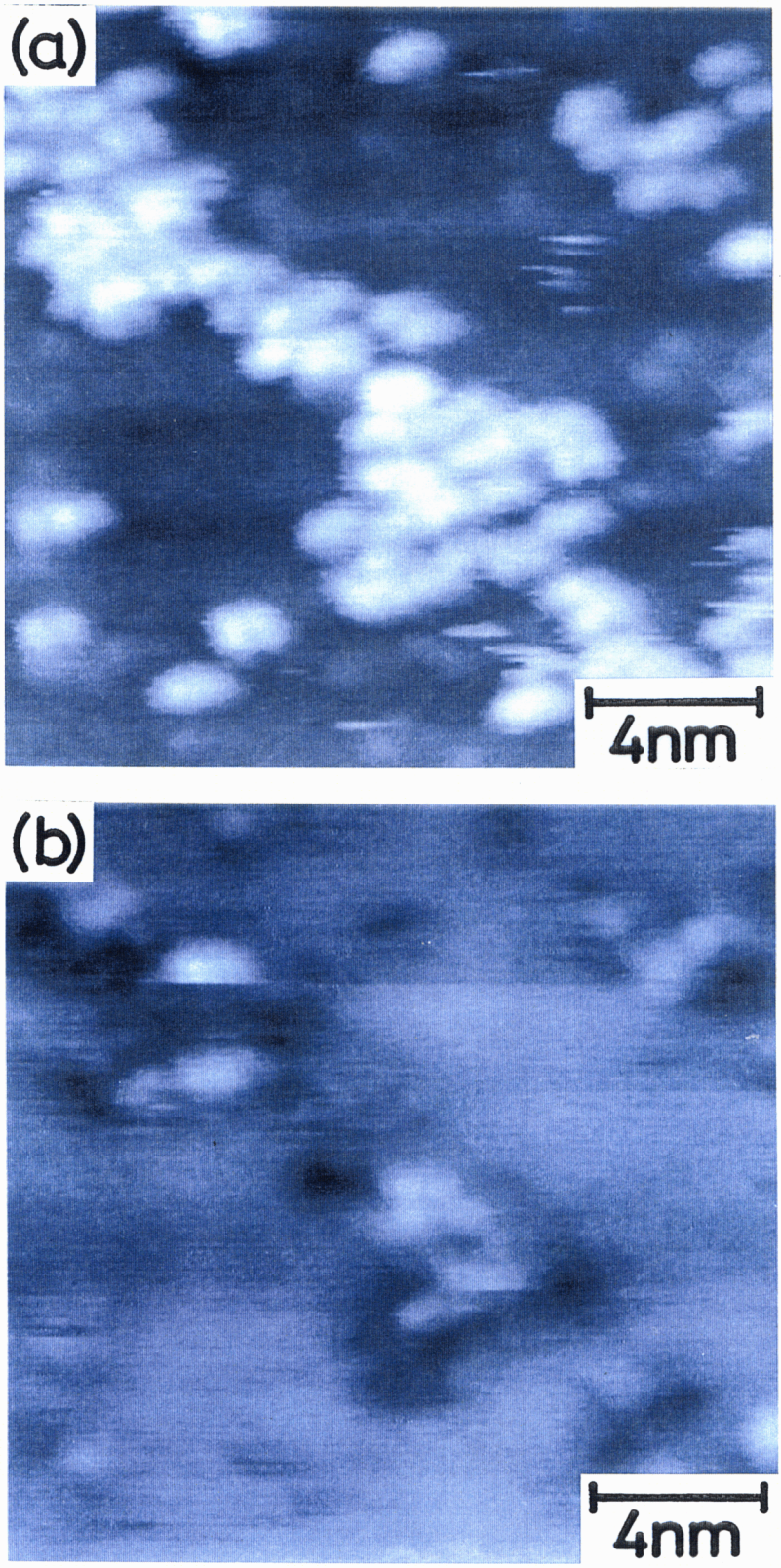

Fig. 3-6 This series of constant current STM images (18 nm by 18 nm by 0.8 nm(x,y,z)) show adenine molecules adsorbed on the identical area of the substrate. (a) This image was obtained with a sample bias of +2 V and tunneling current of 20 pA. (b) This image was obtained with a sample bias of +3 V and tunneling current of 20 pA. In (a) adenine adsorbates appear as protrusions, while in (b) adenine molecules appear as depressions rather than protrusions.

adenine, thymine, guanine, and cytosine. The results of the bias dependence of the four bases are summarized in the form of a height vs. bias voltage diagram, as shown in Fig. 3-7. Since the values strongly depend on tip conditions as described above, I tentatively employ "the moderate values" as the data for each base to reduce the tip effect. This diagram suggests that it is possible to discriminate between nucleic acid bases by means of STM imaging.

Differentiation

To examine the differentiation between similar sized molecules, a comparison was made between adenine and guanine, having the same molecular size. Adenine(as shown in Fig.3-3) appears brighter than guanine(as shown in Fig.3-8), because the heights for adenine and guanine are about 0.50 ± 0.05 nm and 0.24 ± 0.05 nm, respectively, at the bias voltage of -3V. Thus, the result indicates that adenine and guanine molecules having similar sizes and structures can be also distinguished from each other by comparing the heights in the STM images.

Discrimination of co-deposited adenine and thymine

To investigate the possibility of the discrimination in a direct manner, different molecular species were deposited on the same substrate. Fig.3-8 (a) shows image after the deposition of thymine (0.5 monolayer) on adenine (0.1 monolayer). Cross section of Fig. 3-9 (a) is presented in Fig. 3-8 (b). The larger and brighter dots correspond to adenine whereas the somewhat smaller and faint dots correspond to thymine, indicating that discrimination of DNA bases is possible using STM.

3.3.2 Electronic structure and imaging mechanism

The observed STM images of molecules appear as a round shape with dimensions of 0.3 nm (z) and 1 nm (*x*-*y*) that are much higher than expected values (typically 0.1-0.2 nm (z) and 0.5 -0.8 nm (*x*-*y*)). This result suggests that the molecular corrugations do not directly correspond to the molecules, especially molecular orbitals(MO) of the molecule, because MO of an asymmetric molecule should have an asymmetric distribution.

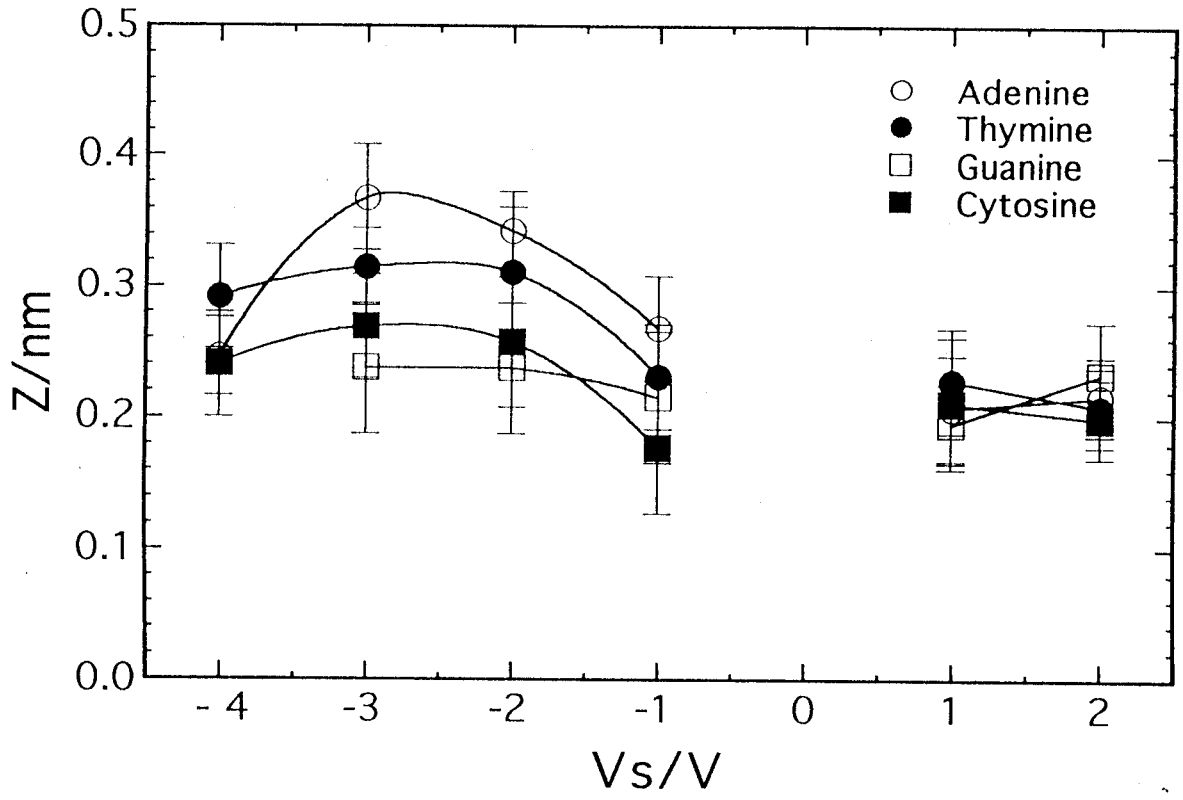

Fig. 3-7 Bias dependence of the four bases, plotted in the heights vs. sample bias voltages. The values strongly depend on tip conditions as described in the text. "The moderate values" are tentatively employed as the data for each base to reduce the tip effect.

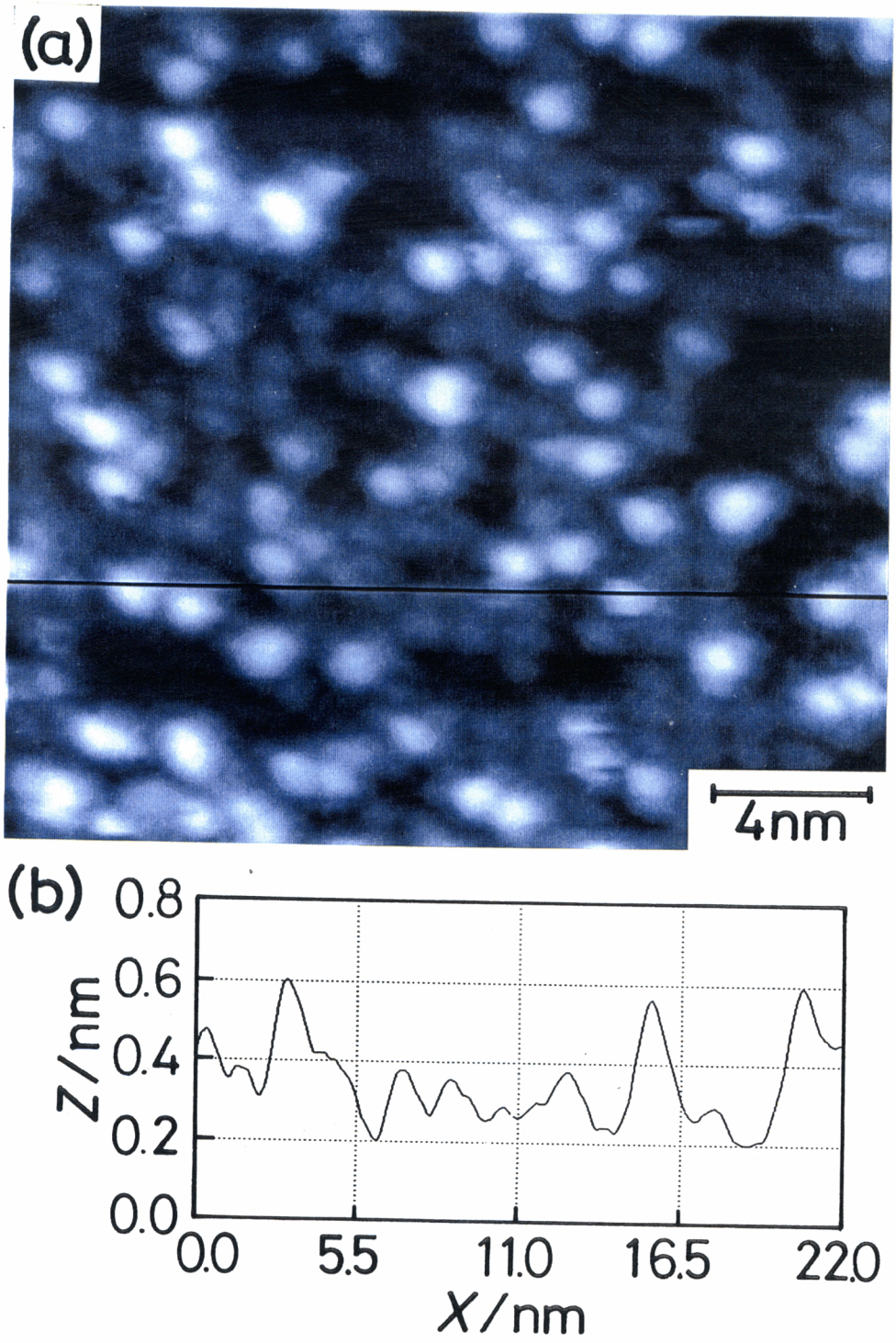

Fig. 3-8 (a) Constant current STM image (22 by 21 nm) taken after the deposition of thymine on adenine. (b) Cross sections of Fig. 3-9 (a). The image was acquired at sample bias of -3 V (tunneling current of 20 pA) to differentiate the adsorbed species.

Moreover the observed lateral dimensions are anomalously large. To understand the imaging mechanism for the base molecules on the $SrTiO_3(100)$ system, explanation of the apparent enlarged and round-shaped molecular image is mandatory.

The molecule-substrate interaction alters both the electronic states of adsorbed molecule and of underling substrate and effective tunneling barrier for electrons to tunnel through. Here in this section, possible origin of observed molecular corrugations are discussed, based on the equations of (1.1),(1.4) - (1.7).

Electronic structure of the $SrTiO_3(100)\sqrt{5}x\sqrt{5}$

The $SrTiO_3(100)$ substrate has a nature which is different from the other metal substrates that are used in conventional studies. The electronic conductivity originates from the oxygen vacancy that induces (Ti^{3+} + oxygen-vacancy) complex state near the E_f. STM image of clean surface maps surface O-vacancy of a $\sqrt{5}x\sqrt{5}$ periodicity (see Fig. 1.4.). Without oxygen-vacancy, STM imaging is impossible because $SrTiO_3(100)$ is an insulator with band gap of 3.2 eV.

The molecule-substrate interaction on the $SrTiO_3(100)\sqrt{5}x\sqrt{5}$

Although this $SrTiO_3(100)\sqrt{5}x\sqrt{5}$ surface has not been extensively investigated, the surface may be relatively inert, because the E_{des} for the oxygen molecule is estimated to be 0.9 eV[40]. This value is fairly small for oxygen. It should be mentioned that there is a well known general tendency of E_{des} for various molecule-solid surfaces[41]:

$$O_2 > HC{=}CH > H_2C{=}CH_2 > CO > H_2 > CO_2 > N_2.$$

In fact the E_{des} ~ 1 eV is obtained for DNA base molecules. Thus the molecule-substrate interaction is not so strong on this $SrTiO_3(100)$ substrate.

The tunneling current

The equation of (1.4) and (1.5) shows that the tunneling current (the height in STM image) is a function of the DOS of the sample(molecule-substrate system) and the tip, and that of the surface work function (tunneling barrier) of the sample (molecule-substrate system) and tip.

There are two possibilities of image formation as follows:

(1) The emergence of additional DOS within the energy window of bias voltage at the adsorption site.

(2) The (local) tunneling barrier of the substrate change at the adsorption site.

The emergence of additional DOS is caused by molecule-substrate interaction. In the present case, the molecule-substrate interaction in the $SrTiO_3(100)\sqrt{5}x\sqrt{5}$ system is not so strong enough to produce additional DOS within the energy window of bias voltage (1~3 V). Moreover, the lateral dimensions of molecular image is nearly twice larger than expected and will not be explained by the DOS.

The local tunneling barrier change means that the tunneling current tunnels between the substrate and tip i.e., not between the molecule and tip. This phenomenon will occur in the case that the molecule-substrate bonding is weak. In other words, the current can not easily commute between the molecule and substrate and the tunneling current that flows between the substrate and tip, feel the molecule as nothing but a tunneling barrier. Since the experiment suggests the weak molecule-substrate interaction for this system, the local tunneling barrier change of substrate may contribute to the image formation in this particular system.

Local tunneling barrier change

The local tunneling barrier of substrate is altered by dipole moment of the adsorbed molecule, as following:

$$\phi_s = \phi_{s\,clean} - e\,\mu / \varepsilon_0$$

where ϕ_s and $\phi_{s\,clean}$ are the work function (tunneling barrier) of substrate where molecule exists and that of does not, respectively. The e is the electronic charge, μ is the dipole moment of the adsorbed molecule, and ε_0 is the vacuum permittivity [42].

Assuming the extreme case that only local tunneling barrier of substrate contributes to the molecular contrast, using over simplified equation of (1.1), the following relationship stands.

$$\exp(-s\,\phi_s^{1/2}) = \exp[-(s+\Delta s)(\phi_s+\Delta\phi_s)^{1/2}]$$

where s is the (initial)substrate-tip distance, the Δs is the apparent height of the

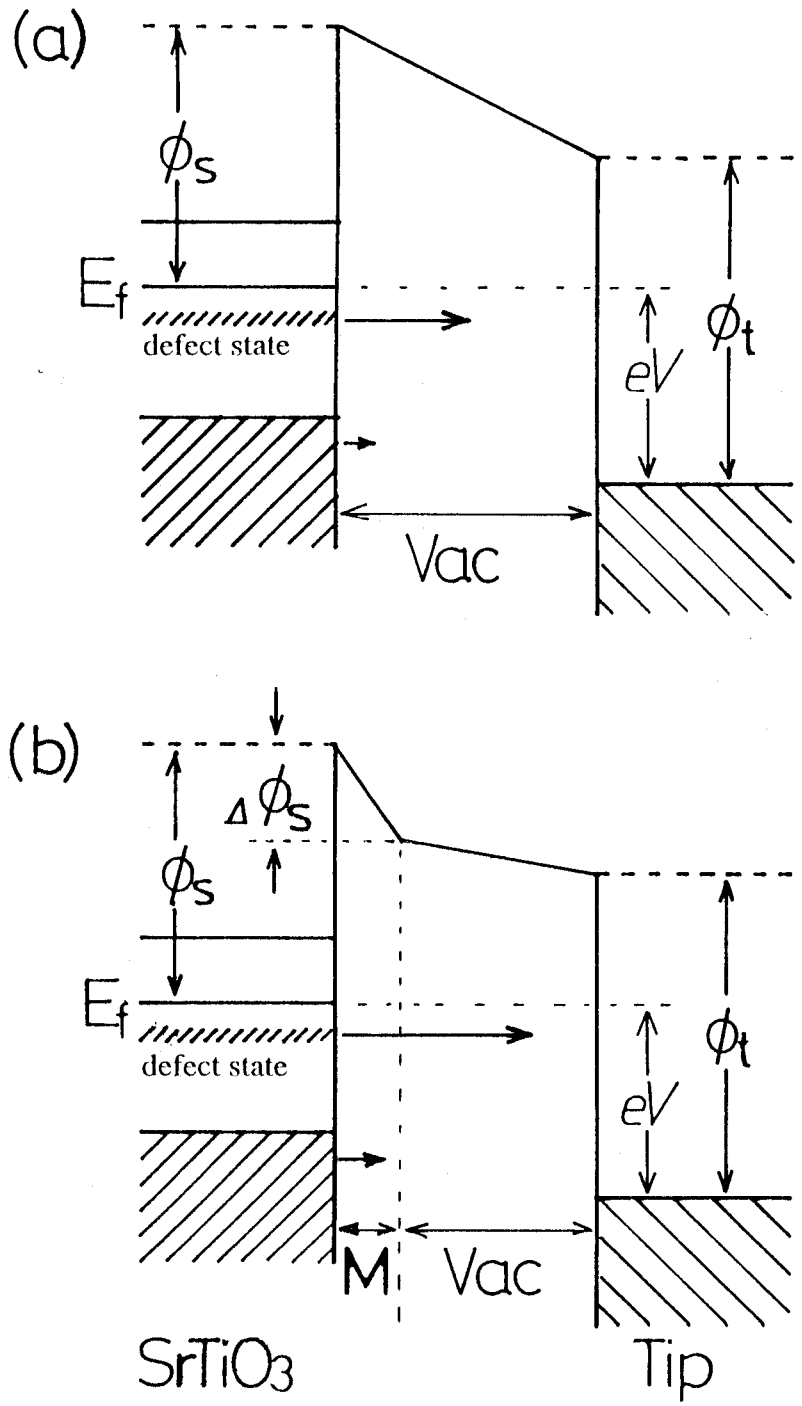

Fig. 3-9. A possible schematic energy diagram between the $SrTiO_3(100)$ surface and tip. (a) That for without DNA molecule between them. (b) That for with molecule between them. "M " represent the area that molecule exits. "Vac" represents vacuum region. "/////" represents oxygen vacancy states of $SrTiO_3(100)$. The presence of the polar molecule lowers work function of the substrate (the tunneling barrier), resulting increase in the tunneling current.

molecule, ϕ_s is the work function of clean substrate, $\Delta\phi_s$ is the work function change due to the presence of the polar molecule. The values of s = 0.7 nm, Δs = 0.2 ~ 0.5 nm and ϕ_s= 3 eV [43] give $\Delta\phi_s$ = -1.19 ~ -1.98 eV. This value may be reasonable because my recent measurement on the apparent barrier height change gives a work function change by -1 ~ -2 eV at the adsorption sites. Thus the work function change due to the dipole moment of the adsorbed molecule may contribute to the observed molecular contrast in STM image. This mechanism is schematically sketched in Fig.3-9.

Band structure effects

Although the work function change gives the molecular contrast in the STM image, the large lateral dimension that is nearly twice larger than expected, remains unclear. There is another factor which contributes to the image formation. That comes from the effects of band structure (in chapter 1.1.3). The Eqs. (1.5)-(1.7) shows tunneling transmission probability becomes the largest when the parallel momentum is zero and that the wavefunctions with the parallel momentum also contribute to the tunneling current to some extent. This contribution of the parallel momentum may not be considerable at clean surface because the geometric and electronic structures are completely periodic along the surface. However, at a site where the molecule adsorbs, the contribution of the parallel momentum may be considerable, because the work function change caused by the molecule gives larger tunneling transmission probability for the wavefunctions with non-zero parallel momentum that can flow between the molecule and *tip located near the molecule*. This contribution will appear as broadening (blur) of the molecular contrast.

At present, the band structure of the $SrTiO_3(100)\sqrt{5}x\sqrt{5}$ is unknown. However the above mechanism may explain the observed images.

3.4 Summary

(1) STM imaging of the four DNA bases deposited on a reduced $SrTiO_3(100)$ clean surface under UHV conditions has been done.

(2) The lateral dimensions of adenine and guanine are approximately 1.5-1.0 nm and of

thymine and cytosine are approximately 1.0-0.6 nm with a sample bias voltage of -1 to -3 V.

(3) By comparing the lateral dimensions of the bases in the STM image, I have found that the discriminations between adenine and thymine, and between guanine and cytosine are possible. Analysis of the bias dependence of the imaged heights of the bases indicates that further discrimination of the bases is possible.

(4) The interaction between molecule and substrate is rather weak (E_{des} ~ 1eV, E_{dif} ~ 0.7 eV), and some molecules tend to diffuse over the surface.

(5) By controlling a tunneling parameter of current, translational molecular manipulation is demonstrated. Possibility of manipulation of the single nucleic acid bases using STM is indicated.

(6) The observed molecular contrast of the base molecules is explained by that polarized adsorbed molecules lower the local work function of the substrate.

The fact that high resolution imaging of molecule which directly corresponds to the electronic states (MO) of molecule is not successfully done. This is strongly related o the electronic states of the underling substrate, as is discussed in this section. In order to study the role of the substrate-molecule interaction that determines both the apparent molecular image in STM and adsorbed structure on the surface, different substrates different from that of $SrTiO_3(100)$ are investigated in next section. The substrate is metal Pd(110) that is relatively chemically active due to the electronic state of dense $4d^{10}$ band at Fermi level.

Chapter 4

The DNA Base Molecules on Pd(110) :STM Imaging and Molecular Orbital Calculation

4.1 Introduction

The imaging of DNA base molecules adsorbed on $SrTiO_3(100)$ has offered important results such as the possibility to discriminate kind of individual base molecules. However, the tentative interpretation of imaging mechanism still require additional experimental information on the effect of substrate (substrate-molecule interaction). As a solution, a metal Pd(110) substrate is chosen. Pd is relatively chemically active due to the electronic state of dense $4d^{10}$ band at Fermi level. A (110) surface of fcc crystal exposes a surface geometric structure with an anisotropic symmetry of C_{2v}. This nature offers different molecule-substrate and molecule-molecule interactions which are observed as apparent molecular corrugation and adsorbed structures different from those for $SrTiO_3(100)$. Herein this chapter, the first STM imaging of isolated DNA base molecules adsorbed on an metal surface under UHV conditions is reported. STM images of apparent molecular contrast corresponds to MO of molecule which is strongly adsorbed on the surface.

4.2 Experimental

Substrate

The experiments were performed in a UHV system ($<1x10^{-10}$ Torr) equipped

with a Beetle type STM (Besocke Delta Phi GmbH) [44]. After repeated sputtering and annealing (1100K) cycles, I obtained a clean (1x1) Pd(110) surface [13][14]. In addition to conventional STM imaging at room temperature, imaging at temperatures from 100K to 300K was also performed. After the cooled sample was transferred onto the STM probe head, the temperature gradually was increased to room temperature within about one hour. During this period, STM observations were performed. The images were taken using a mechanically sharpened Pt-Ir tip.

DNA base molecules of adenine and thymine

Adenine and thymine were purchased from Tokyo Chemical Industry Co., Ltd.. The nucleic acid bases were loaded into an electrically heated Ta cell to bring about the deposition. After introduction into the UHV chamber, the cell was degassed for 1 hour prior to the deposition process. The evaporated species were analyzed by mass spectroscopy. This revealed that single molecules were evaporated from the cell and that deposition of intact isolated molecules is possible.

Deposition of the DNA base molecules

Typical deposition conditions were as follows: During evaporation, the base pressure of $<10^{-10}$ Torr rose to 10^{-9} Torr. The temperature of the cell during the evaporation was about 470K. The coverage of the nucleic acid base was controlled by the deposition time and temperature of the cell.

4.3 Results and discussion

4.3.1 Images

Adenine/Pd(110) at room temperature

Fig.4-1(b) shows an STM image of the Pd(110) surface obtained after adenine deposition (~0.1 ML (1ML=1.07×10^{15} molecules cm^{-2}). The temperature of the Pd(110) substrate was kept at room temperature, both during deposition and STM imaging. In higher resolution images, the isolated adenine molecules are observed as characteristic triangular-shaped protrusions with typical lateral dimensions of ~0.8nm, as shown in

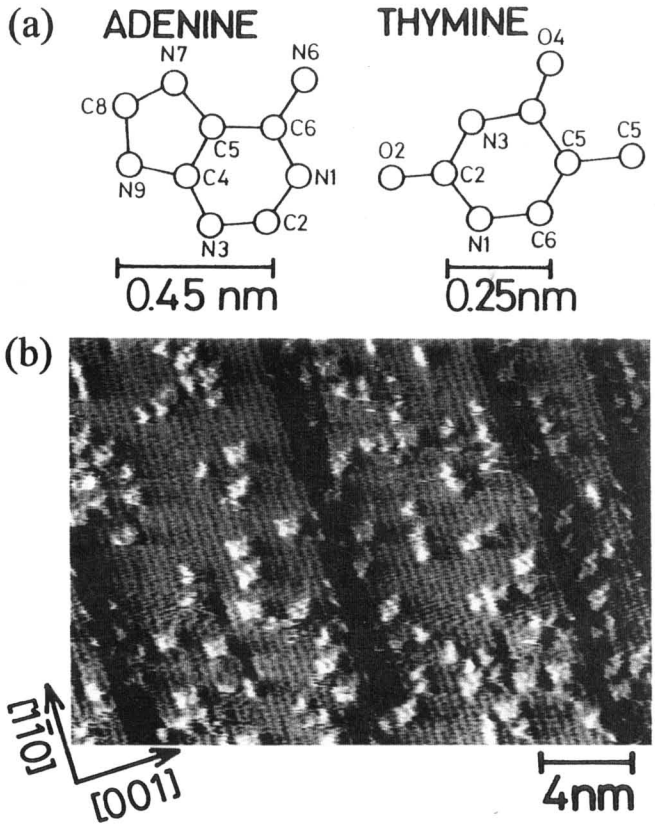

Fig.4-1 (a) Molecular structure of adenine and thymine with molecular scales. (b) A typical large scale image (25x18nm^2) of a Pd(110) (1x1) surface observed after the deposition of adenine (~0.1 monolayer(ML)). Tip bias *Et*=-0.01V, tunneling current *It*=1nA. The image was obtained using a differential data acquisition mode.

Fig.4-2(a). Although the smaller bias voltage tends to result in a higher resolution of the image, the dimension, shape and corrugation height (~0.14 nm) show no appreciable dependence on the tip bias from *Et*=-2 to 2V. The contours of constant charge density (ϕ =0.001) of highest occupied molecular orbital(HOMO) and lowest unoccupied one(LUMO) at 0.1 nm above the molecular ring system of adenine molecule are also shown in Fig.4-2(a). The MO calculations have been performed by the semiempirical PM3 method using the program MOPAC ver.7.01. It should be mentioned that the detailed calculation for the adsorbed molecules including underlying substrate is under investigation using ab-initio method[45]. The charge density of the HOMO is localized around the N1, C2, N3, C6, N6, N7 and C8 sites and that of the LUMO. This distribution can be roughly outlined as a triangle with a lateral dimension of ~0.6 nm. Although the resolution of the observed molecular image is not high enough to distinguish HOMO and LUMO, the observed molecular images appear to be in agreement with the calculated contour of the HOMO or LUMO. These results imply that the deposited adenine molecules have not decomposed on the (1×1) Pd(110) surface at room temperature. Therefore I consider that the electronic structure of isolated adenine molecules has been imaged by STM for the first time. Although it is difficult to determine the adenine adsorption site precisely, it appears that the center of the adenine molecules seems to be located in the middle between the closed-packed Pd rows along [110], (Fig.4-1(b)).

Adenine dimer

Fig.4-2(b) shows an STM image of a (1×1) Pd(110) surface with an increased adenine coverage of ~0.1 ML. As before, the substrate temperature was kept at room temperature during the deposition and STM imaging. In addition to isolated adenine molecules, many dimer-like configuration of adenine molecules are observed which appear to consist of a pair of triangles of ~0.8 nm (each corresponding to a single adenine molecule). The pairs are aligned along the [001] direction and not along the [110] direction, indicating a strong substrate-dependent anisotropy on the pairing mechanism.

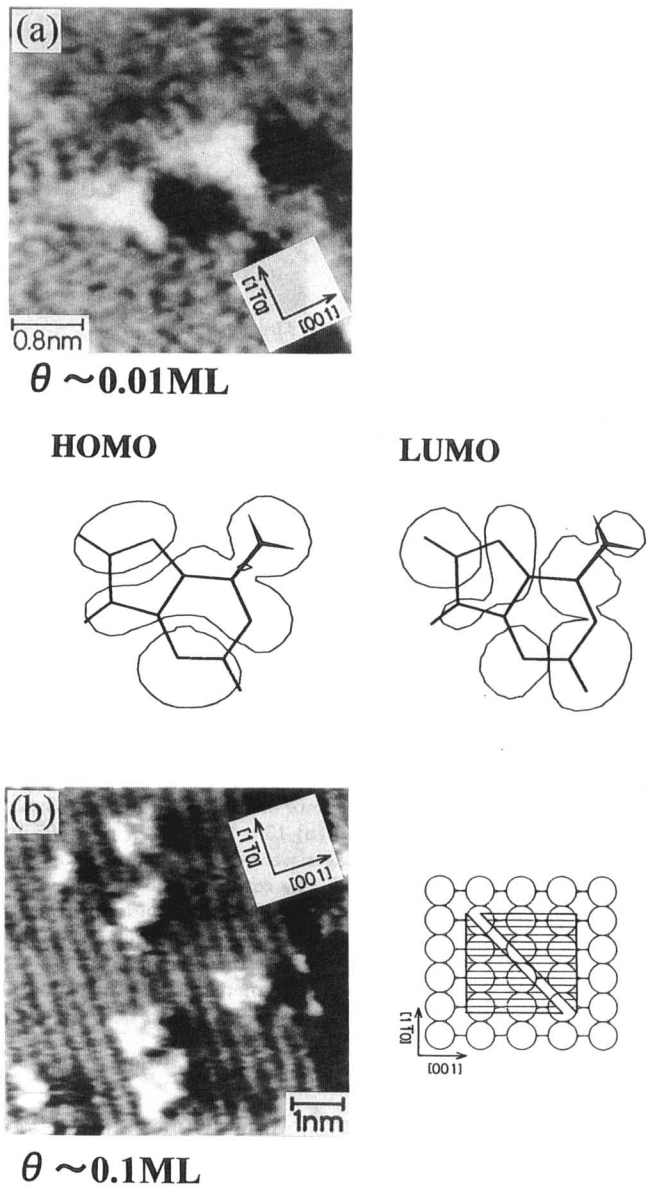

Fig.4-2 (a) An expanded image (4.1x4.1nm^2) shows the isolated adenine molecules. The substrate temperature was room temperature during the deposition and STM imaging. Tip bias *Et*=-0.2V, tunneling current *It*=1nA. The contours of constant charge density (ϕ =0.001) of highest occupied molecular orbital(HOMO) and lowest unoccupied MO(LUMO) at 0.1 nm above the molecular ring system of single adenine molecule are also shown. The MO calculations have been performed by the semiempirical PM3 method using the program MOPAC ver.7.01.
(b) This image (6.4x6.4nm^2) shows paired adenine molecules adsorbed on the (1x1) Pd(110) surface obtained at an adenine coverage of ~0.1ML. The substrate temperature was room temperature during deposition and STM imaging. *Et*=-0.01V, *It*=1nA. All the images were obtained in a differential data acquisition mode.

The interaction energies for the DNA base pairs have been calculated by Hobza and Sandorfy[19] with a nonempirical ab initio selfconsistent field method. They reported three possible adenine homopairs with binding energies of -66.2, -61.7 and -38.8 kJ/mol. Although I can not distinguish which of the pairing structures corresponds to the observed structures, the mere fact that dimers are observed provides evidence for an attractive interaction. It should be noted that there were no appreciable differences between the STM images of isolated adenine molecules at room temperature or at ~100K. This result corroborates our speculation that the adenine molecules are adsorbed on the Pd(110) surface as complete molecules, i.e. not decomposed, at room temperature.

Thymine/Pd(110) at low coverage

Qualitatively different behavior was observed for the nucleic acid base, thymine. Thymine was deposited on the Pd(110) substrate with the same procedure as for adenine. The temperature of the Pd substrate was ~100K during the deposition and ~270K during recording of the image. As shown in Fig.4-3(a), thymine molecules appear as round protrusions with lateral dimensions of ~0.45 nm. The contours of HOMO and LUMO orbitals of dienol type thymine molecule calculated by the semiempirical PM3 method using the program MOPAC ver.7.01 are shown in Fig.4-3(c). Considering that adenine molecules have been observed as triangular protrusions with lateral dimensions of ~0.8 nm, it follows that these dimensions and shapes are distinctly different from each other, indicating the possibility of discrimination between these bases by STM. Closer inspection of Fig.4-3(a) reveals that most of the distances between nearest-neighbor thymine molecules are about ~0.5 nm, and that there are relatively many open spaces. These results indicate that thymine molecules have a tendency to form such islands.

Thymine/Pd(110) at higher coverage

The tendency of thymine molecules to form such islands becomes more prominent at higher coverages. Fig.4-3(b) shows an image with increased thymine coverage of ~0.2 ML. The temperature of the substrate was ~100K during the deposition and ~265K

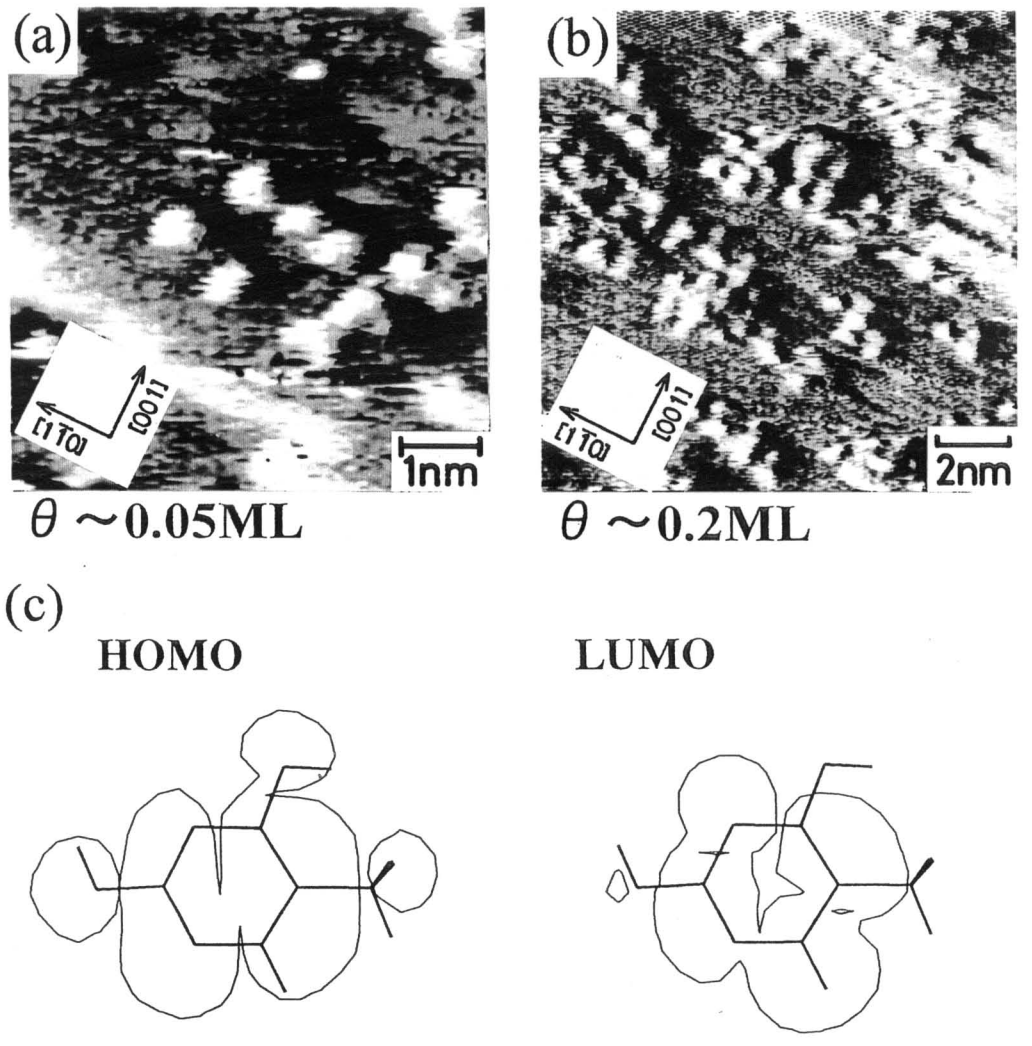

Fig.4-3 Series of STM images of thymine islands on a (1x1) Pd(110) surface with different coverages. The coverages of thymine are approximately (a) ~0.05 and (b) ~0.2ML, respectively. The substrate temperature during deposition was ~100K, and during image recording about 265-270K for both (a) and (b). The STM imaging parameters were as follows: (a) 6.8x6.8 nm^2, *Et*=+0.01 V, *It*=1 nA and (b) 13x13 nm^2, *Et*= +0.05 V, *It*=0.2 nA. All the images were obtained in a differential data acquisition mode. (c) The contours of constant charge density (ϕ =0.001) of the calculated HOMO and LUMO orbitals for dienol type thymine molecule at 0.1 nm above the molecular ring system of single thymine molecule are also shown. The MO calculations have been performed by the semiempirical PM3 method using the program MOPAC ver.7.01.

during recording of the image. No isolated thymine molecule is found, and only thymine islands are observed. This tendency towards island formation even at low coverage region reveals a remarkable attractive interaction between thymine molecules for both [110] and [001] directions. On the other hand, adenine molecules tend to form dimers and are uniformly spread over Pd(110) surface. Theoretical calculations indicate that the interactions of adenine homopairs lead to a larger stabilization energy than in the case of thymine keto-form homopairs(-52.0~-53.2kJ/mol) [19]. A possible explanation for the observed strong interaction between thymine molecules is as follows. Thymine molecules can transform into enol or dienol forms, both of which contain H-bonds[46]. The H-bonds in the enol form may be stronger than the interaction between adenine molecules. Our results suggest that the enol tautomerization plays an important role in the interactions between the bases.

4.3.2 Electronic structure and imaging mechanism

The most important experimental result that is different from those obtained for $SrTiO_3$(100), is that the STM images of apparent molecular shape appear to correspond to that of molecule` MO and the molecular image can be obtained at extremely low bias voltage of 0.01 V. Since only substrate is changed, it is reasonable to suspect that the underling substrate contributes to image formation.

Molecule-substrate interaction

As mentioned earlier, Pd is chemically reactive material[13][14]. This active nature arises from its 4d electronic states that rest at the Fermi level. In fact, the observed images suggest that the molecules are adsorbed stronger than those on $SrTiO_3$(100), because no mobile molecule is observed for Pd(110). Note that some molecules are mobile on $SrTiO_3$(100) surface. The desorption activation energy of DNA base molecules from Pd(110) is not reported so far. Since E_{des} is usually obtained from the thermal desorption technique, molecules which decompose before desorption from the surface cannot be applied by this technique. The E_{des} for benzene is estimated to be 0.9-1.3 eV[47]. The E_{des} of the DNA base molecules from Pd(110) may be larger than 2 eV. However the molecule-substrate interaction is not strong enough to dissociate or

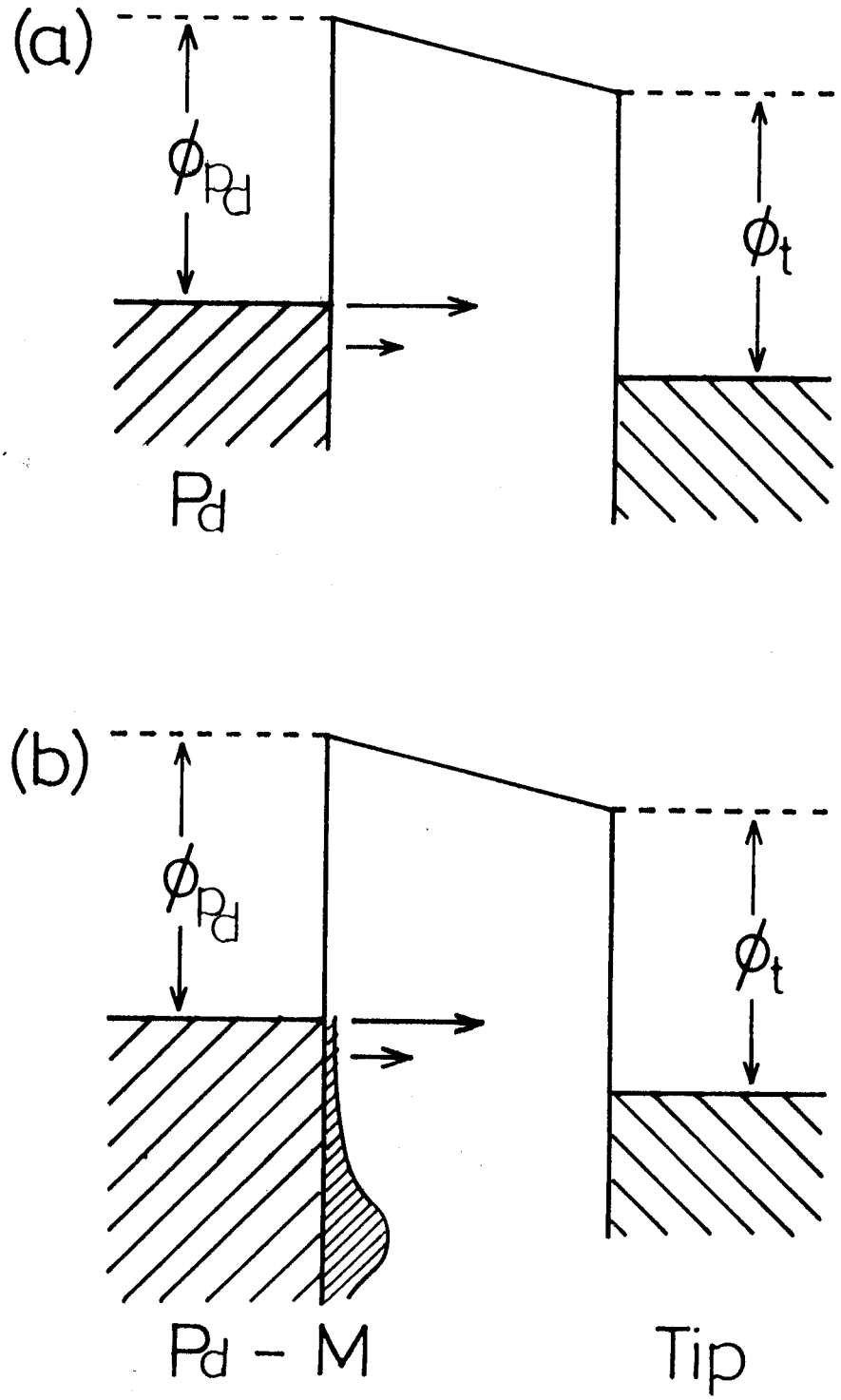

Fig. 4-4 A possible schematic energy diagram between (a) the clean Pd(110) surface and tip, (b) the adsorbed system of the Pd(110)-molecule (Pd-M) and tip. In (b), the partial DOS that originate from the MO of the molecule contribute directly to the molecular contrast.

decompose these molecules.

DOS of the DNA base molecules on Pd(110)

The DOS of adsorbed molecule is predicted by the *News- Anderson* model as shown in chapter 1.3.2[10]. In the case of weak chemisorption in this model, "the density of states in the metal is flat and the adsorbate state is broadened from a single level in the isolated atom to a Lorenzian distribution centered about the original energy level." The observed molecule-substrate interaction is strong enough for "weak chemisorption" but not strong enough for strong chemisorption to dissociate or decompose molecules as discussed in previous section. Therefore, it is reasonable to consider the level of the MO of the molecule are broadened to give an observable DOS from MO of the molecule extended near the $E_f(|Vs| \sim 0.01$ V). In Eq.(1.4), above discussion corresponds that the DOS of substrate ($\rho_s(r, E)$ in Eq.(1.4)) is replaced by that of adsorbed system, as shown in Fig.4.4. In other words, the molecular contrast in STM image is a map of the local DOS of MO of adsorbed molecule in the energy window of bias voltage.

4.4 Summary

(1) STM imaging of DNA base molecules deposited on a clean (1x1) Pd(110) surface under UHV conditions have been done.

(2) The lateral dimensions of adenine and thymine are approximately 0.8 nm and 0.5 nm with a bias voltage of 0.01 to 2 V.

(3) The observed molecular images of the adsorbed base molecules appear to correspond to the shape of MO of each base molecule.

(4) The interaction between molecule and substrate is not weak ($E_{des} > 2$eV, $E_{dif} > 1$ eV), and no molecular diffusion has been observed.

(5) The molecular images represent the local DOS from MO of adsorbed molecules which is broadened to produce observable DOS within the energy window of bias voltage of STM.

The broadening of the MO of the molecule results of the weak chemisorption.

(6) The molecule-molecule interaction is observed.

Adenine shows a strong tendency for dimer formation for adenine .

Thymine forms islands even at low coverages.

However, relatively large E_{dif} > 1eV limited the molecular diffusion to form further molecular super structure such as self-assembly.

In this section, interpretation of imaging mechanism of DNA base molecules adsorbed on Pd(110), an chemically active metal surface, is discussed. The systematic comparison of the results of $SrTiO_3$(100) and Pd(110) systems, has enable to obtain an insight into the imaging mechanism. Since a base molecule should be adsorbed on a surface as intact molecule (not dissociated or decomposed), it is reasonable to change the substrate from the chemically active (4d band at E_f) Pd(110) to chemically less active (4s band at E_f) Cu(111).

Cu is a noble metal of 4s band at E_f and band of closed 3d shell at 2 eV below E_f. This electronic structure may contribute to different substrate-molecule interaction which will be observed as apparent molecular image. Since Cu(111) has chemically less active nature and symmetry of close-pack fcc (111) surface, the E_{dif} may be small enough for molecular diffusion to form self-assembly through molecule-molecule interaction.

In next chapter, results for DNA base molecule-Cu(111) substrate system is shown and discussed.

Chapter 5

The DNA base Molecules on Cu(111) :Low-Dimensional Self-Assembly of the DNA Base Molecules

5.1 Introduction

The results of the previous two molecule-substrate systems, bases/$SrTiO_3$(100) and bases/Pd(110), indicate that the role of substrate that the molecule-substrate interaction determine the electronic states of adsorbed system. The interaction with the chemically active Pd substrate alters the electronic structure of adsorbed molecules to produce new DOS accessible by STM. The large E_{dif} (partly due to the large E_{des}) appears to limit the molecular diffusion necessary for molecule-molecule interaction to self-assemble themselves.

The chemically less active nature of Cu(111) surfaces will offer weak interaction between molecule-substrate. The observed molecular images have shapes similar to those of MO of the molecules at relatively high bias voltage. The molecules in the images tend to be transparent at $|Vs| < 0.1$ V, indicating that molecule-substrate interaction which is less strong than that for Pd(110), produces thinner molecule`s DOS near E_f.

It is also revealed that the small E_{dif} allows molecular diffusion necessary for molecule-molecule interaction to self-assemble themselves into novel low-dimensional super-structures. The dominant molecule-molecule interaction force for the self-assembly formation is attributed to the hydrogen-bonding between DNA base molecules. The mechanisms of image formation and self-assembly process will be discussed in this

chapter.

5.2 Experimental

Substrate and deposition

After repeated Ar ion sputtering and annealing cycles in ultra high vacuum UHV , I obtained a clean flat Cu(111) crystal surface. The bases, adenine, thymine, guanine and cytosine were deposited on the freshly cleaned crystal by evaporating them from an electrically heated stainless steel cell (2 mm in inner diameter and 10 mm long) in which powders of base were loaded. The temperature of the cell was measured with a chromel-alumel thermocouple which is spot-welded to the cell. The purities of the evaporated bases were checked in-situ by mass spectroscopy to verify that deposition of intact bases is possible. STM imaging was performed at room temperature, using a mechanically sharpened Pt-Ir tip.

5.3 Results and discussion

5.3.1 Images

Shape of molecular image

It was found that STM image of *isolated* DNA base molecules is difficult to obtain due to thermal diffusion at room temperature. However, molecules which are close-packed into a monolayer or self-assembled into a super-structure are barely imaged as molecules even at room temperature. Figure 5-1 shows an STM image of adenine molecule packed in to a monolayer. In this image adenine molecules are observed as characteristic triangular-shaped protrusions with typical lateral dimensions of ~0.6-0.8 nm (x-y) and ~0.1 nm (z). This shape is similar to the contour of calculated MO as shown in Figure 4-2(a). From this result, the mechanism of molecular image formation in Cu(111) system resemble to that in Pd(110) and different from that in $SrTiO_3$(100) system. It is apparent that the deposited adenine molecules are not decomposed on the clean Cu(111) surface at room temperature.

The bias dependence of molecular images has revealed that they become transparent at bias voltage($|Vs|$) below 0.1 V. Note that, molecular images are usually obtained at low bias voltage of 0.01 V for Pd(110) system.

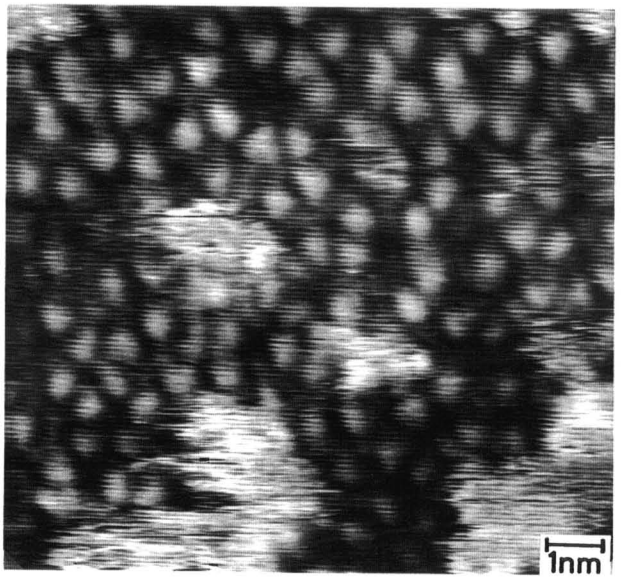

Figure 5-1 STM images of close-packed monolayer of adenine molecules on Cu(111) surfaces at room temperature.(10x9.5x0.2 nm^3, *Vs*=-1V , *It*=50pA.)

Self-assembly of the DNA base molecules

The observed self-assembly of the four bases, adenine, thymine, guanine and cytosine, on the clean Cu(111) surfaces at room temperature is shown in Fig.5-2(a)-(d). Coverages of each base are 1 monolayer (ML) for adenine and guanine, 0.5 ML for thymine and 0.1 ML for cytosine. One can see 1-D chains form networks in Fig.5-2(a) for adenine, 2-D islands in Fig.5-2(b) for thymine, 2-D square lattices in Fig.5-2(c) for guanine and 1-D zig-zag networks in Fig.5-2(d) for cytosine. Since no isolated

molecules are observed due to molecular diffusion at room temperature, these self-assembled structures which are unique to each base suggest that the corrugation of the potential (the activation energy of diffusion(E_{dif})) is not strong enough to freeze molecular diffusion on the Cu(111) surface. I consider that the bases can self-assemble themselves spontaneously on the clean Cu(111) surfaces with little influence of the substrate.

The E_{dif} can be estimated in a same way as in Chapter 3. Assuming that isolated molecules defuse over the surface within the shorter period of a time constant of the feedback circuit(~0.001 s). The activation energy for surface diffusion is derived from an Arrhenius equation shown as (1.2). $t = t_0 \exp(E_{des}/kT)$
assuming $T = 300$ K, $t_0 = 10^{-12}$ s, $t < 0.001$ s, $k = 1.38 \times 10^{-23}$ J/K ($= 8.62 \times 10^{-5}$ eV/K),
then $E_{dif} < 0.5$ eV is estimated.

5.3.2 Self-assembly mechanism

Adenine

The self-assembled adenine (Fig.5-2(a)) has network structures consisting of 1-D chains with apparent widths of ~ 0.5 nm, topographic heights of 0.1-0.2 nm and lengths of 1-5 nm. The width of the chains, ~ 0.5 nm, is close to the lateral dimension of the adenine molecules, as shown in the inset of Fig.5-2(a). The height of 0.1-0.2 nm is the value usually observed for the height of molecules of π system lying flat on a metal substrate [48][49]. These results suggest that the observed network structures consist of 1-D adenine molecular chains with each molecule lying flat and neighboring each other on the surface. Accordingly, there is a possibility that the molecule-molecule interactions through the hydrogen-bonding is responsible for the formation of the self-assembly of adenine [19].

In order to investigate the observed structure theoretically, molecular orbital calculations have been performed for the adenine dimer and trimer structures by the semiempirical PM3 method using the program MOPAC 93. The optimum structures of dimers (AA I ~ AA IV) obtained from the calculations are shown in Fig.5-3(a). The 1-D adenine chains cannot be assembled only from the most stable pair, AA I , but

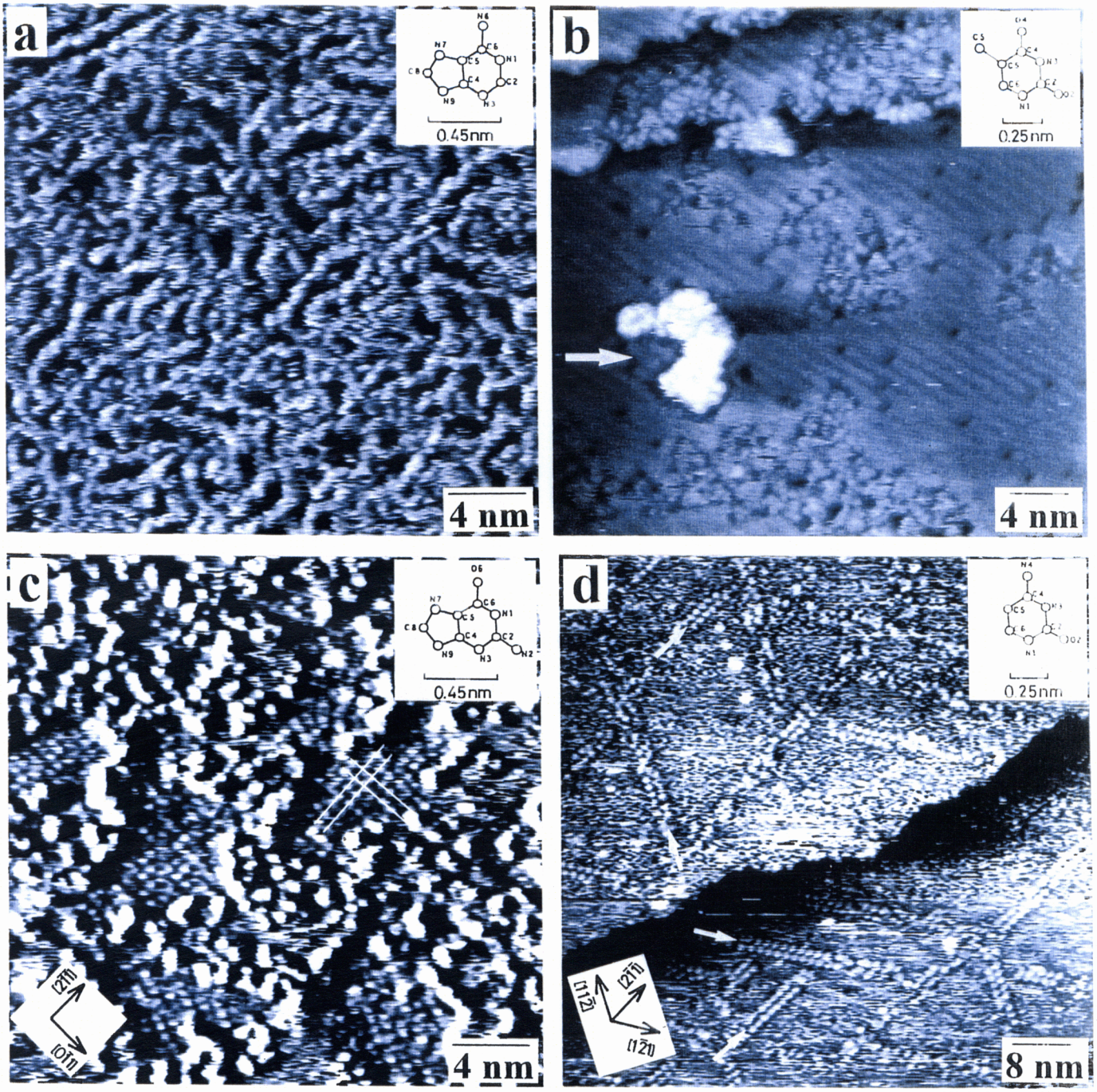

Fig.5-2 A series of unprocessed constant-current (a, b and d) and constant-height (c) STM images of the self-assembled nucleic acid base molecules on Cu(111) surfaces at room temperature. (a) Adenine, coverage (θ)(1 monolayer (ML), 28x28x0.4 nm^3, *Vs*=-1V , *It*=20pA. (b) Thymine, θ (0.5 ML, 35x35x0.8 nm^3, *Vs*=-1V , *It*=0.2nA. (c) Guanine, θ (1 ML, 35x35nm^2, *Vs*=-1V , *It*=0.1nA. (d) Cytosine, θ (0.1 ML, 70x70x0.3 nm^3, *Vs*=-2V , *It*=0.1nA.

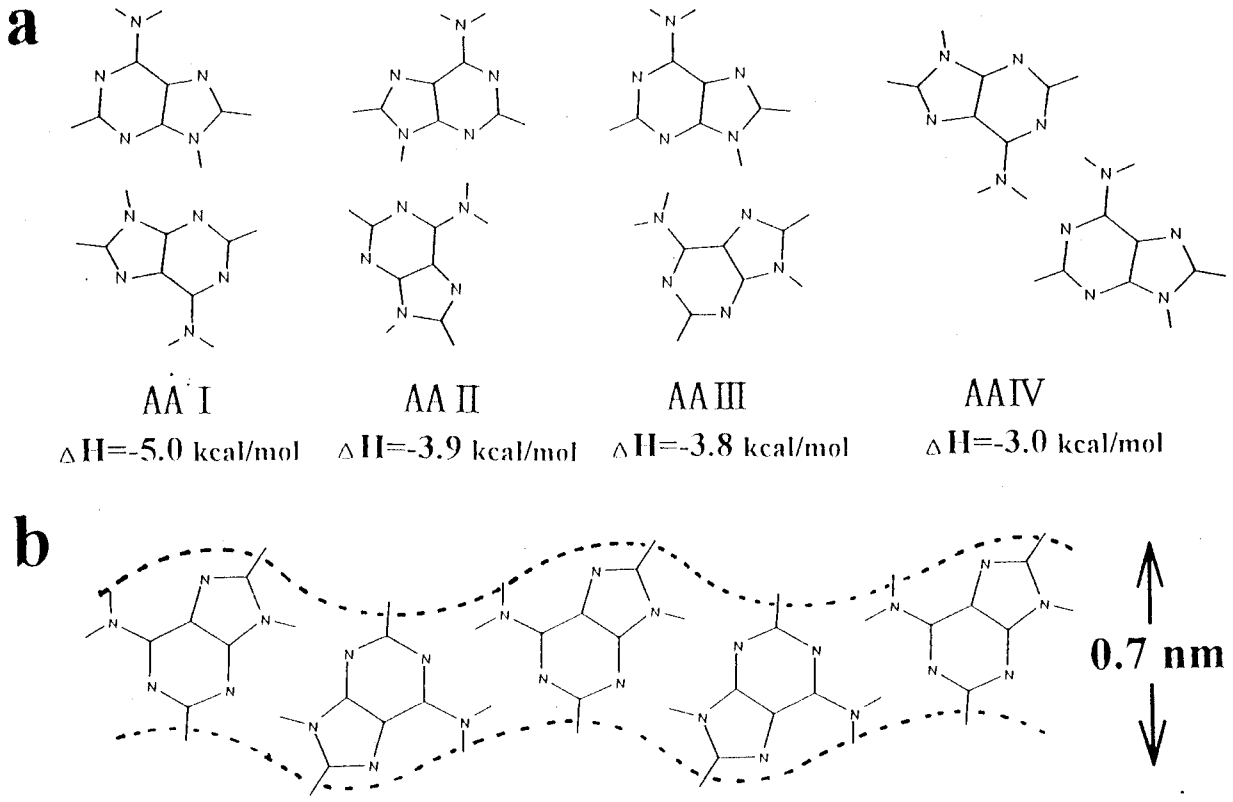

Fig.5-3 (a) The four most stable structures of adenine dimers obtained from molecular orbital calculation by PM3 method using the program MOPAC 93. ΔH is the energy difference of the heat of formation between adenine monomer and each dimer. (b) One of the proposed structures of adenine molecule chains consisting of the sequence of alternating AAI and AA IV pairs. The obtained ΔH are -3.6 kcal/mol for the adenine trimer of AAI and AA IV pairs and -5.8 kcal/mol for adenine molecular string of infinite sequence of alternating AAI and AA IV pairs.

require a participation of another type of pair. Considering that AA II and AA III pairs can take a three-way branch and AA IV does not, 1-D molecular chains can be assembled from sequences of AA I and AA IV pairs. In fact, the trimer constructed from the sequence of AA I and AA IV is a stable structure, as shown in Fig.5-3(b). On the basis of this result, the formation of adenine network is possible by the sequence of the alternating AA I and AA IV pairs with the insertion of AA II or AA III at a various points. Since the rows in the observed network are not completely well ordered as a line, other sequences with less stable combinations may contribute to form the network. I believe that the mechanism of self-assembly of the adenine network can be essentially explained by the above base-base pairing sequence through hydrogen bonds.

Thymine

Distinctly different behavior has been observed for thymine. Thymine tends to form islands of 0.2-0.3 nm height with open spaces around them (see Fig.5-2(b)). Assuming that thymine lies flat on the surface with single or multiple molecular height (0.2-0.3 nm), the growth mode of the observed islands is 2-D. This result indicates thymine has strong aggregation forces.

Guanine

The other purine base, guanine of the first surface layer forms 2-D square (0.6x0.6 nm^2) lattices mixed with the second disordered aggregates, as shown in Fig.5-2(c). All the axes of the square lattices are directed along <110> and <112> directions, indicating that the three-fold symmetry of underlying substrate contributes to the formation of the square guanine lattices to some extent. On closer inspection, the distance between neighboring guanine molecules randomly aggregated on the second (top most) layer imaged as bright spots in Fig.5-2(c) is 0.65-0.75 nm and is larger than that on the first layer. These values suggest that the guanine molecules in the first layer are relatively close packed. Therefore, the 2-D molecular interactions may cause the square lattice which is not completely commensurate over the underlying substrate.

Cytosine

The other pyrimidine base, cytosine forms 1-D zig-zag networks, as shown in Fig.5-2(d). All the 1-D zig-zag networks are identically oriented in a threefold symmetric mesh of <112>. The distance between the neighboring bright dots along the propagating direction is ~1.2 nm and is larger than that for a base pair, typically about 0.6 nm. The dots have the height of about 0.1 nm and the fairly large lateral size of 0.7-1 nm, presumably the single dot consists of several cytosine molecules. Moreover, the dots in the 1-D zig-zag network are often destroyed into smaller dots, indicating the dots consist of clusters of cytosine molecules. Cotton and Scholes studied benzotriazole (BTA) adsorbed on Cu surfaces; the molecule has similar structure to the DNA bases. They concluded that the BTA adlayer consists of Cu-BTA complex on the surfaces [50]. There is a possibility that the dots in the 1D zig-zag network consist of a Cu-cytosine complex. The mechanism of formation of 1-D zig-zag networks, however, remains unclear. Grtter and Drig studied self-assembled quasidendritic patterns of Co on Pt(111) surfaces [51]. The observed that Co dendrite arms are oriented to the <112> direction of the (111) surfaces and have no side branches. They concluded that the cause of dendritic growth is the presence of a local reconstruction (induced by the growth of Co islands) of the Pt surface, which acts as a template for the Co adlayer [51]. Considering that the observed 1-D zig-zag network of cytosine have surprisingly similar threefold symmetric structure to that for Co quasidendrite on Pt(111), I suggest that the driving force of the formation of 1-D zig-zag network of cytosine is also attributed to a local reconstruction of underlying substrate, which is induced by the growth of cytosine cluster.

5.3.3 Electronic structure and imaging mechanism

The characteristic feature point of the molecular image observed on Cu(111) substrates is following.

1. The shape of molecular image is similar to the contour of MO of isolated molecule.
2. The molecules in the STM image become transparent at low bias voltage of $|Vs| <$ 0.1 V.

The former suggests that the imaging mechanism is essentially the same as the case of Pd(110). Thus the problem is the explanation of the latter.

Molecule-substrate interaction: E_{des}

In the mechanism of image formation, the E_{des} (the molecule-substrate interaction) is important as discussed in the previous chapter. The E_{des} of the DNA base molecules from Cu(111) substrate is not known. The fact that the molecules stay at the surface much longer than the order of a day indicates that E_{des} > 1eV. Although the specific value is unknown, the molecule-substrate interaction is strong enough to make the molecules chemisorb on the surface .

DOS of the DNA base molecules on Cu(111)

As discussed in the case of Pd(110), the level of the MO of the molecule are broadened to give a observable DOS from MO of the molecule near E_f. However, the fact that molecules in the STM image become transparent at low bias voltage of $|Vs| <$ 0.1 V, is the different from the case of Pd(110) and remains unclear. This indicate that very low DOS of the molecule in the energy region of $|Vs| < 0.1$ eV.

In the case of weak chemisorption in the *News- Anderson* model, the electronic interaction of the metal and molecule cause the Lorenzian broadening of MO of the adsorbate in weak chemisorption. The magnitude of this broadening depends on the magnitude of the interaction. That is to say that the smaller E_{des} results in lower DOS of MO of the adsorbate. It is well known that Cu(111) is less chemically active in comparison to Pd(110). This is due to difference of the electronic structure. Pd(110) has 4d band at E_f. On the other hand, Cu(111) has 4s band at E_f. A possible energy diagram for above discussion is outlined in Fig.5-4. Figure 5.4(a) shows the case for high bias voltage $|Vs| > 1$ V. A partial DOS of adsorbate in the relatively large energy window of the bias voltage($|Vs| > 1$ V), can contribute to tunneling current to produce molecular contrast in STM images. On the other hand, in (b), too spare DOS of adsorbate in the (relatively narrow) energy window of the bias voltage ($|Vs| < 0.1$ V), so that it can not contribute to tunneling current to produce molecular contrast in STM images.

It is emphasized that the above discussion is consistent with the interpretation of imaging mechanisms discussed in the previous section (Pd(110) system).

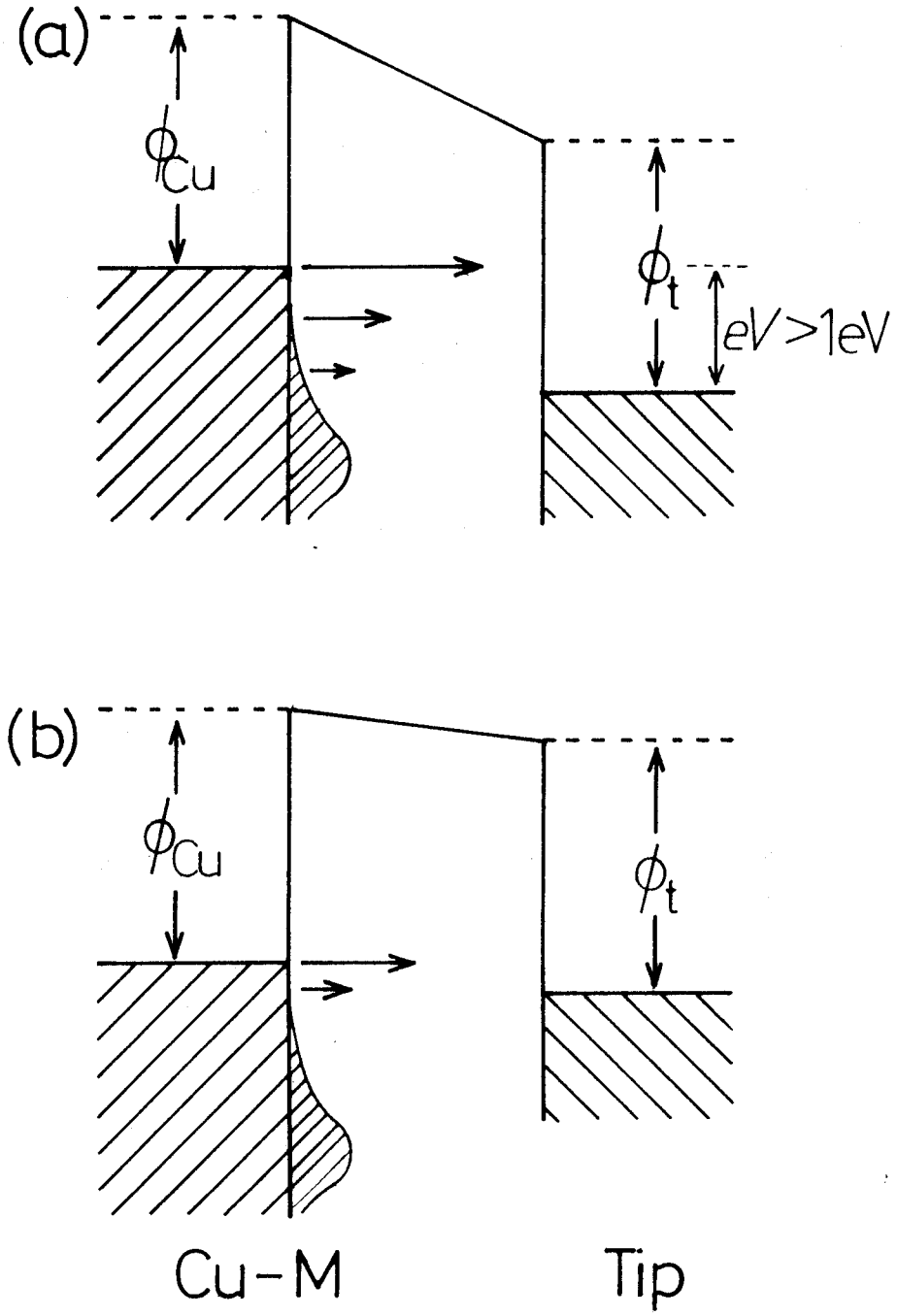

Fig.5-4. A possible energy diagram for imaging mechanism of the adsorbed system of Cu(111)-DNA base molecule. (a) The energy window of bias voltage is high enough for partial DOS of the adsorbed molecule(M) can tunnel to appear as molecular contrast in STM images. For the case of ($|Vs| > 1$ V). (b) The other case ($|Vs| < 0.1$ V). The energy window of bias voltage is too small. No detectable current from partial DOS of the adsorbed molecule(M) tunnels to give rise a molecular contrast in STM images.

5.4 Summary

(1) STM imaging of DNA base molecules deposited on a clean Cu(111) surface under UHV conditions has been done.

(2) The lateral dimension of adenine is approximately 0.8 nm with bias voltage of 1 to 2 V.

The molecules in the STM image become transparent at low bias voltage of $|Vs| < 0.1$ V.

(3) The observed molecular images of the adsorbed adenine appear to correspond to the shape of MO of the base molecule.

(4) The interaction between molecule and substrate is not strong (E_{des} > 1eV, E_{dif} <0.5 eV). No isolated molecules are imaged as "molecular images" due to thermal diffusion at room temperature.

(5) The molecular images represent the local electronic states from MO of adsorbate which is broadened to produce observable finite DOS within the energy window of bias voltage(1-2 V) of STM. The broadening and level shift of the MO result form the interaction with the Cu 4s band at Fermi level.

(6) The novel phenomena on the self-assembly of DNA base molecules is observed by means of STM for the first time.

Adenine: 1D molecular chains

Thymine: 2-D islands

Guanine: 2-D square lattices

Cytosine: 1-D zig-zag molecule-cluster networks

(7) The mechanism for observed self-assemblies is understood based on the balance of E_{dif} (surface corrugation), hydrogen-bonding (molecule-molecule interaction) and kT(thermal energy).

The order of them is following. E_{des} > hydrogen-bonding > E_{dif}

(8) It is found that molecular orbital calculations (without considering a substrate) reproduce some of the observed self-assembly and that base-base interaction induced by hydrogen-bonding is essential to this phenomenon.

(9) The self-assembled super-structures have substrate dependent structure (epitaxial nature). To understood the mechanisms further, role of the substrate must be considered. Molecule-molecule interaction is stronger than E_{dif} and kT.

The STM images obtained for the DNA base molecule-Cu(111) substrate system confirm the proposed mechanisms of image formation and of self-assembly. As a next step to the goal of this thesis, it is necessary to image and manipulate actual DNA molecule adsorbed on a well-defined solid surface under UHV conditions.

Chapter 6

Discussion for Imaging and Self-Assembly Mechanism on Different Substrates

In this chapter, essential mechanisms of imaging and self-assembly of DNA-base molecules are discussed on basis of interactions of molecule-substrate and molecule-molecule.

6.1 Imaging mechanism

The apparent molecular contrast in STM images observed for the three different substrates (see Fig.6.1) have characteristic features which are unique to each substrate (cluster, 2-D gas, self-assembly, etc.). It is true that the apparent feature (lateral dimension, height and their bias dependence) does depend on the tip condition of both geometric and electronic structure. However, the systematic investigation on the three different substrates indicates that the role of tip is negligible in comparison to that of the substrate (molecule-substrate) system. Thus it is reasonable to assume that imaging mechanism depends mainly on the electronic properties and geometric structure of molecule-substrate system. This means that in Eq.(1.4), as re-shown in the end of this paragraph, the second term(ρ_t) is negligible in comparison to the other terms(ρ_s and T). The electronic properties and geometric structure of molecule-substrate system, are determined by the molecule-substrate interaction. Some of the important results are summarized in Table 6.1.

$$I = \int_0^{eV} \rho_s(r, E)\ \rho_t(r, -eV + E)\, T(E, eV, r)\, dE \qquad (1.4)$$

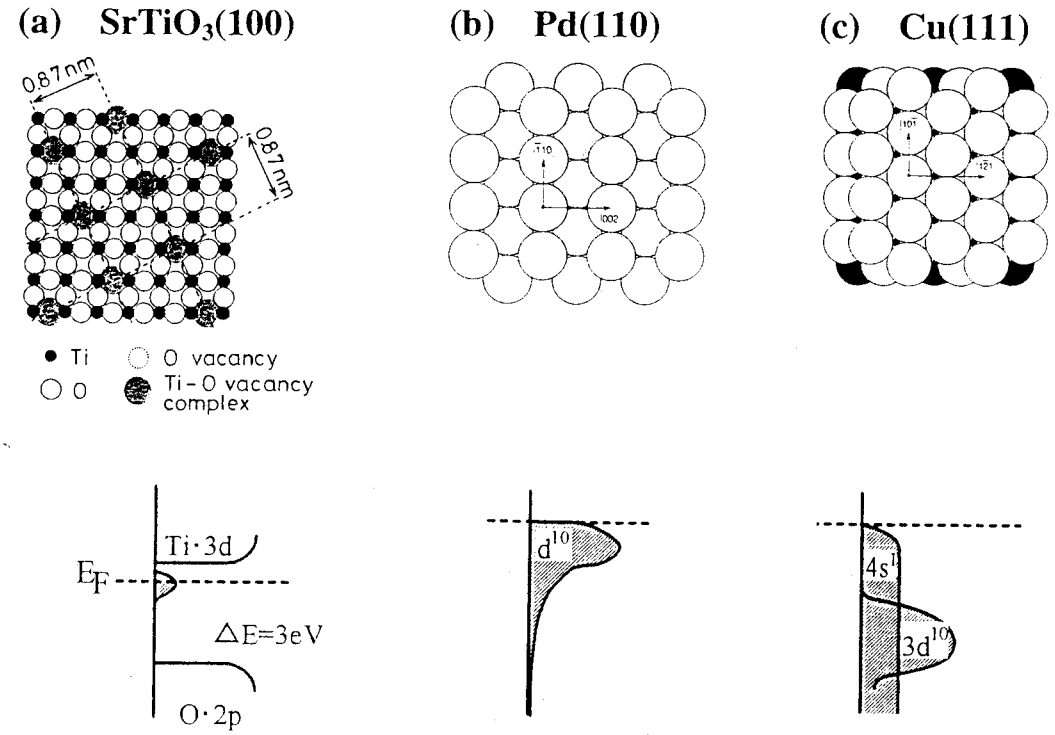

Fig. 6.1. The simple models of the surface structure and electronic structure (density of states near the Fermi level (E_f)) of the three different substrate surfaces. (a) $SrTiO_3(100)\sqrt{5}x\sqrt{5}$-R26° , (b) Pd(110) and (c) Cu(111).

TABLE 6.1. Electronic Properties of substrate and Molecular Images

Substrate	$SrTiO_3(100)\sqrt{5}x\sqrt{5}$	Pd(110)	Cu(111)
Electronic State of Substrate	semi-metal O-vacancy	dense 4d band	flat 4s band
Molecular Image	Round & Large (blurred)	MO like	MO like
Bias dependence	Strong	Observable even at $\|Vs\| \sim 0.01$V	Transparent at $\|Vs\| < 0.1$ V

Pd(110) and Cu(111)

The molecule-substrate interaction for the metal surfaces causes the broadening of single level of the MO of the molecule to produce observable partial DOS from the MO of the molecule in the energy window of the bias voltage, as sown in Fig.6.2(b) and (c). The fact that the molecular contrast in the STM images has a apparent shape and lateral dimensions similar to that of contour of the MO, is consistently explained.

There is different bias dependence between Pd(110) and Cu(111) as listed in Table (6.1). This is explained by the difference of the electronic structures of the substrate. The interaction of Pd(110) system which has 4d band at E_f is stronger than that of Cu(111) which has 4s band at E_f. Consequently the broadening of the MO in the Pd(110) system is larger than that in the Cu(111) system.

In the two metal systems of Pd(110) and Cu(111), the molecular contrast in the STM images corresponds to the partial DOS of the adsorbed system (the first term of Eq.(1.4)).

$SrTiO_3$(100)

As discussed in chapter 3.3.2, the observed molecular contrast of the base molecules correspond to DOS of underlying $SrTiO_3$(100) substrate where polarized adsorbed molecules lower the local work function of the substrate. This imaging mechanism is completely different from that for Pd(110) and Cu(111) substrates The essential reason is the polar adsorbed molecule. The majority of the tunneling current can flow between the *substrate* and tip, feeling the molecule as nothing but a tunneling barrier, as shown in Fig.6.2(a).

Moreover, the molecule-substrate interaction on this surfaces may cause the broadening of single level of the MO of the molecule to produce observable partial DOS from the MO of the molecule in the energy window of the bias voltage, as discussed in the case for Pd(110) and Cu(111) surfaces. However the fact that the molecular contrast on $SrTiO_3$(100) surfaces has a apparent shape and lateral dimensions much larger than that for contour of the MO indicates that the dominant tunneling current dose not come from the partial DOS from the MO of the adsorbed molecule..

Therefore, the molecular contrast on $SrTiO_3(100)$ originates mainly from the contribution of the tunneling barrier height (the third term, $T(E, eV)$ in Eq.(1.4) is dominant). The molecular contrast corresponds to the change of the local tunneling barrier height (work function of the $SrTiO_3(100)$ substrate) lowered by the presence of polar adsorbate, because those wave functions of tunneling electron who pass through the polar adsorbed molecule can obtain larger decay length (larger T).

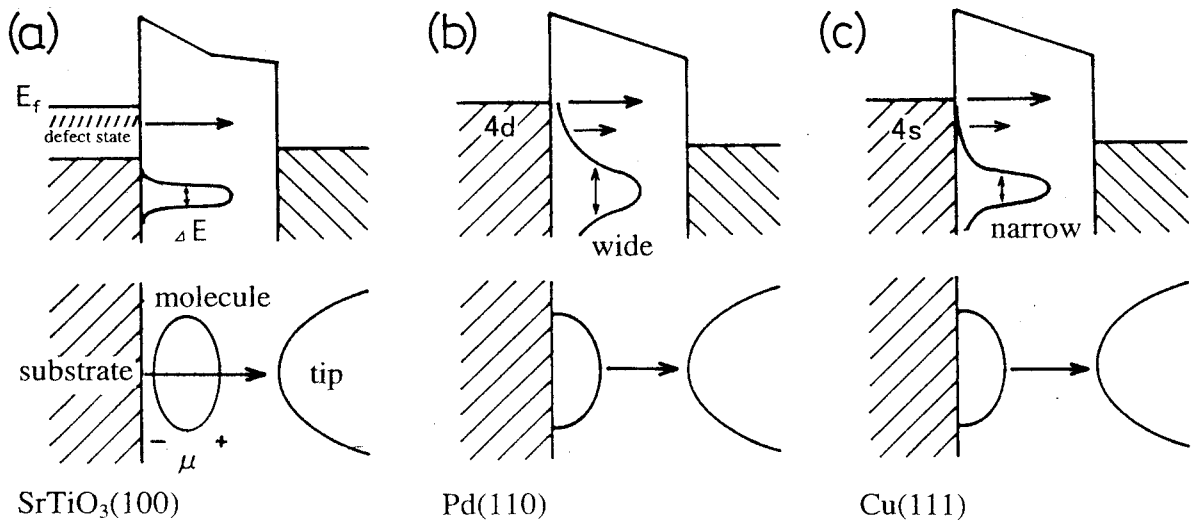

Fig.6.2 Schematic illustration of imaging mechanism for the three substrates, (a) $SrTiO_3(100)$, (b) Pd(110) and (c) Cu(111).

8.2 Chemisorption and self-assembly of DNA molecules on solid surfaces

The DNA base molecules are chemisorbed on the solid surfaces. The molecule-substrate interaction (E_{des}) contributes to the imaging mechanism as discussed. The self-assembly is related to E_{dif} rather than E_{des}. The important factors that have been observed are listed as follows.

1. E_{dif} (activation barrier for surface migration)and kT(thermal energy)

2. Molecule-molecule interaction (hydrogen-bonding ~ 0.1-0.5 eV)

3. Epitaxy (surface structure of the substrate)

In chapter 5, it is concluded that the phenomena of self-assembly is understood based on the balance of E_{dif} , hydrogen-bonding and kT. In this section, the above factors and observed surface super structures of the DNA base molecules are discussed. The results of observed assembly and the relating data (E_{dif}) are summarized in Table 6.2.

The observed adsorbed structures of *all* the three different substrates can be totally understood as discussed below.

TABLE 6.2. Self-assembly, E_{dif} and substrate structures

Substrate	$SrTiO_3(100)\sqrt{5}x\sqrt{5}$	Pd(110)	Cu(111)
Isolated molecule	~ immobilized	immobilized	mobile
Self-assembly of molecules	isolated, small cluster	isolated, dimer, small cluster	self-assembled superstructures
E_{dif} (eV)for molecules	~ 0.7 eV	> 1 eV	< 0.5 eV
Structure of substrate periodicity	$\sqrt{5}x\sqrt{5}$ 0.87x0.87 nm	[110] row 0.39 nm	fcc(111) close-pack 0.26 nm

$SrTiO_3(100)\sqrt{5}x\sqrt{5}$

The molecule-substrate interaction(small E_{des}) is not strong. However E_{dif} ~ 0.7 eV is not small enough for free molecular diffusion with thermal energy (kT ~ 0.025 eV) at room temperature, as illustrated in Fig.6.3(a). This results in the existence of isolated observed assembly of molecules as mere cluster. The driving force of cluster of DNA base molecules is molecule-molecule interaction through hydrogen-bonding. The hydrogen bonding energy (E_{hb}) is 0.1-0.5 eV and is a little smaller than that of the E_{dif} ~ 0.7 eV. This order of two energies means that the molecules can not self-assemble themselves into an intrinsic molecular superstructure, ignoring the surface periodicity of

the E_{dif} (periodicity ~ 0.87 nm). Thus the observed structure of the molecules on this surface is explained. The order of the interactions (E_{des}, E_{dif}, $E_{hb} > kT$) are as follows.

$$E_{des,}\sim 1 \text{ eV} > E_{dif,}\sim 0.7 \text{ eV} > E_{hb}\, 0.1\text{-}0.5 \text{ eV} > kT$$

Pd(110)

The surface immobilizes the molecules. The $E_{dif} > 1$ eV is estimated, as illustrated in Fig.6.3(b). This large E_{dif} prohibits diffusion of adsorbed molecules. However, the dimmer (adenine) and cluster (thymine) are found. Two possible mechanisms of these molecular assembly are as follows;

First, these assemblies are formed during the process of evaporation, before arriving at the surface. Second, the translational energy of gas phase molecule (evaporated from the cell) may be redistributed into the surface diffusion energy at adsorption process.

One of the unique point is that adenine dimer is aligned along the [001] direction and not along the [110] direction. Although the reason for this anisotropy is not clear, this is an effect of the structure of underling substrate.

The order of the interactions (E_{des}, E_{dif}, E_{hb} and kT) in this system are as follows.

$$E_{des,} > 2 \text{ eV} > E_{dif,} > 1 \text{ eV} > E_{hb} \sim 0.1\text{-}0.5 \text{ eV} > kT$$

Cu(111)

The characteristic point of this substrate has the extremely small $E_{dif} < 0.5$ eV with periodicity of 0.26 nm, as illustrated in Fig.6.3(c). The adsorbed molecules can freely diffuse over the surface. They interact each other to form hydrogen-bonding (E_{hb} ~ 0.1-0.5 eV). This results in the observed self-assembled structures which are unique to each base. The hydrogen bonding are anisotropic bonding because they are typically formed as -OH***O-, O-H***N-. Thus unique structure of these self-assemblies originates from the anisotropic structure of each base.

In addition, the effect of epitaxy contribute to the self-assembly to some extent. The axis of the self-assembled super-structures tend to be directed along <110> and <112> directions of the underling substrate. This suggests a possibility of a local reconstruction of underlying substrate which is induced by the presence of adsorbed molecules (molecule-substrate interaction).

The order of the interactions (E_{des}, E_{dif}, and E_{hb}) in this system are as follows.

$$E_{des,} > 1 \text{ eV} > E_{hb} \sim 0.1\text{-}0.5 \text{ eV} \sim E_{dif} > kT$$

As discussed in this section, the self-assembly is understood by the balance of the E_{des}, E_{dif}, and E_{hb}, with epitaxy (periodicity) of the underling substrate.

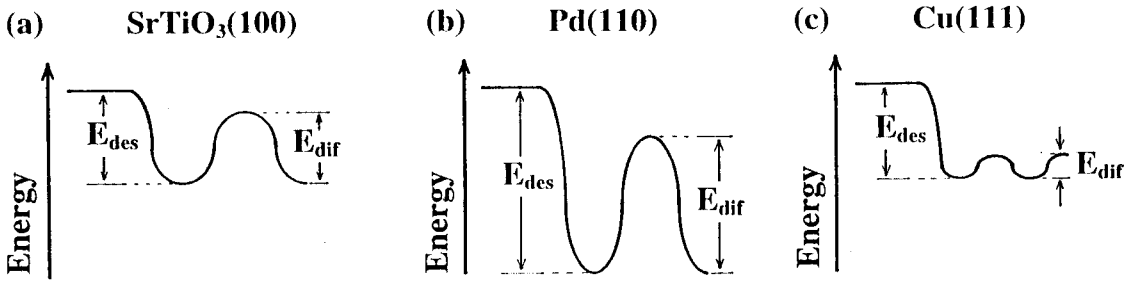

Fig.6.3 Schematic potential energy diagram showing the E_{des} and E_{dif} for adsorbed molecules on (a) $SrTiO_3$(100), (b) Pd(110) and (c) Cu(111).

Chapter 7

STM Imaging and Molecular Structure of DNA Oligomer on Cu(111)

7.1 Introduction

The experimental results of three different substrates ($SrTiO_3$(100), Pd(110) and Cu(111)) have shown that discrimination of the DNA base molecules is possible. However, one of the important keys to the DNA sequencing by STM is the development of a reliable and reproducible sample preparation technique. The DNA molecules can not be deposited by thermal evaporation due to thermal decomposition. It is well known that conventional methods such as air-evaporation, electrochemical deposition, and dropping of DNA-containing solution directly onto a substrate, result in the deposition of aggregated DNA [52][53][54].

In order to overcome above difficulty, a new sample preparation technique has been developed. The technique is a pulse injection method of DNA oligomer containing aqueous solution onto Cu(111) surfaces. The STM images revealed that the surface of Cu(111) retains its atomic flatness even after the injection of DNA-containing solution and that the deposition of intact DNA oligomers without aggregation is possible. The observed internal structure (bulges) of deposited DNA may suggest the promising possibility of sequencing DNA by means of STM.

7.2 Experimental

A schematic of the apparatus is shown in Fig.7-1. The UHV apparatus basically consists of an STM chamber and a preparation chamber. After repeated sputtering and

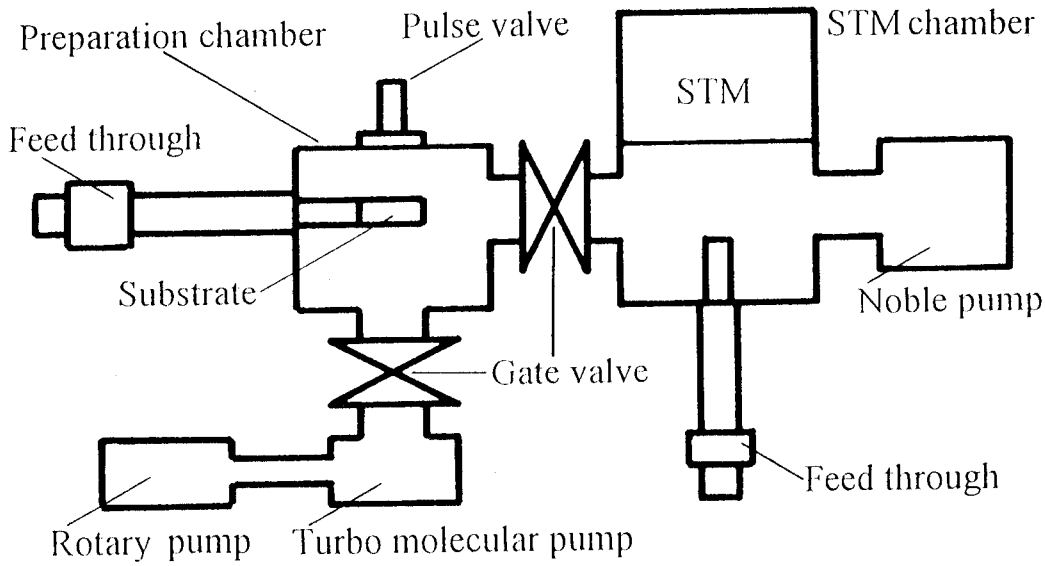

Fig.7-1 Schematic diagram of the pulse injection and STM apparatus used for this study.

annealing cycles in the preparation chamber, I obtained a clean flat Cu(111) surface. The single-stranded DNA oligomer purified by HPLC, pAAAAA, containing five adenines was purchased from Vector Research Co. (Japan). The distilled water, purified by passage through a Barnstead-II purifier, was used in this study. The concentration of the sample was 0.1 mM/l. In order to make aggregated DNA to dissociate, the pulse valve (General Valve Co., Series 9) was warmed by hand-made electric heater at ~90℃ for few minutes before the injection. The conditions of the pulse injection were following. The temperature of the Cu(111) substrate was room temperature. The height of the pulse valve above the substrate surface was 130 mm. The temperature of the sample (pAAAAA, 0.1 mM/l) was ~90℃. Amount of injected sample was ~0.1 ml for 10 shots of the pulse with each pulse duration of 1.5 ms. Under these conditions, I estimate an approximate coverage of pAAAAA at around hundred of the molecules on the area of 100×100 nm^{-2}. After the deposition by the injection, the Cu(111) substrate was

transferred to the STM chamber to perform STM observation. The STM measurements were performed using electrochemically etched W tips.

7.3 Results and discussion

Figure 7-2 shows a typical STM image (*Vs*=-2 V, *It*=10 pA,100x100x0.4 nm^3), obtained after the injection of the aqueous sample solution. One can see distribution of bright objects on an atomically flat terrace in this image. Some of them are preferably located at the step edges(not shown). These objects does not appear when control experiments (injection of H_2O without DNA) are performed. This result indicates that the surface of Cu(111) retains its atomic flatness even after the exposure to the injection of DNA-containing aqueous solution. These bright objects have topographic heights of 0.2-0.3 nm. The heights of 0.2-0.3 nm is relatively larger than those usually observed for the height of nucleic acid bases adsorbed on Cu(111) substrate, typically 0.1-0.2 nm(see chapter 5). Assuming that deposited single-stranded pAAAAA (~3 nm long, when straight) takes flat (rather than steric) conformation to the substrate plane, the height of 0.2-0.3 nm may be explained. Although there is a distribution of apparent shapes and widths of these objects, smaller objects tend to have round shape with ~3 nm width. On closer inspection, they appear to have internal structure of several bright maxima. However, the resolution of the images is not high enough to determine definite structure model. As is seen in chapter 5, self-assembly of DNA bases adsorbed on Cu(111) are found that individual molecules are difficult to be resolved at room temperature but can be resolved at liquid nitrogen temperature[55]. Since STM imaging was performed at room temperature in this experiment, limited resolution may be due to the thermal perturbation at room temperature. I presume that imaging at low temperature enable us to obtain higher resolution to sequence DNA. Thus I think that round bright objects with ~3 nm are isolated pAAAAA and larger objects are clusters of the pAAAAA, which may be formed during surface diffusion before losing translational energy. I tentatively propose a model for the observed isolated pAAAAA, as shown in Fig.7-3. In this model, the hydrophilic chain of each sugar and phosphate is located to form a circle inside, while each hydrophobic adenine is located towards outside the circle.

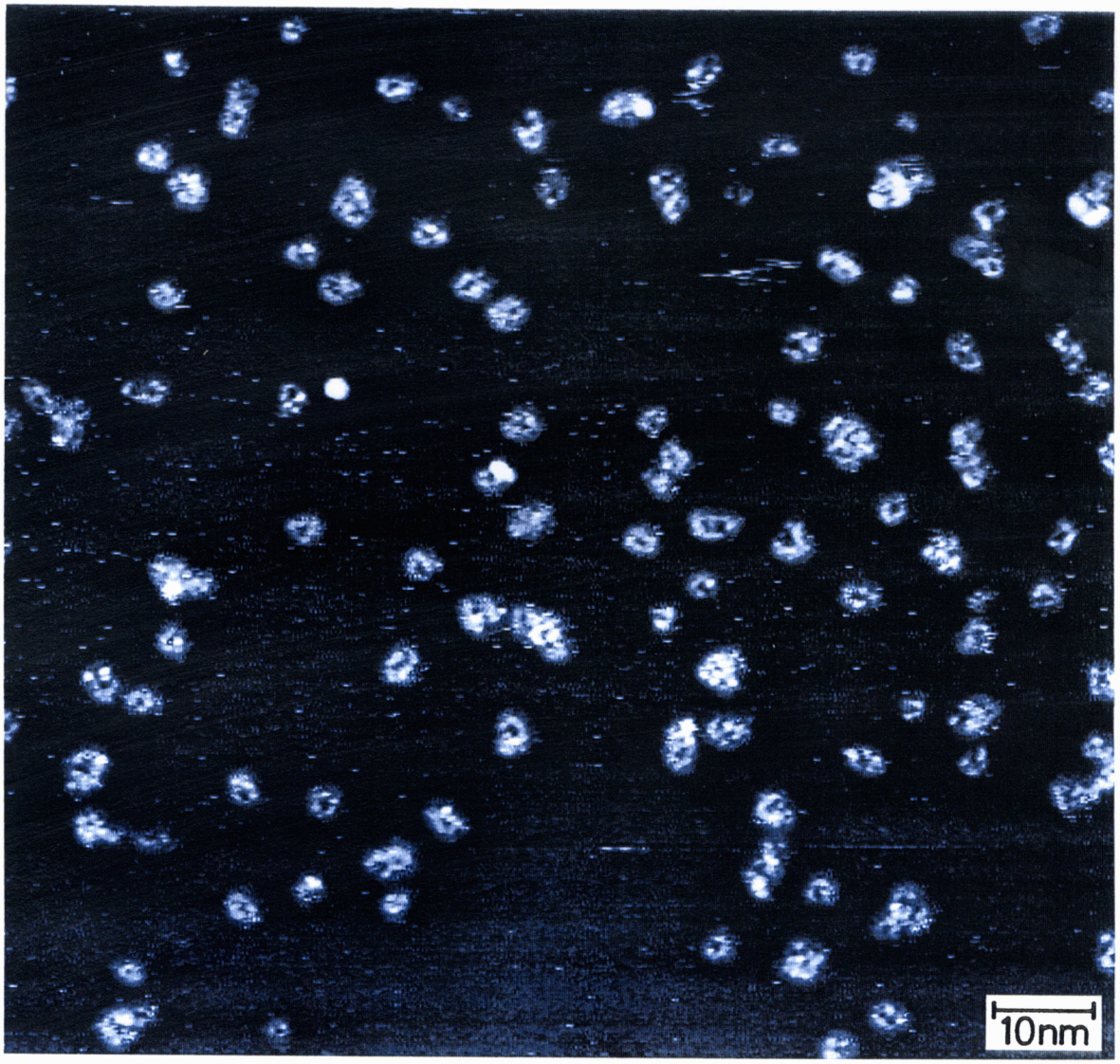

Fig.7-2 A typical STM image (*Vs*=-2 V, *It*=10 pA,100x100x0.4 nm^3), obtained after the injection of the DNA sample on a clean Cu(111) substrate. Bright objects which have not been observed at control experiments, are seen on an atomically flat terrace.

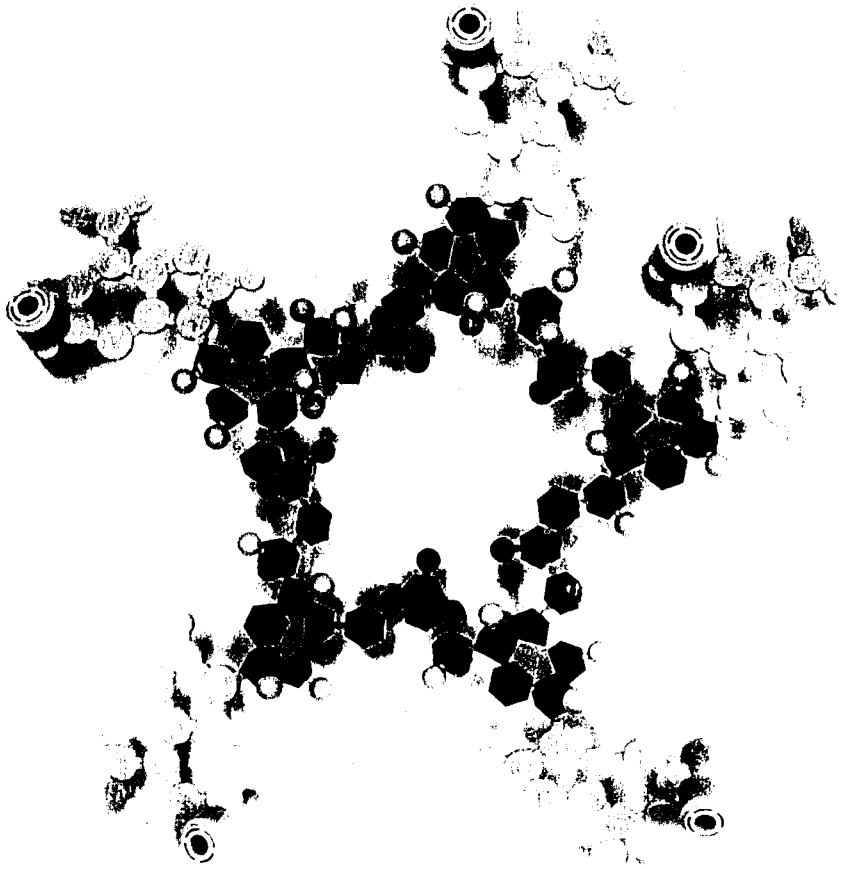

Fig.7-3 A proposed model for the observed isolated pAAAAA on the Cu(111) surface. In this model, hydrophilic chain of the sugar and phosphate is located to form a circle inside, while hydrophobic adenines are located outside the circle. The diameter of this model is ~3 nm, in good agreement of the observed value of ~3 nm.

The diameter of this model is ~3 nm, in good agreement with the observed value of ~3 nm. It should be emphasized that the deposition of intact DNA oligomer without aggregation is possible using pulse injection of DNA-containing solution. Rather simple sample-preparation method may contribute to the studies on molecules which cannot be evaporated or deposited without degradation or aggregation.

Chapter 8

Molecular Manipulation of DNA Oligomer on Cu(111)

8.1 Introduction

As shown in the previous chapter, the pulse injection of aqueous solution containing DNA oligomer onto Cu(111) surfaces is performed as a novel sample-preparation technique for STM studies of biomolecules. It is found that the surface of Cu(111) retains its atomic flatness even after the exposure to the injection of aqueous solution and that the deposition of intact DNA oligomer without aggregation is possible.

In this chapter, manipulation of intact and real DNA oligomer prepared by the pulse injection method is tried as a next step to the goal of manipulation of actual DNA molecule adsorbed on a well-defined solid surface under UHV conditions.

8.2 Experimental

The experimental setup and sample preparation method are same as in the previous chapter. The images were typically taken with a sample bias *Vs* of -0.5 to -3 V and a tunnel current of 10 pA using electrochemically etched W tips. The positioning of the deposited DNA oligomer was performed by lowering the tunnel voltage: *Vs* to -1 mV, similar to that reported in the literatures[35][56][57].

8.3 Results and discussion

J.K.Gimzewski et al. have positioned C_{60} adsorbed on Au(110) by a lateral pushing action of the tip of STM at lowered sample voltage: *Vs*=-4 mV [35][56][57]. In order to

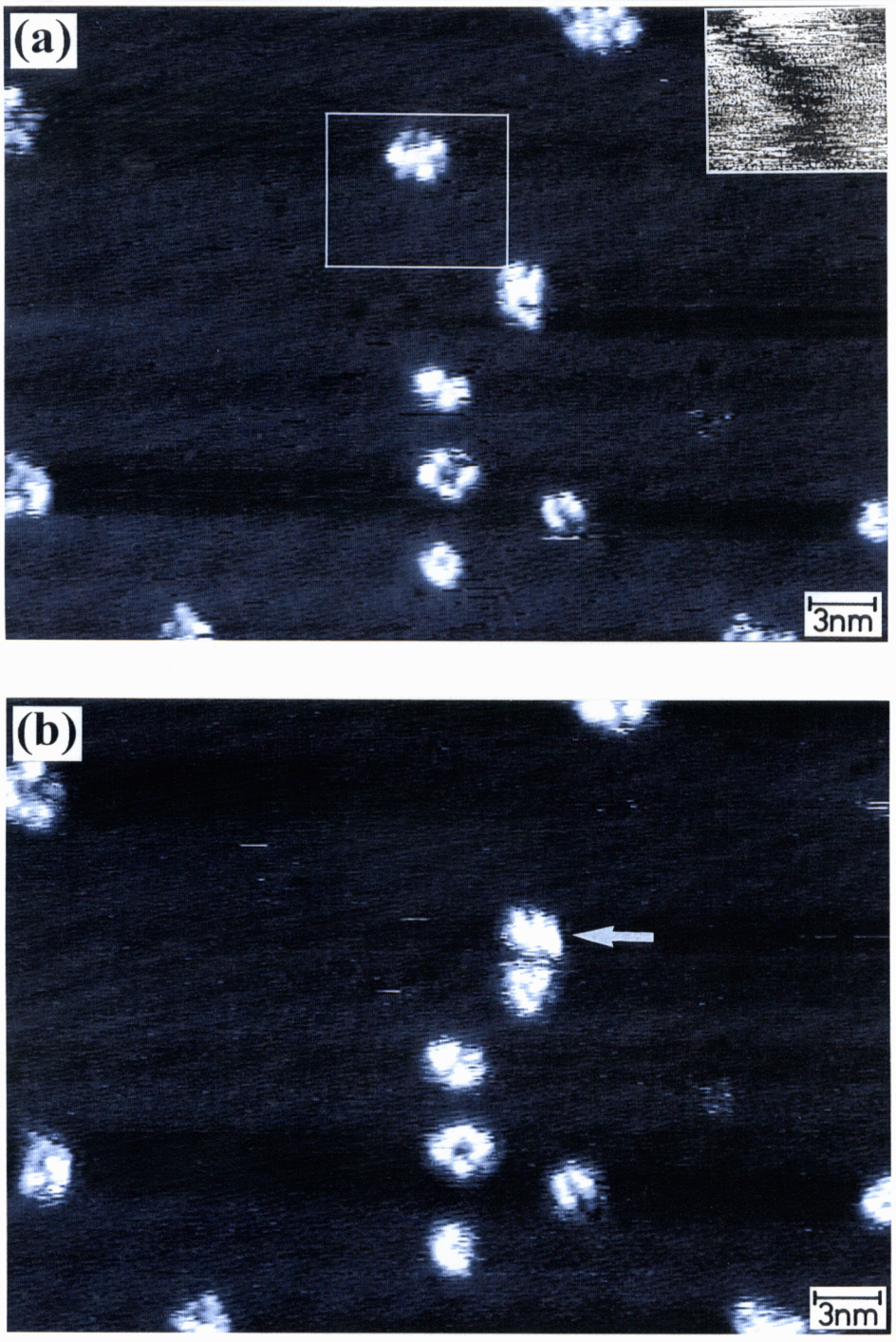

Fig.8-1 A series of STM image of an identical region (40x28x0.4 nm^3) of the surface, taken (a) before and (b) after the operation of manipulation of pAAAAA. Both images were taken at *Vs*=-2 V and *It*=10 pA. Manipulation was performed by scanning at *Vs*=-1 mV and *It*=10 pA on a region (10x9 nm^2), indicated with a white open square in (a). An STM image (10x9x0.2 nm^3) during manipulation is also shown in the inset of (a), indicating a trajectory of the molecule.

examine a possibility of manipulation of DNA, positioning of the pAAAAA DNA oligomer has been performed by a lateral pushing of the scanning tip. Figure 8-1(a) is an image of a region (40x28x0.4 nm^3) taken at *Vs*=-2 V and *It*=10 pA prior to the manipulation. Then, manipulation was performed with the STM tip coming approximately 0.8 nm closer to the surface by scanning at *Vs*=-1 mV and *It*=10 pA on a region (10x9 nm^2), as indicated with a white open square in Fig.8-1(a). An image simultaneously recorded during this manipulation is also shown in the inset of Fig.8-1(a), indicating a trajection (negative contrast) of the molecule in manipulation. After this operation, an image of the same region was obtained, as shown in Fig.8-1(b). This image reveals a lateral displacement of the molecule, as indicated with a white arrow. This attempt indicates that the positioning of the DNA oligomer has been achieved by means of STM as a step towards further manipulation.

8.4 Manipulation mechanism

The molecular manipulation is the controlled perturbation against molecule(s). In other words the tip-molecule interaction is essentially important as well as the molecule-substrate interaction.

$SrTiO_3$(100)

For the manipulation of adenine molecules on $SrTiO_3$(100) surface, more molecules are moved by increasing the tunneling current (from 20 pA to 200 pA), as shown in Fig.3.4. The mechanism is not still unknown because the increase in the tunneling current makes distance between tip and sample closer to increase the electric field. The detailed experiments and theoretical calculation are under investigation[58].

Cu(111)-DNA oligomer

The manipulation of DNA oligomer was performed with the STM tip coming approximately 0.8 nm closer to the surface by scanning at *Vs*=-1 mV and *It*=10 pA as discussed in chapter 8. The interaction force for this movement is the lateral pushing (Born repulsive interaction) of the scanning tip, because such a low bias voltage makes the tip go near the Cu(111) surface by ~ 0.8 nm and that is near enough for the molecule

to be "pushed". The DOS from the molecule in the energy window of such low bias voltage is not observable by STM. The molecules are transparent with $|Vs| < 0.1$ V.

The role of E_{dif} is important in this mechanism. The E_{dif} means the required energy for diffusion. The large E_{dif} prohibits the diffusion of the molecules pushed by the tip. This may result in decomposition of the molecules. Thus, for manipulation of the molecules without destruction, the E_{dif} should not be too large. It should be mentioned that in this sense the Cu(111) surface is an appropriate substrate for manipulation by the lateral-pushing mechanism. This is schematically sketched in Fig.8.2.

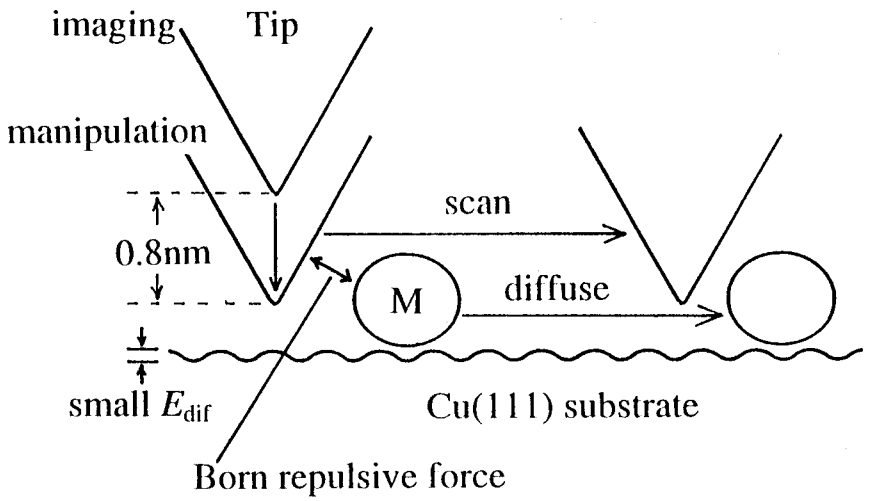

Fig.8.2 The schematic view of the manipulation on Cu(111) surface. "M" represents an adsorbed molecule.

Chapter 9

Concluding Remarks

The UHV-STM study of DNA-related molecules on solid surfaces has been performed. The extensive modification of the UHV-STM system and development of a new sample preparation method have been achieved. The goal of the present study is to elucidate the possibility of the sequencing and manipulation of the DNA using STM based on the understanding of the interactions of molecule-substrate and between molecules.

The observed STM images, of molecules adsorbed on the three different substrates ($SrTiO_3$(100), Pd(110) and Cu(111)) have revealed that the understanding of the molecule-substrate, molecule-molecule and molecule-tip interactions are essential for the mechanism of the image formation, self-assembly and molecular manipulation.

The questions cast in chapter 1.1 are answered in the chapters, though they may be tentative and far from complete. However it is clear that this thesis has opened a substantial way to both experimental and theoretical studies in future.

Acknowledgments

I wish to express my deepest gratitude to my advisor Professor Tomoji Kawai for his contribution both to my research and to my development as a scientist.

It has been very fortunate for me to be able to meet many researchers through the research described in this thesis. Interaction especially with Dr. Maki Kawai and Dr. Jun Yoshinobu of the institute for chemical and physical research (RIKEN) has been absolutely invaluable and unforgettable.

I have benefited from working with a number of members in our research group. I would like to thank Dr. Katsuki Kitahama, Dr. Takuya Matsumoto, Dr. Hitoshi Tabata and Dr. Masaki Kanai for their encouragement and interest for my work.

Finally, I must thank the members of my family, father Takao, mother Takako, sister Hisako, grandmother Masa and late grandfather Choujiro (who passed away last January 20) for everlasting support.

References

[1] G.Binnig, H.Rhorer, C.Gerger, E.Weibel.Phys.Rev.Lett.,**49** (1983) 57.

[2] C.J.Chen; "*Introduction to Scanning Tunneling Microscopy*", Oxford University Press(1993).

[3] R.Wiesendanger; "*Scanning Probe Microdcopy and Spectroscopy*", Cambridge University Press(1994).

[4] *Scanning Tunneling Microscopy II*, ed.Wiesendanger and H.-J.Guntherodt, Springer Series in Surface Sciences 28,(Berlin, Heidelberg, New York: Springer).

[5] T. P. Beebe Jr, T.E. Wiollson, D.F. Ogletree, J. E. Katz, R. Balhorn, M. Salmeron and W. J. Siekhaus, Science, **243** (1989) 370.

[6] R. J. Driscoll, M. G. Youngquist and J. D. Baldeschweiler, Nature **346** (1990) 294.

[7] G. L. Patricia, G. Arscott, V. A. Bloomfield and D. F. Evans, Science **244** (1989) 28.

[8] S. M. Lindsay, T. Thundat, L. Nagahara, U. Knipping and R. L. Rill. Science **244** (1989) 1063.

[9] G.Binnig and H.Rhorer. Rev. Mod. Phys. **56** (1987) 615.

[10] J.K.Norskov. Rep.Prog.Phys.,**53** (1990) 1253.

[11] C. R. Clemmer and T. P. Beebe Jr. Science **251** (1991) 640.

[12] H.Tanaka,T.Matsumoto,T.Kawai and S.Kawai,Jpn.J.Appl.Phys.**32**(1993)1405

[13] J.Yoshinobu, H.Tanaka, M.Kawai. Phys.Rev.B,**51**(1995)4529.

[14] H.Tanaka, J.Yoshinobu, M.Kawai. Surf.Sci.,**235**(1995)L505.

[15] S.J.Stranick, M.M.Kamna, and P.S.Weiss. Science **266** (1994) 99.

[16] A. Sommerfeld and Bethe, *Handbuch der Physik*, ed. H. Geibeeeger and K. Schell (Springer-Verlag, Berlin), Vol.**24/2**, (1933) 450.

[17] J. N. Israelachvili, *Intermolecular and Surface Forces*, Academic Press, New York 1985.

[18] W.Saenger, *Principles of Nucleic Acid Structure*, (Springer-Verlag, Berlin),

[19] P.Hobza and C.Sandorfy: J.Am.Chem.Soc.**109**(1987)1302.

[20] H. Ohtani, R. J. Wilson, S. Chiang and C. M. Mate, Phys. Rev. Lett. **60** (1988)

2398.

[21] D. P. E. Smith, A. Bryant, C. F. Quate, J. P. Rabe, Ch. Gerber and D. J. Swalen, Proc. Natl. Acad. Sci. USA **84** (1987) 969.

[22] D. P. E. Smith, H. Horber, Ch. Gerber and G. Binnig. Science **245** (1989) 43.

[23] K. B. Blodgett, J.Am.Chem.Soc. **57** (1935) 1007.

[24] I. K. Yanson, A. B. Teplitsky and L. F. Sukhodub, Biopoly. **18** (1979) 1149.

[25] M. Aida, J. Comp. Chem. **9** (1988) 362.

[26] J. B. O. Mitchell and S. L. Price, Chem. Phys. Lett. **154** (1988) 267.

[27] N. J. Tao, J. A. DeRose and S. M. Lindsay, J. Phys. Chem. **97** (1993) 910.

[28] D. M. Eigler and E. K. Schweizer. Nature **344** (1990) 524.

[29] R. S. Becker, J. A. Golvchenko and B. S. Swartzentruber, Nature **325** (1987) 419.

[30] M. Aono, A. Kobayashi, F. Grey, H. Uchida and D. -H. Huang, Jpn. J. Appl. Phys. **32** (1993) 1470.

[31] C. Girard, C. Joachim, C. Chavy and P. Sautet, Surf. Sci. **282** (1993) 400.

[32] T. Nakayama, D. H-. Huang and M. Aono. Microelectronic Eng. in press.

[33] Y. Z. Li, L. Bvazque, R. Piner, R. P. Andres and R. Reifenberger. Appl. Phys. Lett. **54** (1989) 1424.

[34] T. C-. Shen, C. Wang, G. C. Aben, J. R. Tucker, J. W. Lyding, Ph. Avouris, R. E. Walkup. Science **268** (1995) 1590.

[35] T. A. Jung, R. R. Schlitter, J. K. Gimzewski, H. Tang, C. Joachim. Science **271** (1996) 181.

[36] K. Kouguchi, T. Matsumoto and T. Kawai. Science **267** (1995) 71.

[37] J.T.Kim, M.Kanai, T.Kawai and S.Kawai,Jpn.J.Appl.Phys.**33** (1993) 5027.

[38] P.S.Weiss and D.M.Eigler, Phys. Rev. Lett, **71** (1993) 3129.

[39] V.M.Hallmark and S.Chiang, Surf. Sci, **286** (1993) 190.

[40] H.Tanaka,T.Matsumoto,T.Kawai and S.Kawai, Surf.Sci, **318** (1994) 29.

[41] D. O. Hayward and B. M. Trapnell, "*Chemisorption*", Butterworths, London (1964).

[42] J. K. Spong, H. A. Mizes, L. J. LaComb Jr, M. M. Dovek, J. E. Frommer and J. S. Foster. Nature **338** (1989) 137.

[43] V. E. Henrich. Prog. in Surf. Sci. **9** (1979) 143.

[44] K.Besocke: Sur.Sci. **181** (1987)145.

[45] H.Tanaka, J.Yoshinobu, M.Kawai, M.Aida, T.Kawai: to be submitted.

[46] M.Aida and S.Nishimura: Mutation Research, **192** (1987)83.

[47] M. Fujisawa, T. Sekitani, Y. Morikawa and M. Nishijima, J. Phys. Chem. **95** (1987) 145.

[48] H.Tanaka, J.Yoshinobu, M.Kawai, and T.Kawai, Jpn.J.Appl.Phys., **35** (1996) L244.

[49] V.M.Hallmark, S.Chiang, K.-P.Meinhardt and K.Hafner, Phys. Rev. Lett. **70** (1993) 3740.

[50] J.B.Cotton and I.R.Scholes, Brit. Corrosion J. **2** (1967) 1.

[51] P.Grtter and U.Drig, Surf. Sci. **337** (1995) 147.

[52] J.A. Derose, S.M. Lindsay, L.A. Nagahara, P.I. Oden and T. Thundat, J. Vac. Sci. Technol. B **9** (1991)1199.

[53] M.G. Youngquist, R.J. Driscoll, T.R. Coley, W.A. Godard and J.D. Baldeschwieler, J. Vac. Sci. Technol. B **9** (1991).1304

[54] R.W. Keller, D. Bear and C. Bustamante, J. Vac. Sci. Technol. B **9** (1991)1291.

[55] T. Nakagawa, H. Tanaka and T. Kawai, Surf. Sci. 370 (1997)L144.

[56] J.K. Gimzewski, S. Modesti, T David and R.R. Schlittler, J.Vac. Sci. Technol. B **12** (1994)1942.

[57] P.H.Beton, A.W. Dunn and P. Moriarty, Appl. Phys. Lett. **67** (1995)1075.

[58] R.Akiyama, T. Matsumoto, H. Tanaka and T. Kawai, submitted to Jpn. J. Appl. Phys.